

Combined astrometric imaging and coronagraphy

Olivier Guyon (UofA)

Michael Shao (NASA JPL)

Stuart Shaklan (NASA JPL)

Robert Woodruff (LMC)

Bijan Nemati (NASA JPL)

Mark Ammons (UofA)

Eduardo Bendek (UofA)

Marie Levine (NASA JPL)

Joe Pitman (Expl. Sci.)

Improvements to original concept, error budget, exoplanet science

Error budget, mission architecture

Optical design for wide field telescope compatible with coronagraphy

Numerical simulations, modeling approach

Lab demo design & operation

Lab demo optical design & operation

System engineering, mission architecture

System engineering

Tom Milster (UofA)

Jim Burge (UofA)

Neville Woolf (UofA)

Roger Angel (UofA)

Josh Eisner (UofA)

Ruslan Belikov (NASA Ames)

Daniel Eisenstein (UofA)

Ann Zabludoff (UofA)

Dennis Zaritsky (UofA)

Jay Daniel (L3/Tinsley)

Mask manufacturing, scaling of mask manufacturing to full scale PM

Mask manufacturing, scaling of mask manufacturing to full scale PM

Exoplanet science, concept definition

Exoplanet science, concept definition

Exoplanet and star formation/evolution science

Compatibility with coronagraphy

Extragalactic science enabled with wide field camera

Extragalactic science with wide field camera

Extragalactic & galactic science with wide field camera

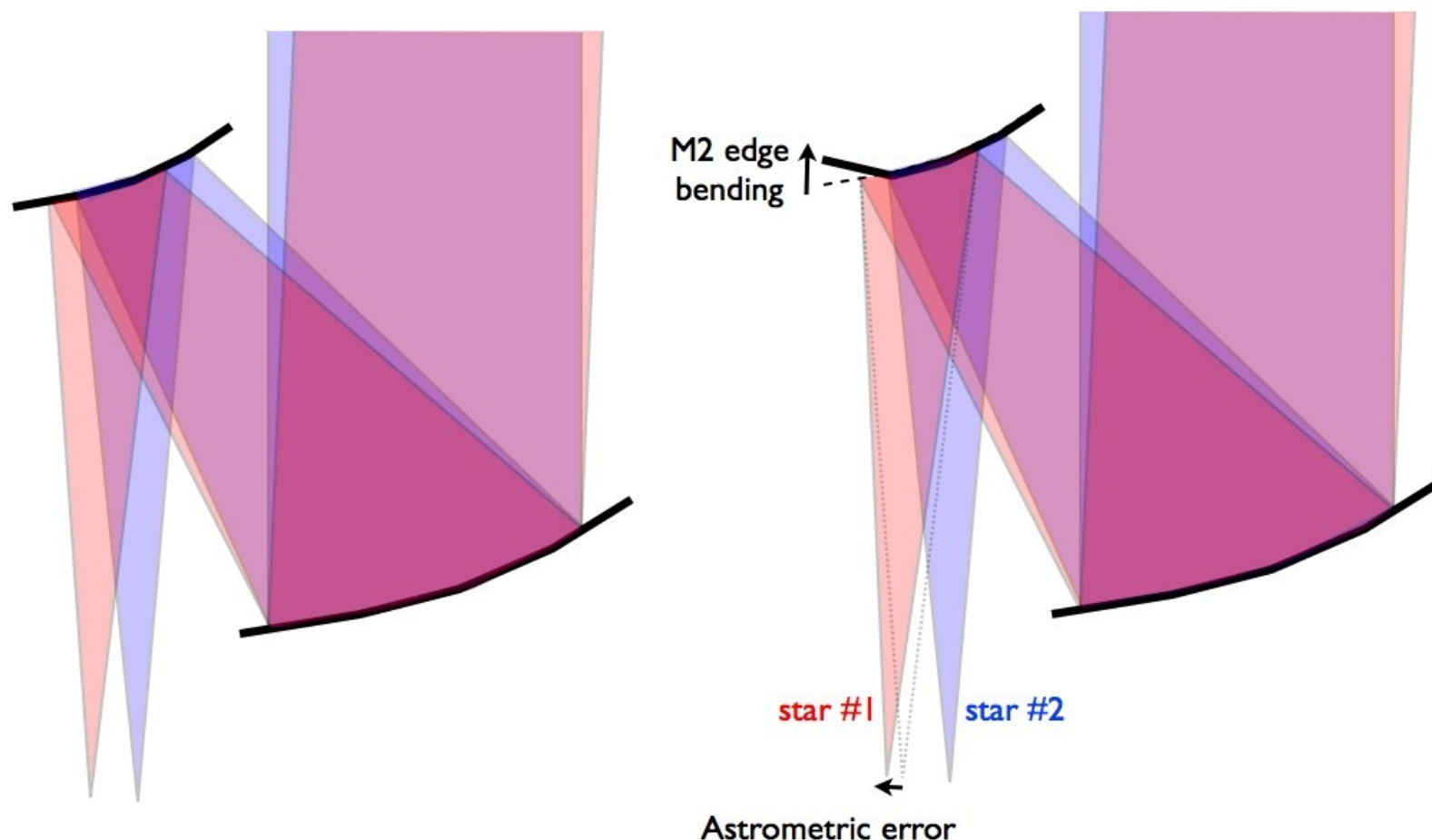
Optics manufacturing

Principle: use background stars around coronagraph target as an astrometric reference

With a 1.4-m telescope in the visible, 0.25 sq deg offers sufficient photons from stars at the galactic pole to provide an astrometric reference at the <50 nano-arcsec after taking into account realistic efficiency, zodi light and pixel sampling.

Why is imaging astrometry difficult ?

On-axis and off-axis stars illuminate different (but overlapping) parts of M2.
Edge bending on M2 is seen by star #1, but not star #2.



(1) Light from different stars on the sky travels different paths \rightarrow small bending of optics produces field distortions

(2) The detector can move between observations (especially when using large mosaics)

(3) Pixels are not perfect and their response changes with time

+ (4) Central star is much brighter than background stars

Astrometric error in the photon noise limit

For each star, pixel coordinate errors due to photon noise (star + zodi) and sampling are computed.

Estimation uses a 2D polychromatic finely sampled PSF which is moved by a small amount and then binned to the pixel scale. The flux change for each pixel is compared to the noise, and all values are combined with SNR^2 weighting.

Simulation on the right shows the single axis astrometric error for a 2 day observation, 0.03 sq deg at galactic pole, Polychromatic PSF, Nyquist sampling detector at 0.6 μm , 80% optical throughput, 90% detector peak QE (0.36 μm effective bandwidth)

$m_V = 22.5 / \text{sqarcsec zodi}$

Combined astrometric accuracy = 0.1265 μas

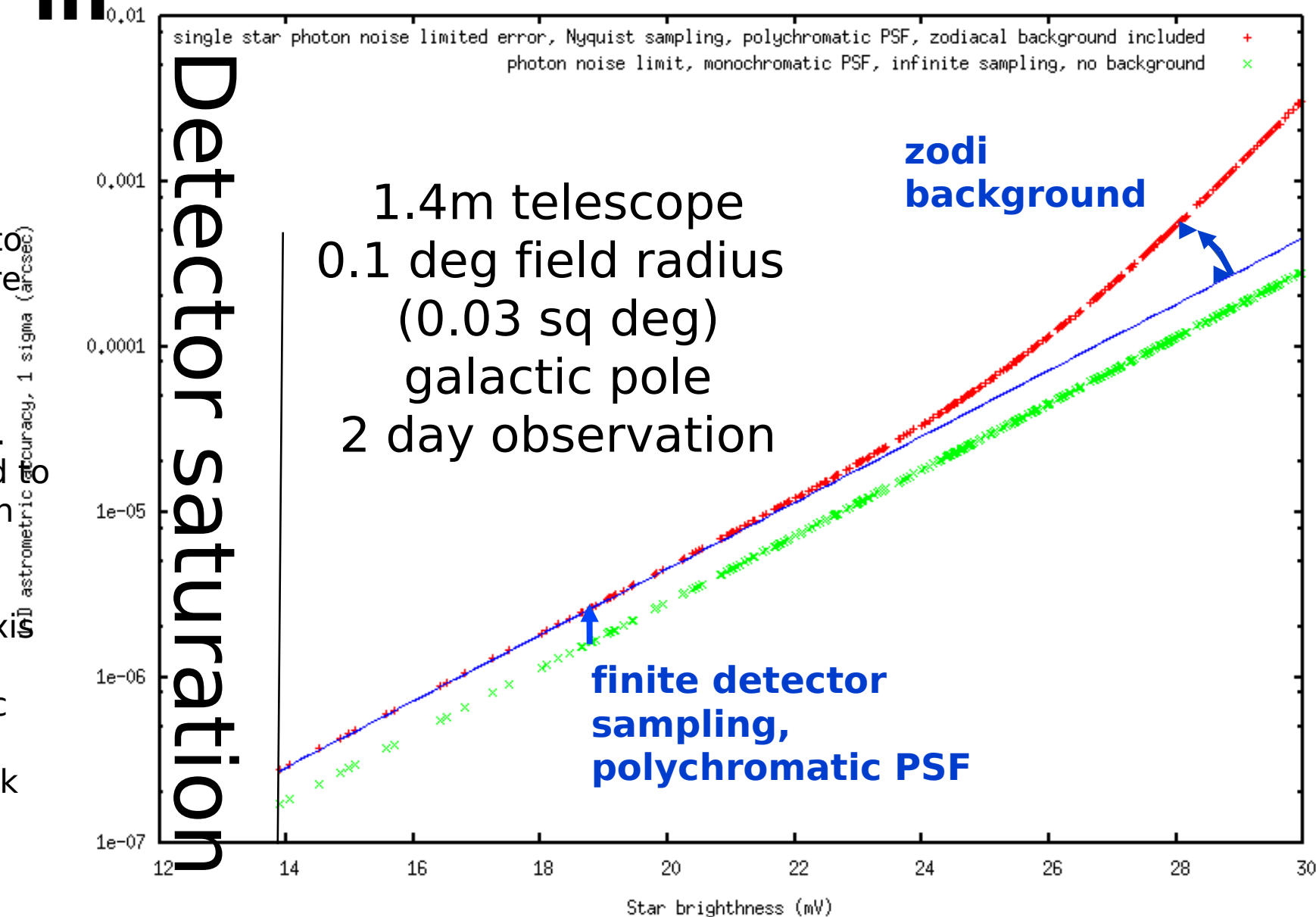
For a 0.25 sq deg (0.5 x 0.5 deg): 0.044 μas

A small number of bright stars (m_V) contribute to most of the measurement accuracy:

If only stars fainter than $m_V=17$ are included, accuracy = 0.46 μas

If only stars brighter than $m_V=17$ are included, accuracy = 0.1315 μas

Note: At high galactic latitude, extragalactic sources may be used to increase sensitivity ?



Green points show theoretical 1D astrometric error:

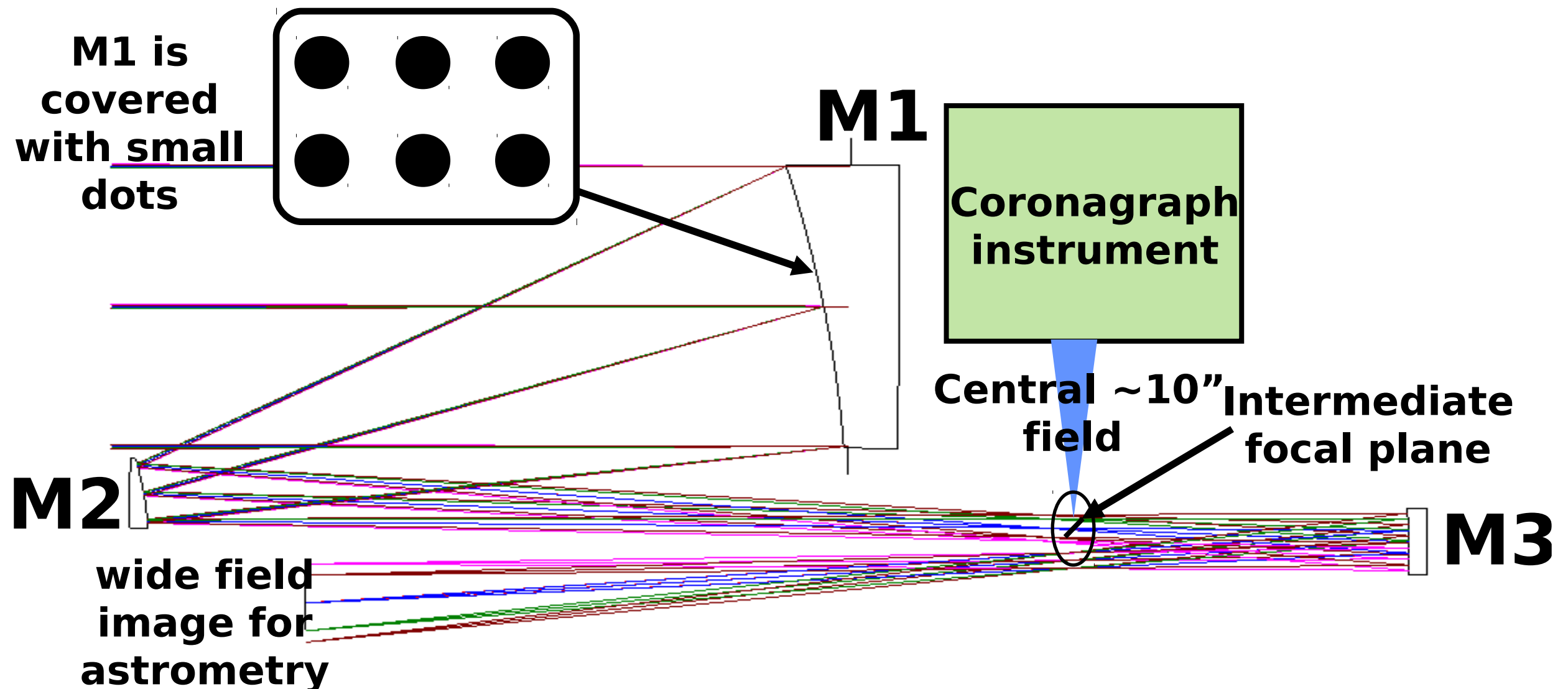
$$\sigma = 0.318 (\lambda/D) / \sqrt{N_{\text{photon}}}$$

Red points show 1D astrometric error when zodi, PSF polychromaticity and pixel sampling are taken into account. The difference between the 2 curves is explained by an offset due to detector sampling and PSF polychromaticity (independent of star magnitude) + an increase in measurement error at the faint end due to zodiacal light photon noise.

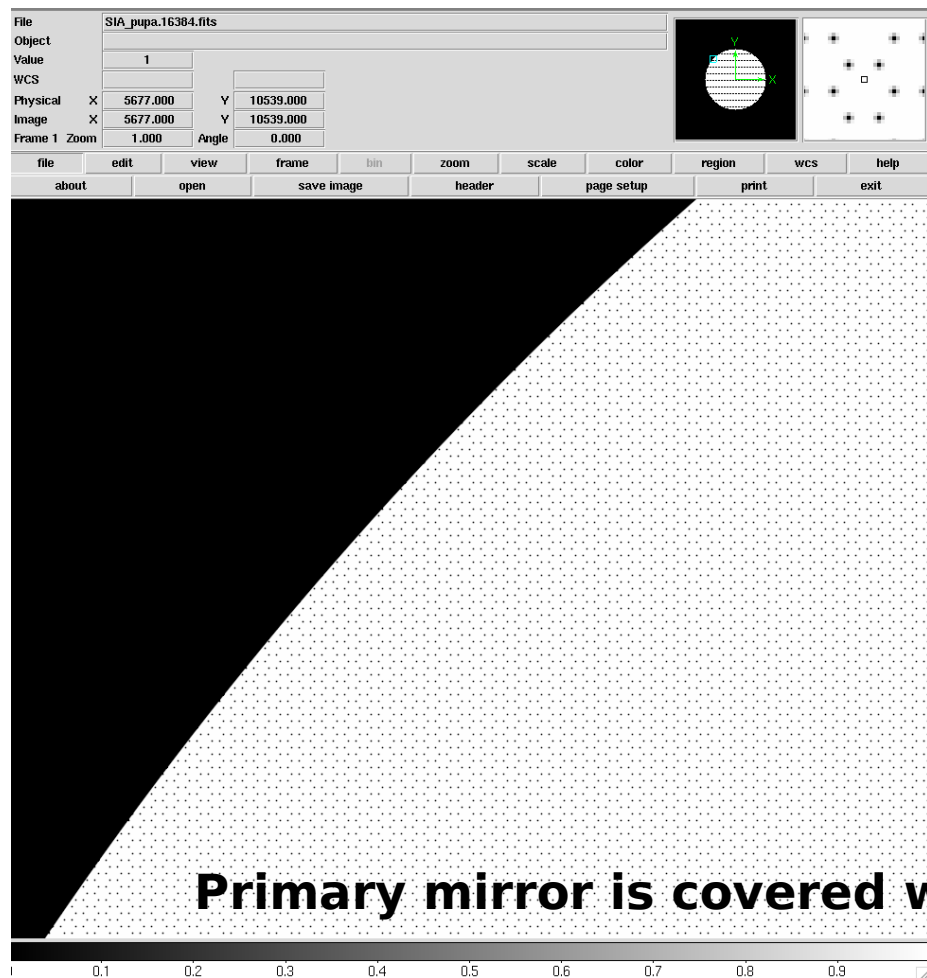
Optical Layout for simultaneous coronagraphy and astrometry

The telescope is a conventional TMA, providing a high quality diffraction-limited PSF over a 0.5×0.5 deg field with no refractive corrector. The design shown here was made for a 1.4m telescope (PECO).

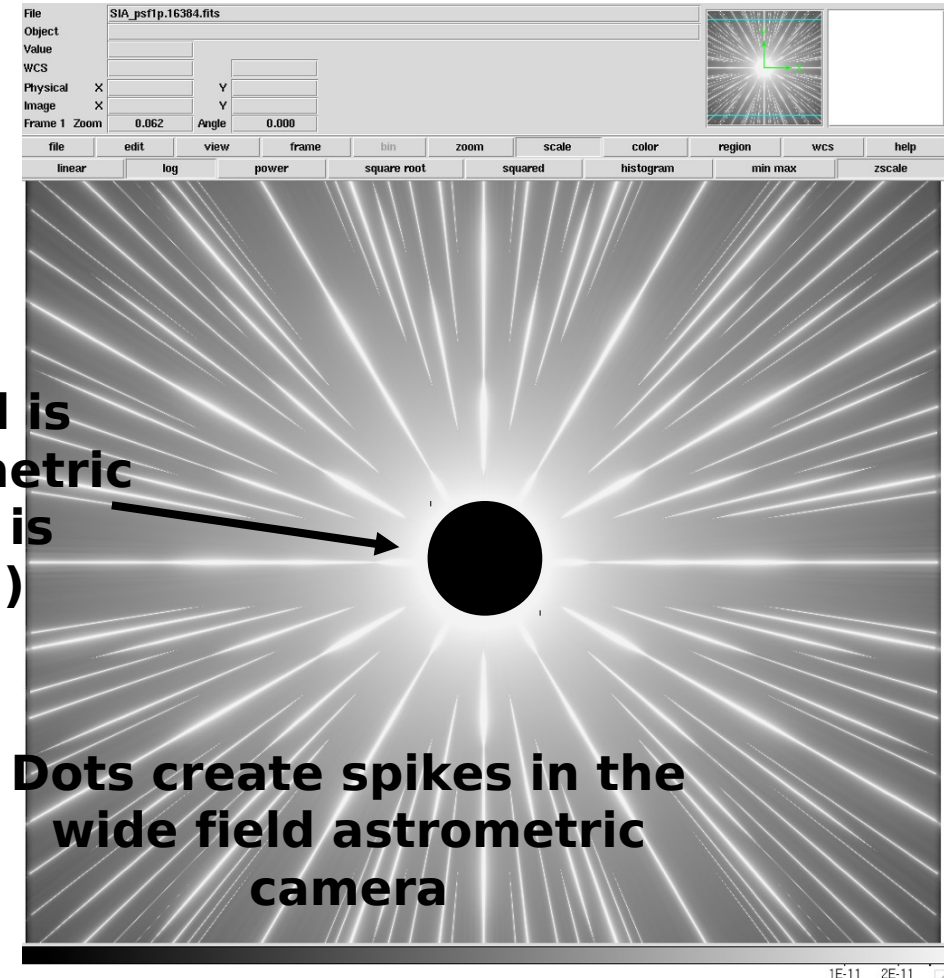
Light is simultaneously collected by the coronagraph instrument (direct imaging and spectroscopy of exoplanet) and the wide field astrometric camera (detection and mass measurement of exoplanets)



Dots on primary mirror create a series of diffraction spikes used to calibrate astrometric distortions



The center of the field is missing from the astrometric camera (central light is sent to coronagraph)

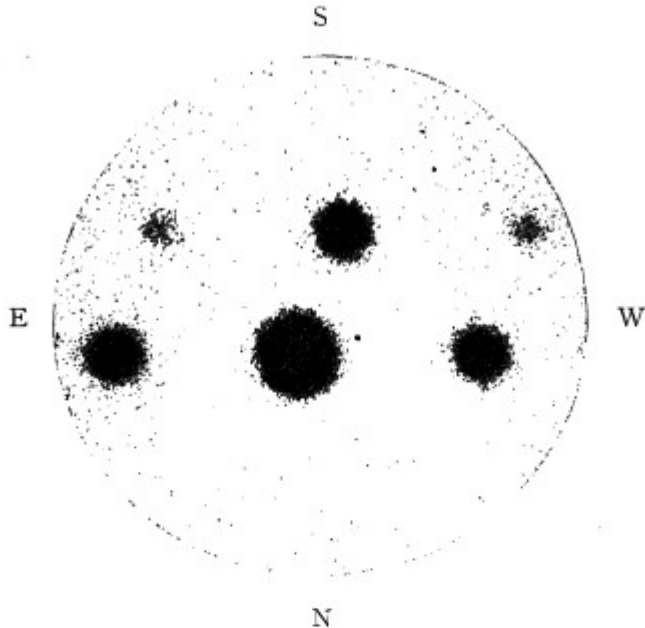


Primary mirror is covered with small dots

Dots create spikes in the wide field astrometric camera

All astrometric distortions (due to change in optics shapes of M2, M3, and deformations of the focal plane array) **are common to the spikes and the background stars**. By referencing the background star positions to the spikes, the astrometric measurement is largely immune to large scale astrometric distortions.

Instead of requiring ~pm level stability on the optics over yrs, the stability requirement on M2, M3 is now at the nm-level over approximately a day on the optics surfaces, which is within expected stability of a coronagraphic space telescope. (Note: the concept does not require stability of the primary mirror).



A 5-seconds exposure of Castor, enlarged 75 times. The separation of the components is 3".74 or 0.198 mm on the plate. The first order spectra are one magnitude fainter than the central image. Taken December 1, 1939, by K. Aa. Strand, with the Sproul 24-inch refractor, aperture reduced to 13 inches, Eastman IV G emulsion, Wratten No. 12 (minus-blue) filter.

age of the fainter component, a compensation for possible magnitude error is provided by using the mean of the measured positions of the two spectral images instead of the central image. As long as the difference in intensity between the images does not exceed half a magnitude, the magnitude error is usually negligible; it is therefore sufficient to have a limited number of gratings, producing first-order spectra which are a whole number of magnitudes fainter than the central image. For example, in his work with the Sproul refractor, Strand^a used four gratings, made of duraluminum, giving differences of one, two, three, and four magnitudes, respectively, between the central image and the first-order spectra. The bars are mounted on 10 cm-wide annular frames, cut from sheets of duraluminum, 3 mm thick. The constants of the four gratings are given below.

CONSTANTS OF SPROUL OBJECTIVE GRATINGS					
Grating	—width of—		extinction	first order minus central image	
	bar	opening	for central image	mag. difference	distance
1	11.25 mm	11.21 mm	1.51 mag	.98 mag	.270 mm = 5".10
2	7.12 mm	15.06 mm	.84 mag	2.05 mag	.273 mm = 5.15
3	3.98 mm	14.80 mm	.52 mag	3.01 mag	.322 mm = 6.08
4	3.20 mm	19.06 mm	.34 mag	3.95 mag	.272 mm = 5.13

"Long-focus photographic astrometry", van de Kamp, 1951

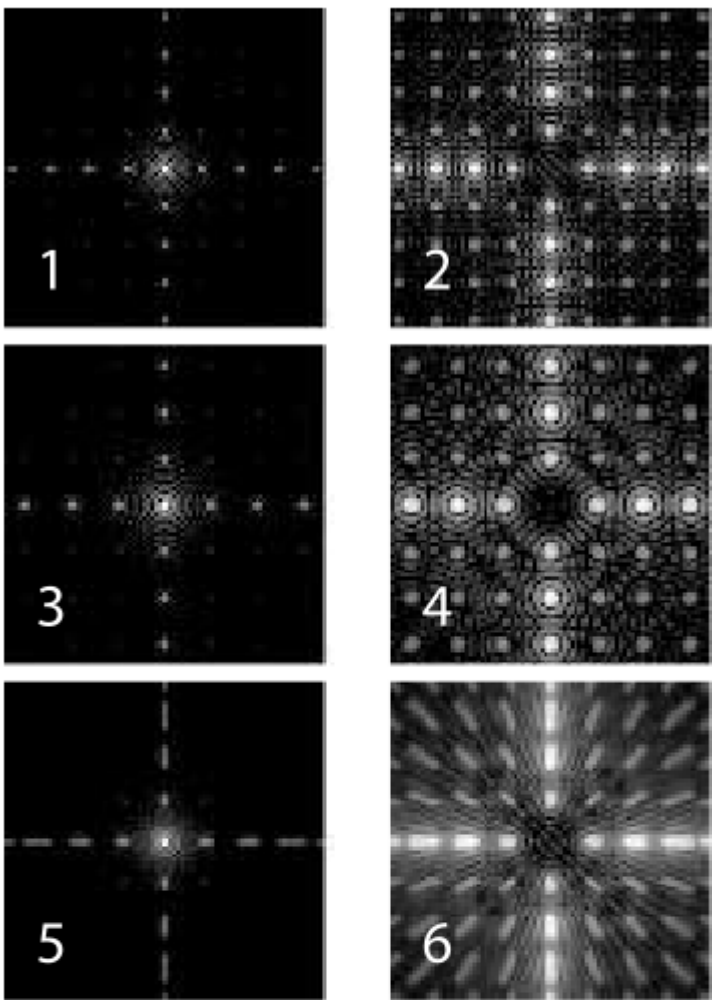
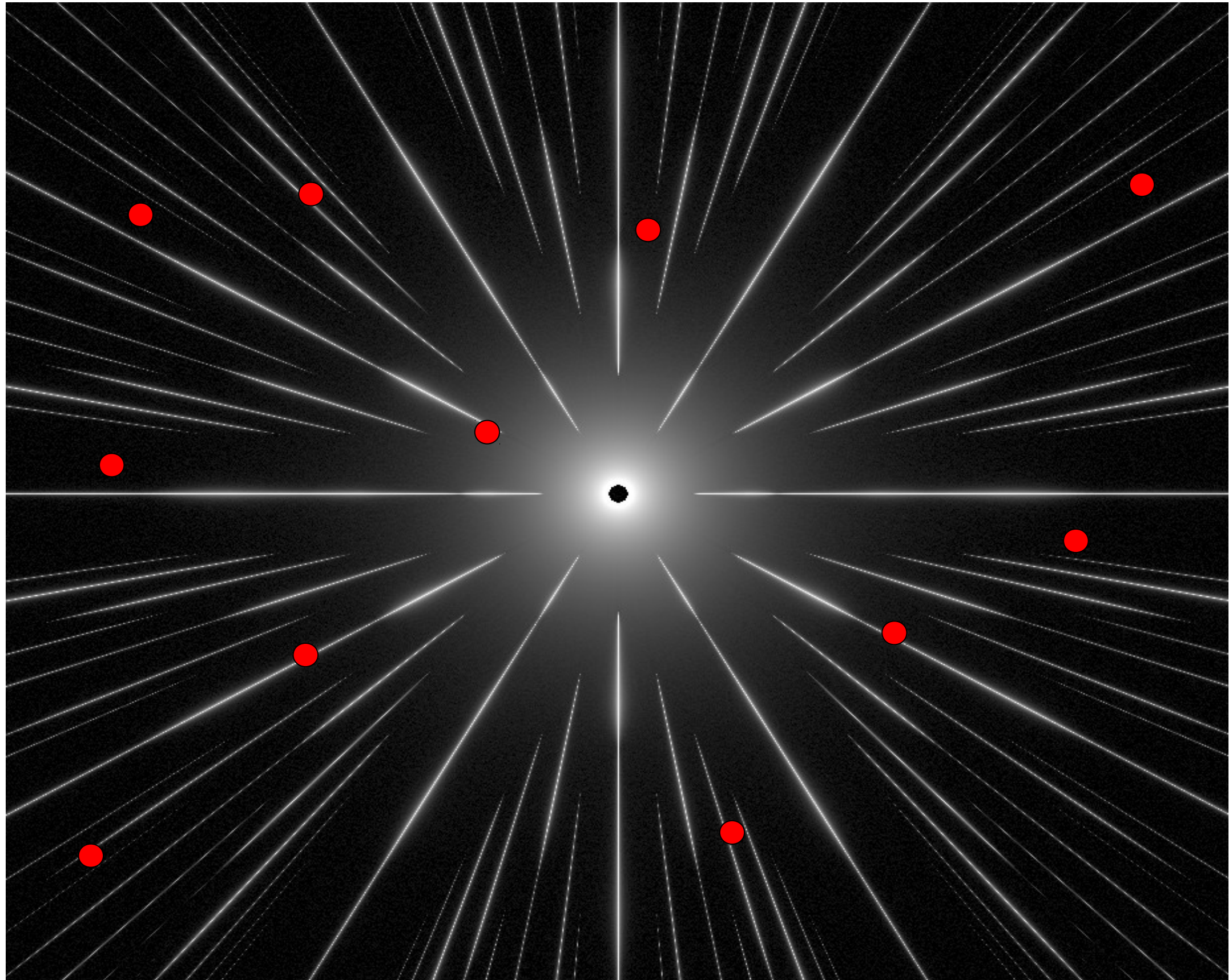


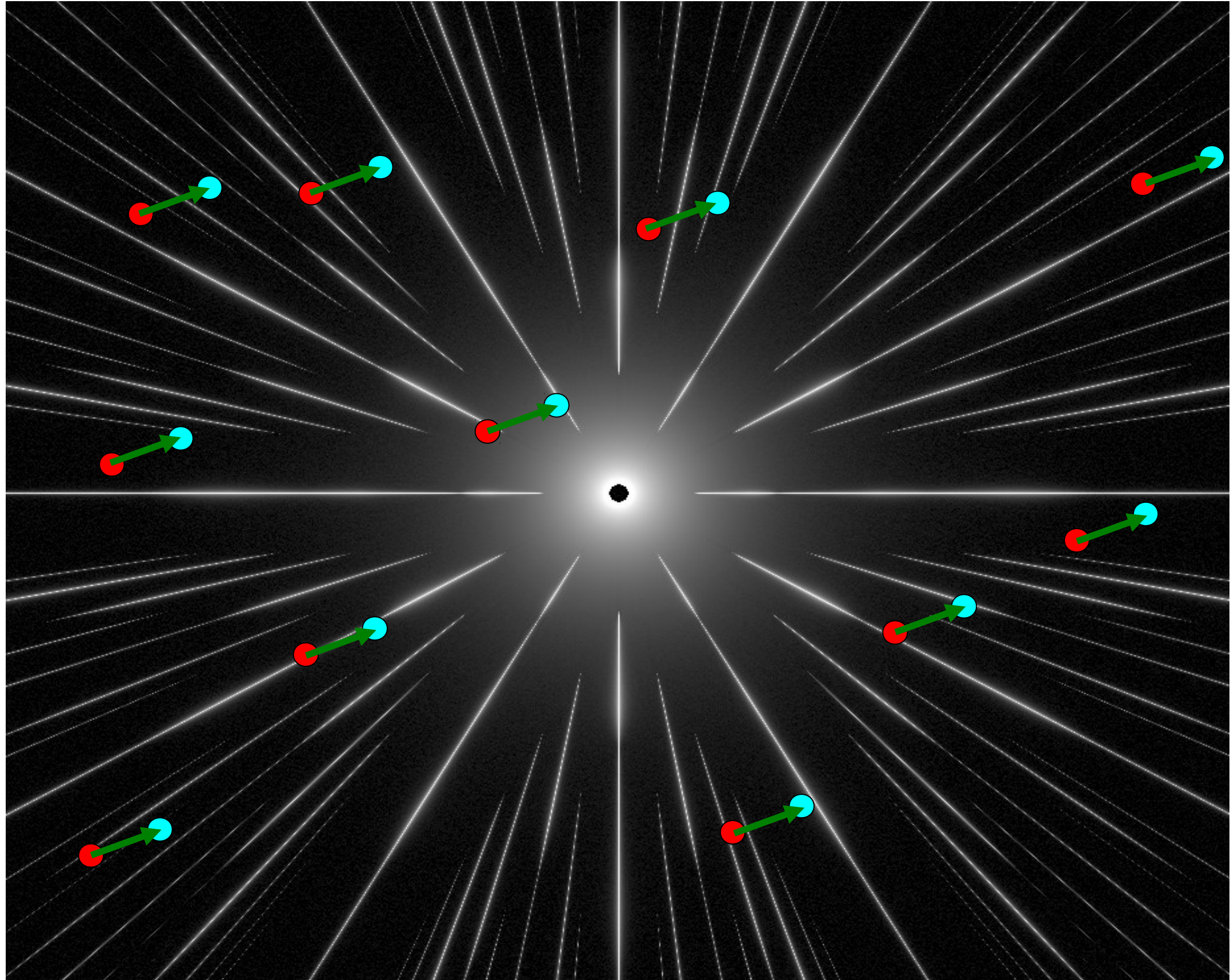
FIG. 1.—Monochromatic and broadband direct and coronagraphic PSFs with a square-geometry reticulate pupil mask. All images are on a logarithmic gray scale stretching 10 mag fainter than their peaks. The pupil is 128 pixels across, and the grid has a wire spacing of 16 pixels, with 2-pixel-wide wires. (1): Direct PSF for the shortest wavelength of a 20% bandwidth filter with uniform transmission within the bandpass, in the absence of phase errors. The satellite PSFs off the origin but along the horizontal and vertical axes are fainter than the central core of the PSF by a factor $\epsilon^2 = (g/d)^2$, where g is the wire thickness and d is the wire spacing. The satellite spots off the axes are ϵ^4 fainter than the corresponding central peak. (2): Coronagraphic PSF at the shortest wavelength of the filter. The off-axis sea of satellite spots are more visible in the coronagraphic image because the core has been suppressed. (3) and (4): Direct and coronagraphic PSFs for the longest wavelength of the filter. (5) and (6): Direct and coronagraphic PSF for the full bandpass. The length of any particular radial streak in this last pair of images (in resolution elements at the central wavelength of the bandpass) is approximately the fractional filter bandwidth multiplied by the radial distance of the spot at band center. The streaks all point toward the origin, so the smearing has no effect on astrometric precision according to Fraunhofer regime image formation theory. We suggest using the four satellite peaks closest to the core as fiducials for the position of the central occulted star in coronagraphic images.

"Astrometry and Photometry with Coronagraphs", Sivaramakrishnan, Anand; Oppenheimer, Ben R., 2006

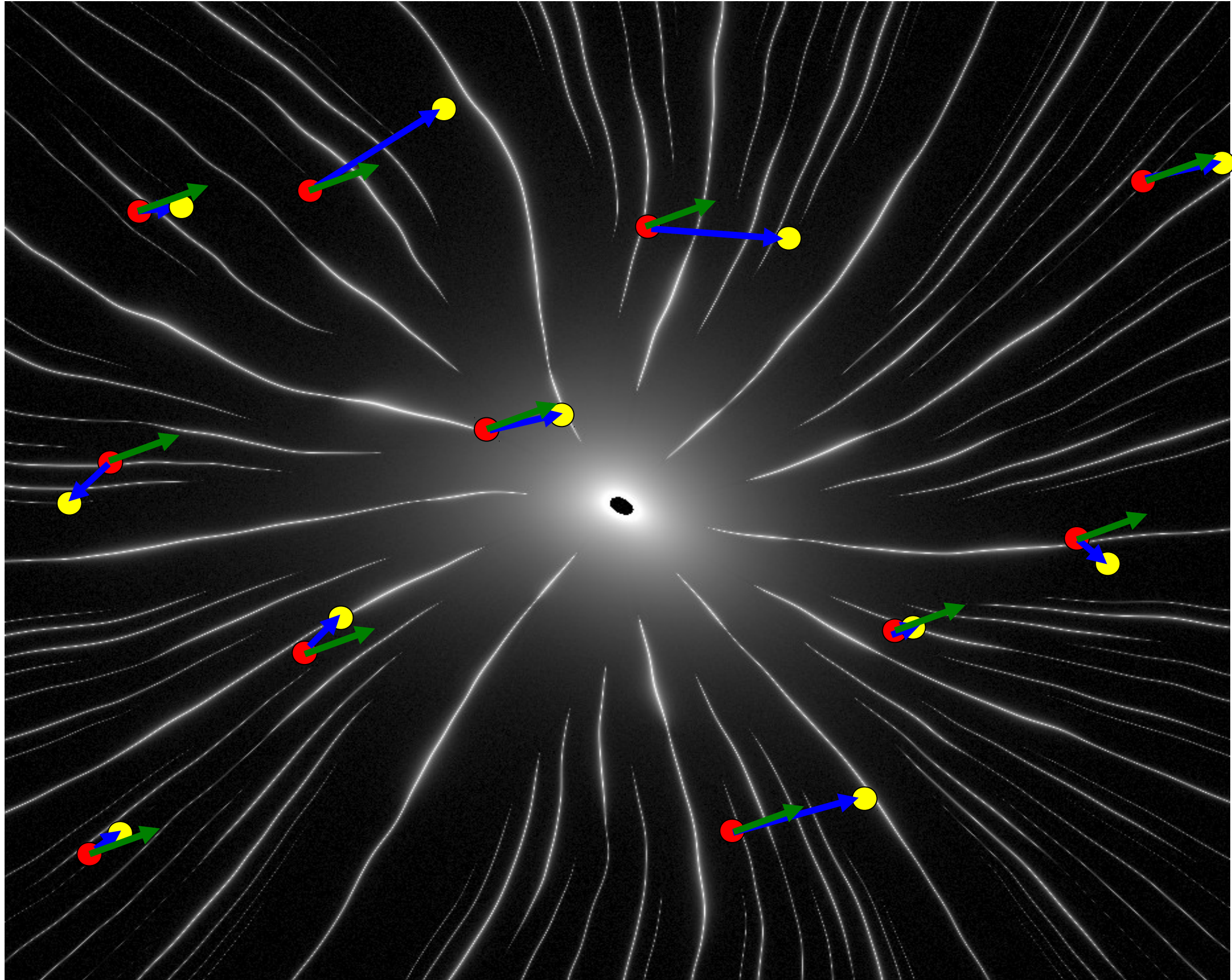
Red points show the position of background stars at epoch #1 (first observation)



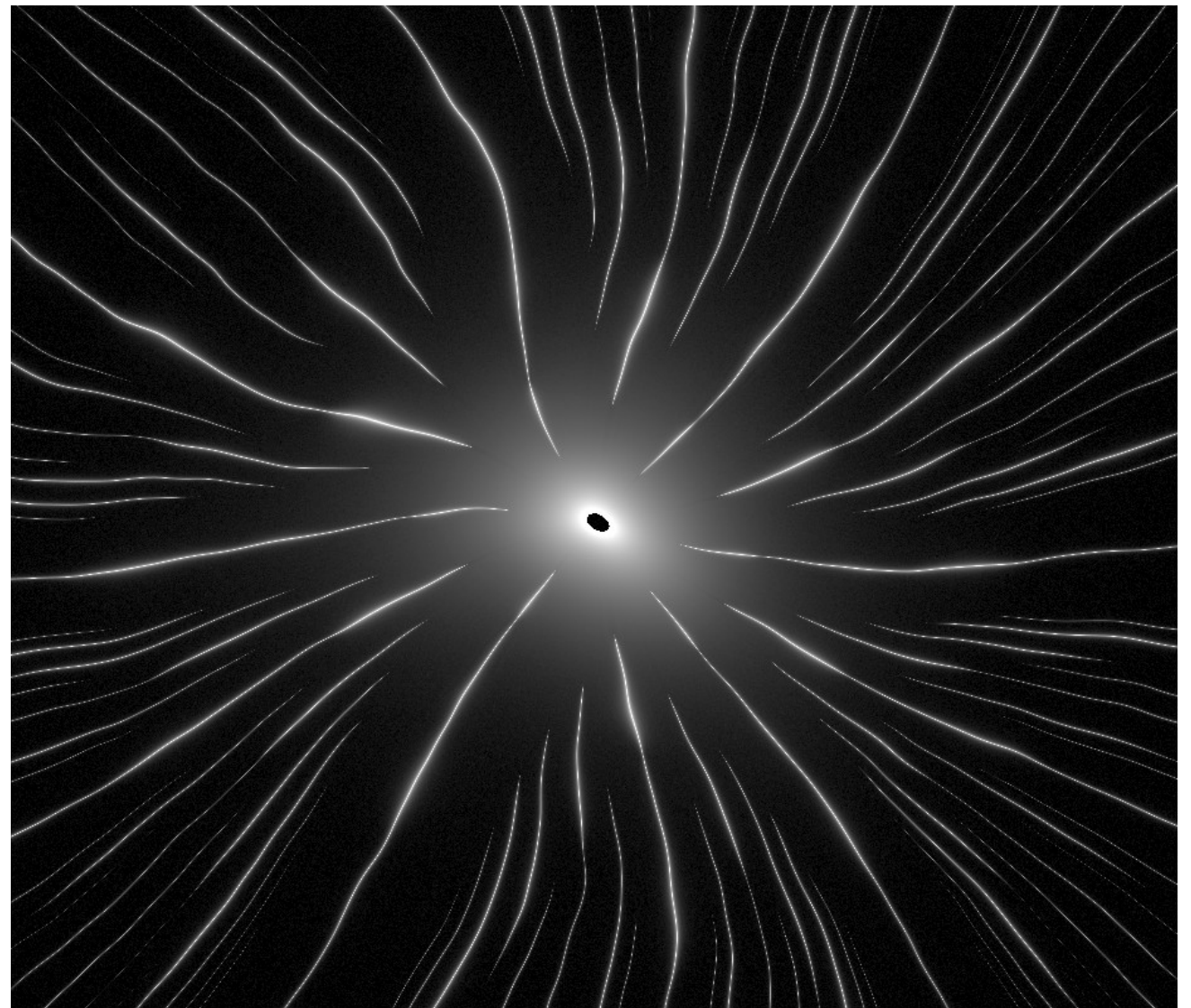
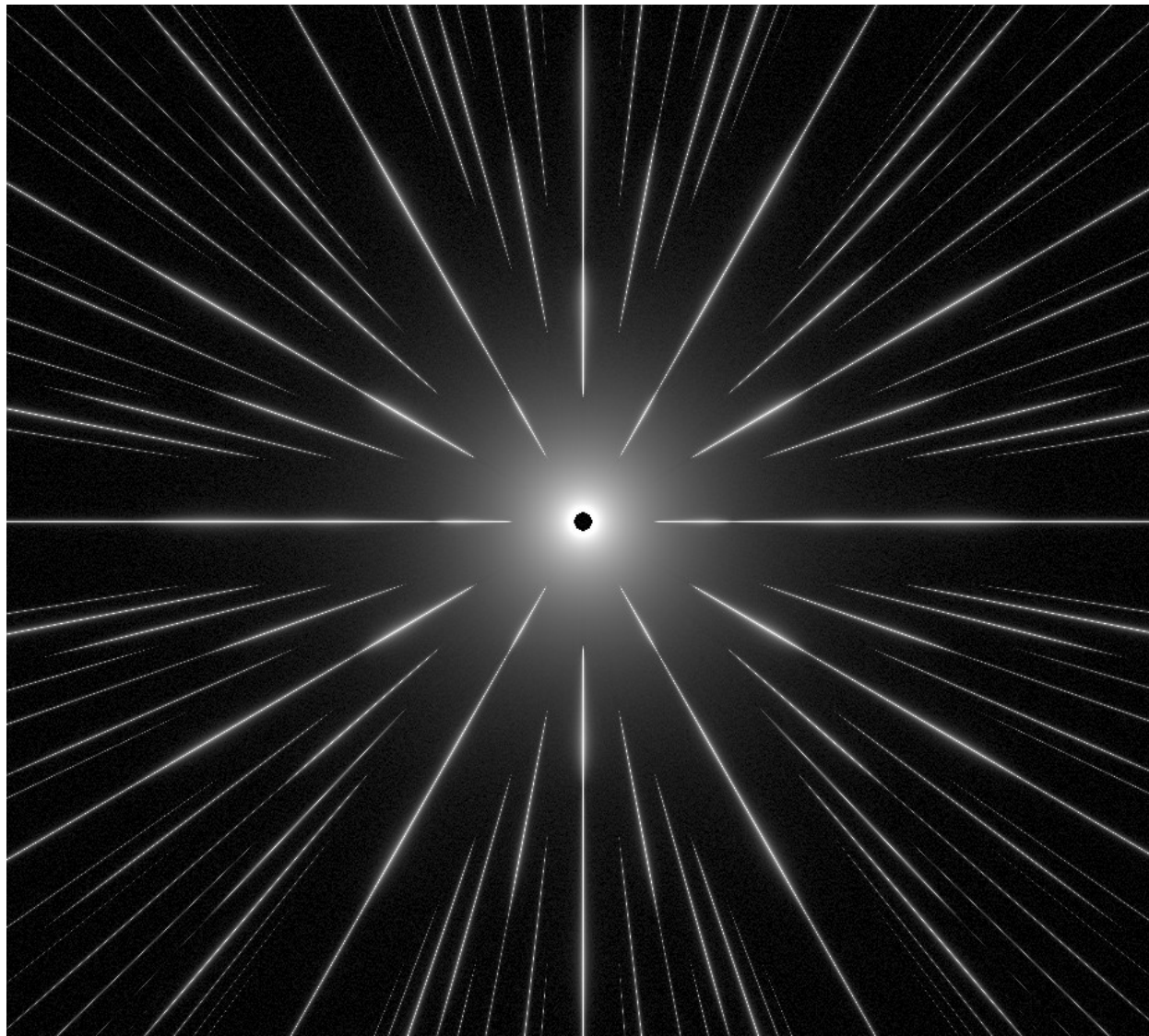
**Blue points show the position of background stars at epoch #2 (second observation)
The telescope is pointed on the central star, so the spikes have not moved between
the 2 observations, but the position of the background stars has moved due to the
astrometric motion of the central star (green vectors).**



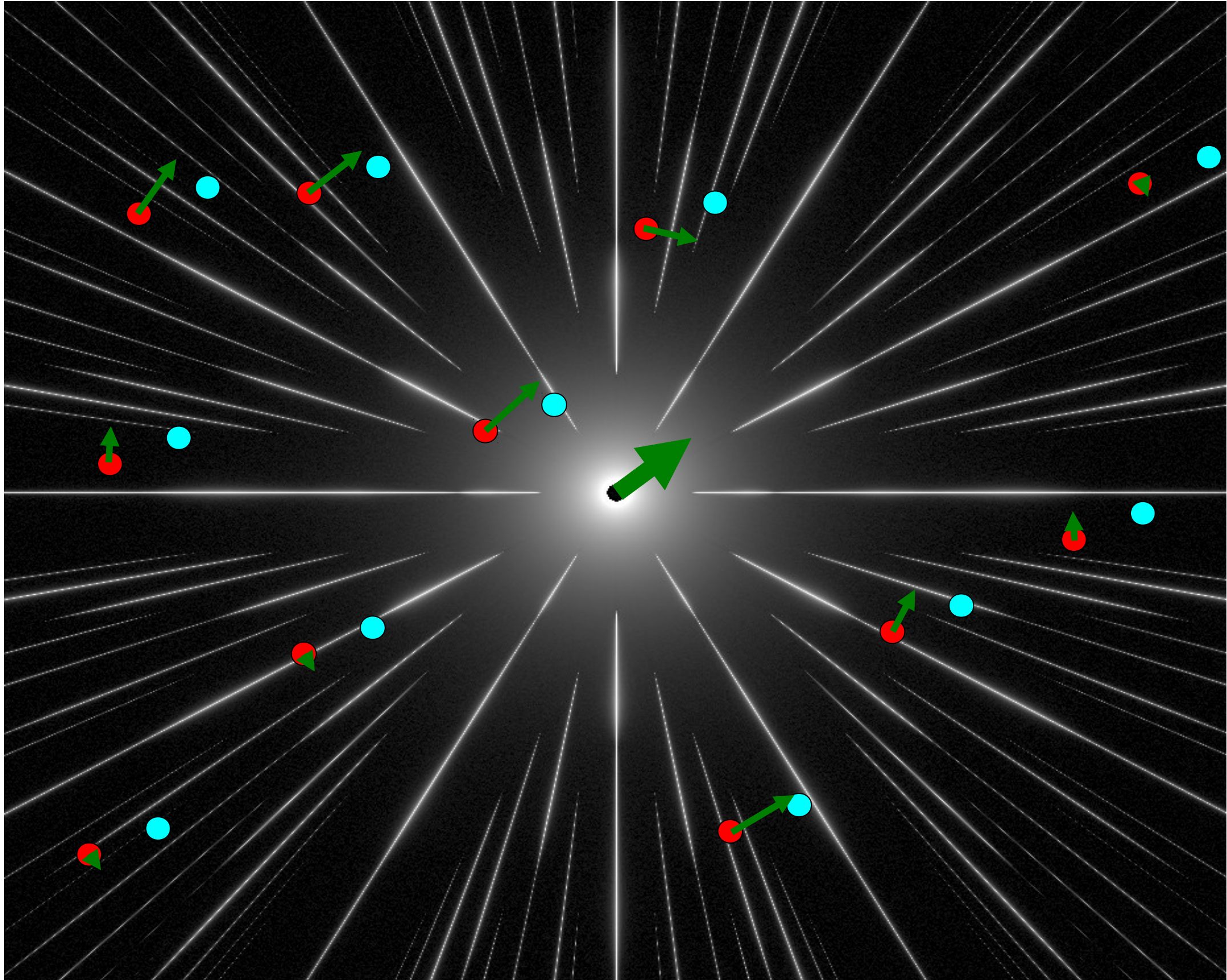
Due to astrometric distortions between the 2 observations, the actual positions measured (yellow) are different from the blue point. The error is larger than the signal induced by a planet, which makes the astrometric measurement impossible without distortion calibration.



The measured astrometric motion (blue vectors in previous slide) is the sum of the true astrometric signal (green vectors) and the astrometric distortion induced by change in optics and detector between the 2 observations. Direct comparison of the spike images between the 2 epochs is used to measure this distortion, which is then subtracted from the measurement to produce a calibrated astrometric measurement.



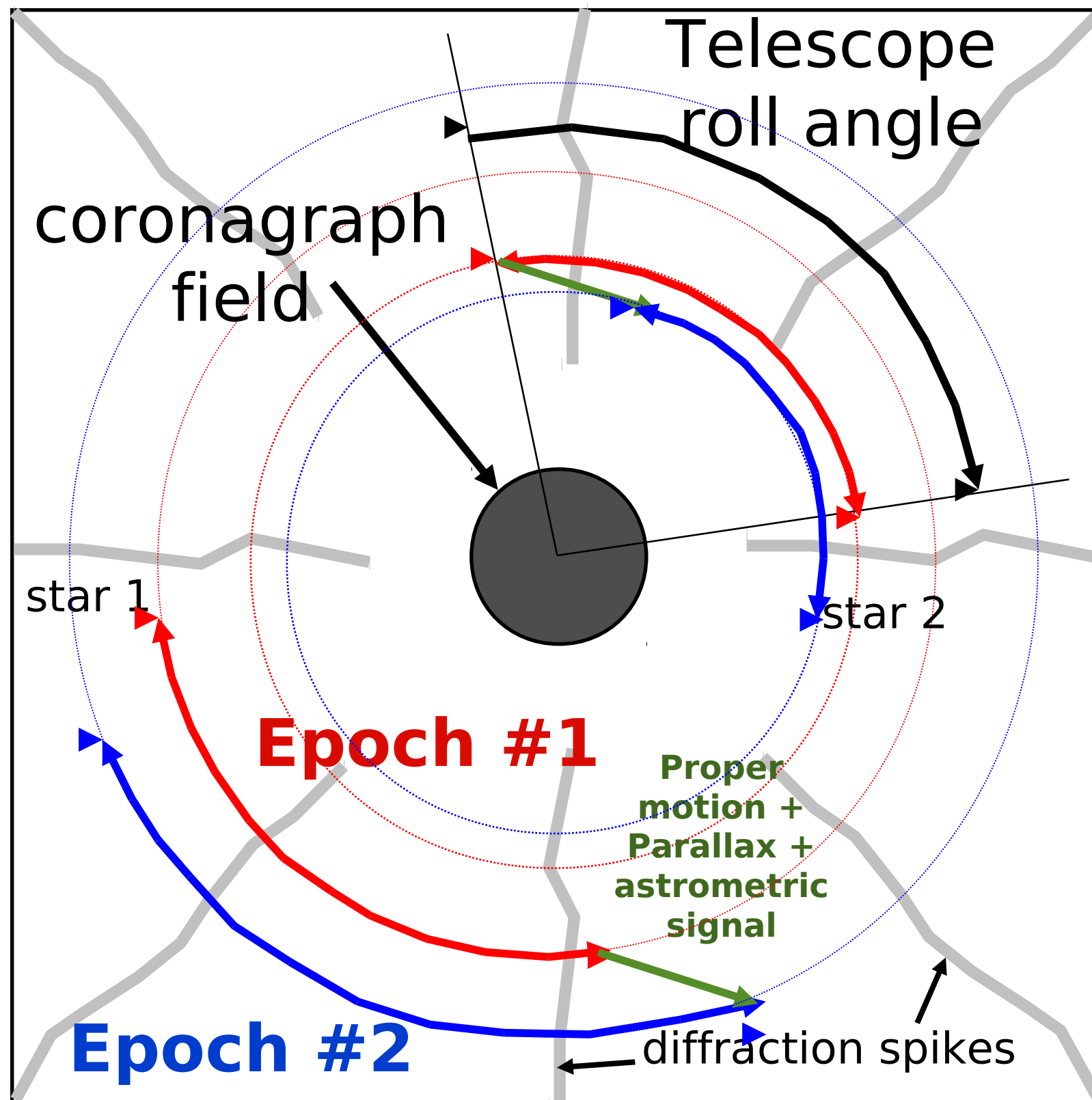
The calibration of astrometric distortions with the spikes is only accurate in the direction perpendicular to the spikes length. For a single background star, the measurement is made along this axis (1-D measurement), as shown by the green vectors. The 2-D measurement is obtained by combining all 1-D measurements (large green vector).



Observation scheme

A slow telescope roll is used to average out small scale distortions, which are due to non-uniformity in the pixel size, (spectral) response, and geometry

The green vector is what should be measured



Science goals and
required astrometric
accuracy

Science goals

Primary science goal:

Measure planet mass with 10% accuracy ($1-\sigma$) for an Sun/Earth analog at 6pc.

This allows mass measurement of all potentially habitable planets (Earth-like & SuperEarths) imaged by PECO.

SNR>5 detection at $R=5$ in less than 6 hrs along 20% of the planet orbit, assuming 45% system efficiency, and 1 zodi (no WF errors)

Table 4-2: Stars with Earth-like planets in habitable zones (1 AU equiv) easily detectable with PECO

HIP#	dist (pc)	max el (λ/D)	*rad (λ/D)	SNR (1s, tp)	t20% (s, tp)	Comment
71683	1.3	11.5	0.06	0.49	35	Alf Cen A G2 V, V=0
71681	1.3	6.6	0.04	0.45	44	Alf Cen B K2 IV, V=1.3
8102	3.6	2.3	0.01	0.08	2750	Tau Cet G8.5 V, V=3.5 **
16537	3.2	2.2	0.01	0.09	2968	Eps Eri K2 V, V=3.7 **
3821	6.0	2.3	0.01	0.04	14329	Eta Cas G0 V V=3.5 ***
2021	7.5	3.1	0.01	0.03	14878	Bet Hyi G0 V, V=2.8
99240	6.1	2.2	0.01	0.03	19636	Del Pav G8 IV, V=3.6

Table extracted from PECO SRD (http://caao.as.arizona.edu/PECO/PECO_SRD.pdf)

Simulated observations

Planetary system characteristics

Star	Sun analog
Distance	6 pc
Location	Ecliptic pole
Orbit semi-major axis	1.2 AU
Planet mass	1 Earth mass
Orbit excentricity	0.2
Astrometric signal amplitude	0.5 μ as
Orbit apparent semi-major axis	200 mas

Observations

Number of observations	32 (regularly spaced every 57 days)
Coronagraph: planet position measurement accuracy in coronagraphic image	2.5 mas per axis (= 3.6 mas in 2D): corresponds to diffraction-limited measurement with 100 photon at 550 nm on PECO
Coronagraph: Inner Working Angle	130 mas (coronagraph cannot see planet inside IWA)
Astrometry: accuracy	Variable (to be matched to science requirements)

Combined solution derived from simultaneous coronagraphy and astrometry measurements

Known variables:

- **Star location** on the sky (effect of parallax is known except for star distance, aberration of light perfectly known)
- **observing epochs**
- **Stellar mass** (assumed to be known at the 5% accuracy level)
- **measurement noise levels** for astrometry ($\sim \mu\text{as}$), coronagraphy planet position (few mas) and star mass ($\sim 5\%$)

Measurements

Astrometry:

star position
(nb of variables =
 $2 \times \text{\#observations}$)

Coronagraphy:

planet position
(nb of variables =
 $2 \times \text{\#observations}$)

Solution

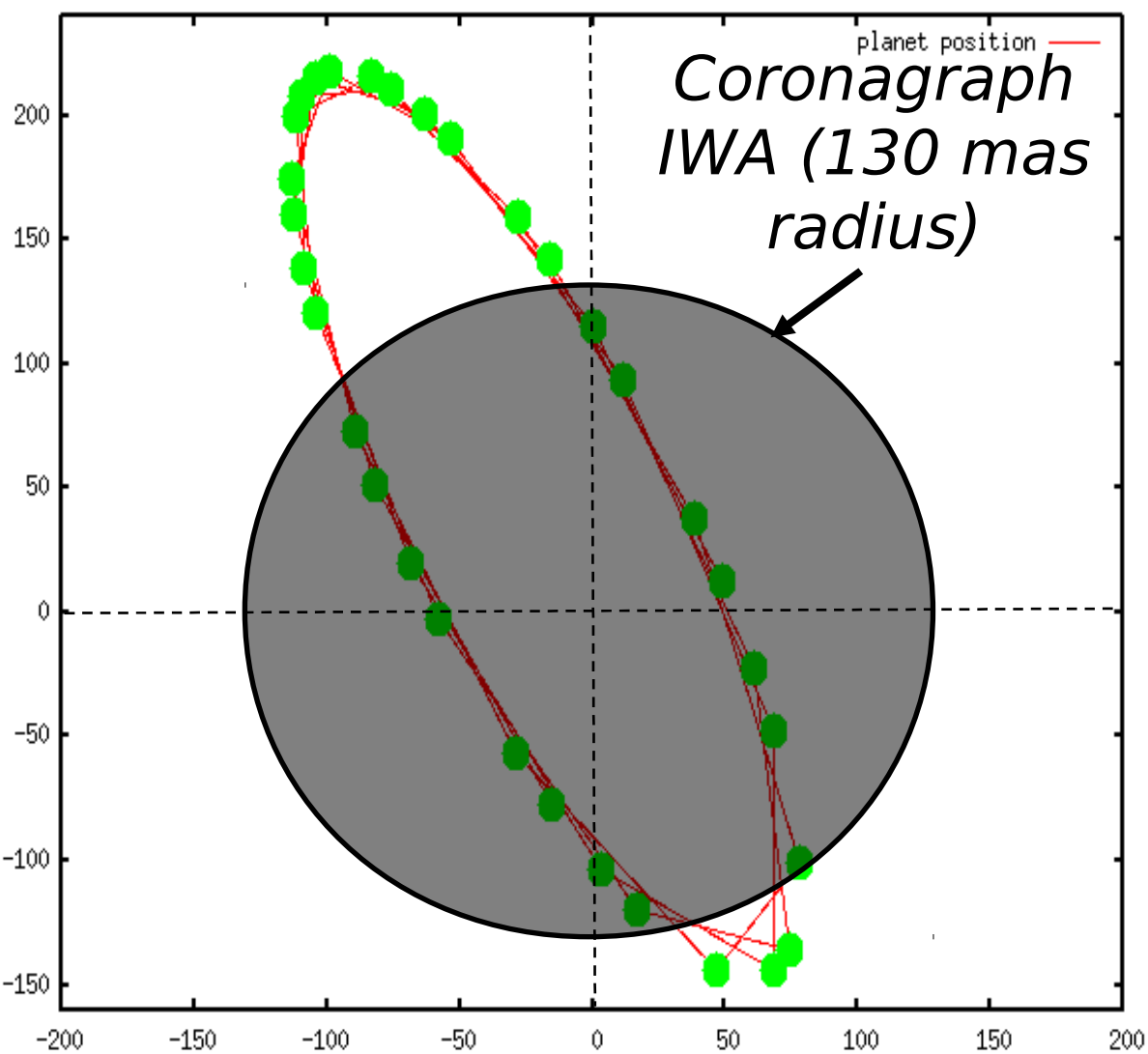
Maximum likelihood solution for
11 free parameters to be solved for:

- star parallax (1 variable)
- proper motion (2 variables)
- star mass (1 variable)
- planet mass (1 variable)
- orbital parameters (6 variables)

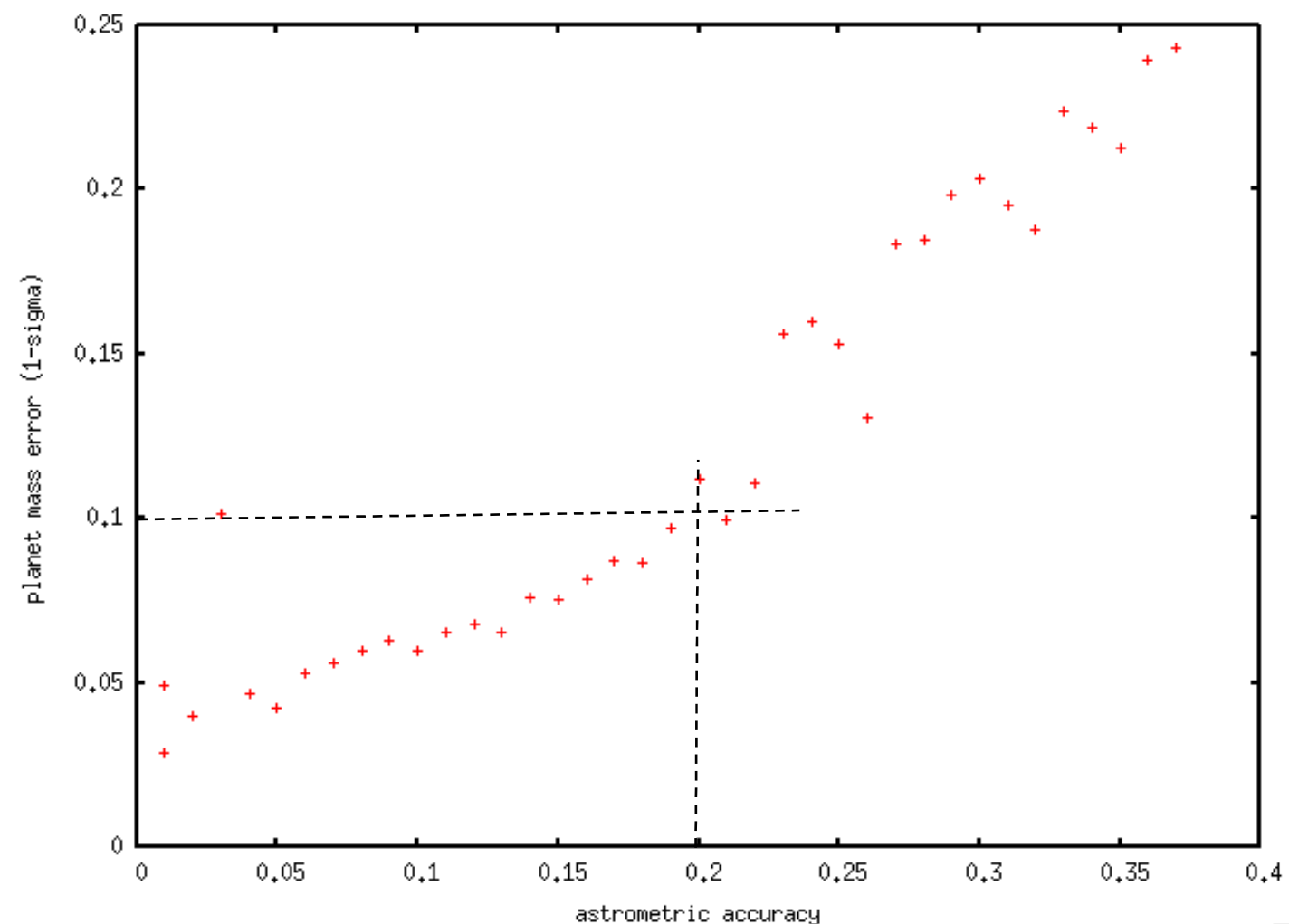
Combined solution for simultaneous coronagraphy + astrometry

Planet on a 1.2 AU orbit (1.3 yr period), $e=0.2$

orbit orientation on sky: planet outside the coronagraph IWA for 17 out of the 32 observations.



Required single measurement
astrometric accuracy = $0.2 \mu\text{as}$ (1-sigma, 1D)



Combined solution from simultaneous coronagraphy and astrometry: method adopted to derive measurement accuracy

Known variables:

- Star location on the sky (effect of parallax is known except for star distance, aberration of light perfectly known)
- observing epochs
- measurement noises on astrometry ($\sim \mu\text{as}$), coronagraphy planet position (few mas) and star mass ($\sim 5\%$)

System defined by 11 free parameters to be solved for:

- star parallax (1 variables)
- proper motion (2 variables)
- star mass (1 variable)
- planet mass (1 variable)
- orbital parameters (6 variables)

Repeat $N \gg 1$ times

Measurements:

Astrometry: star position (2x #observations)

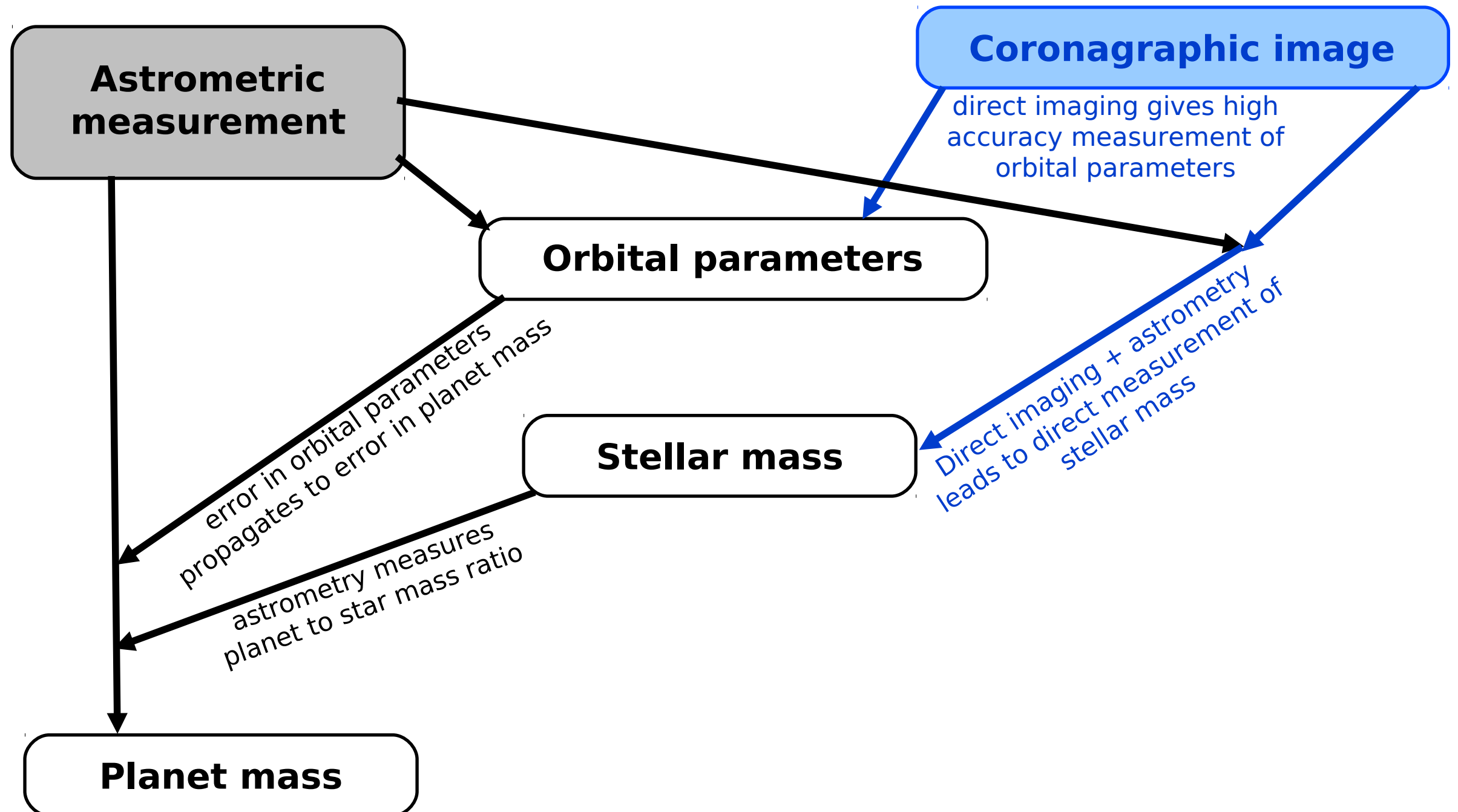
Coronagraphy: planet position (2x #observations)

Stellar mass: derived from stellar luminosity (1)

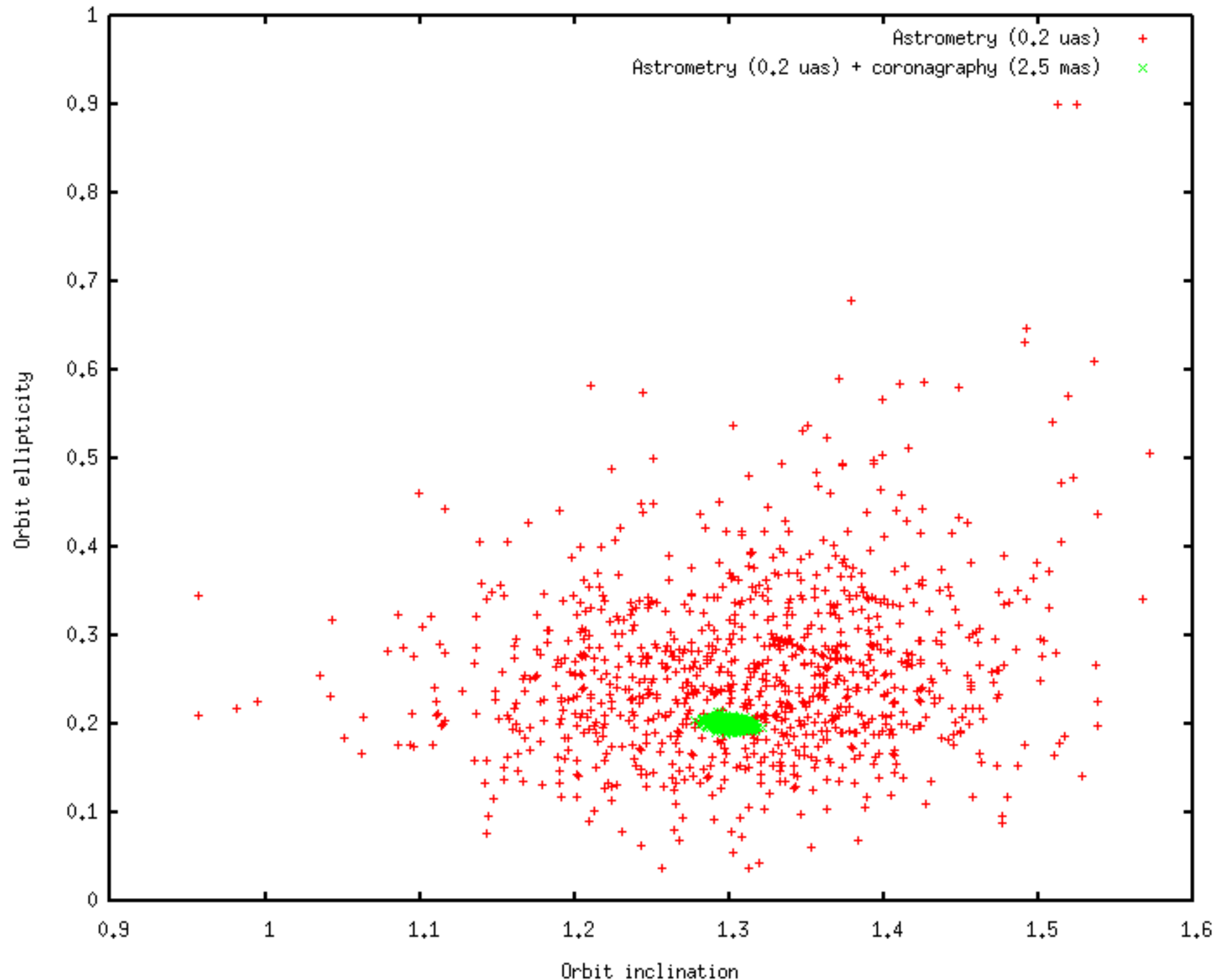
Maximum likelihood solution for 11 parameters

Estimate error on each parameter separately (projection off all solutions on a single axis)
Study covariance between parameters

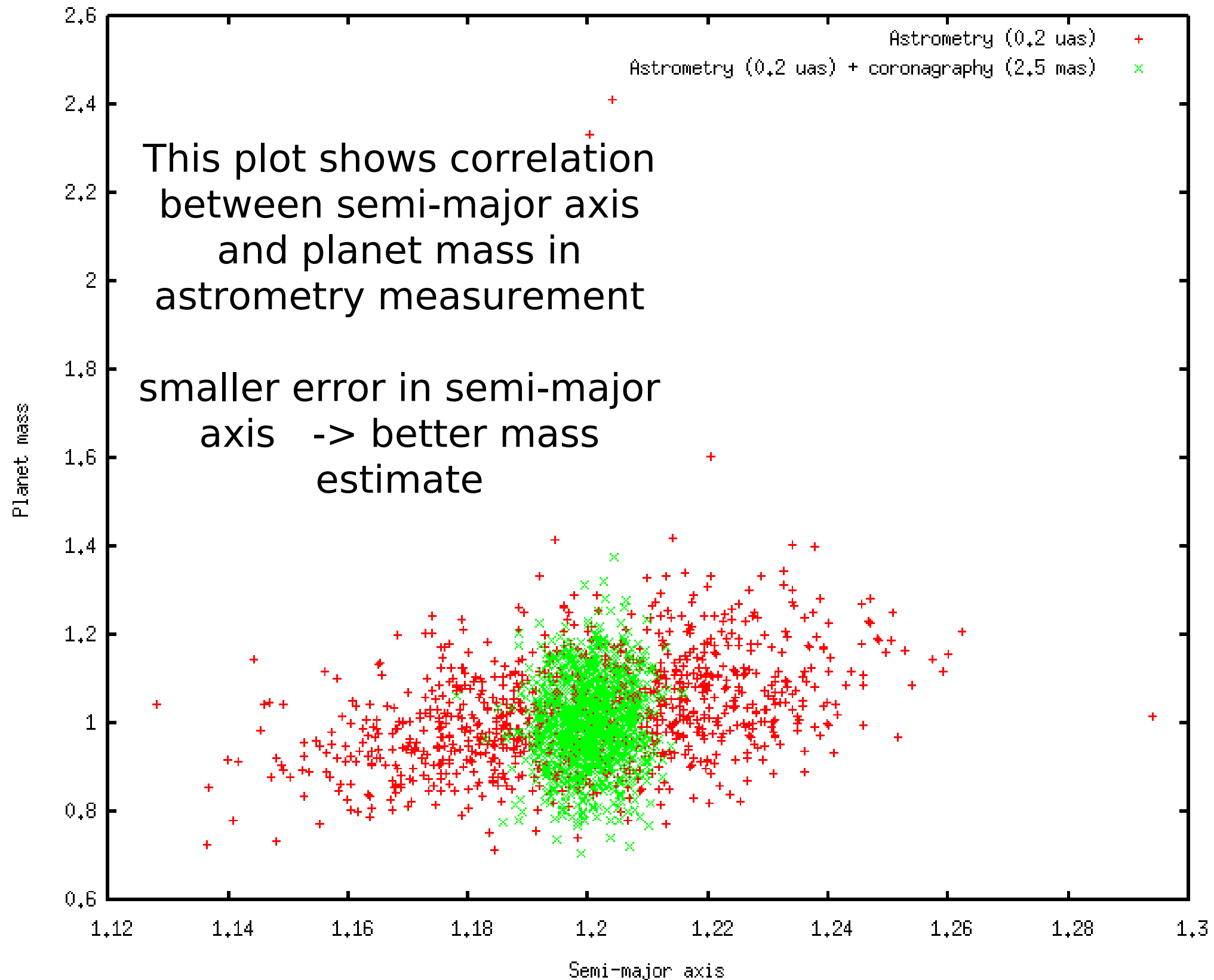
Coronagraphic image measures orbital parameters and stellar mass (with astrometry) -> reduced planet mass error



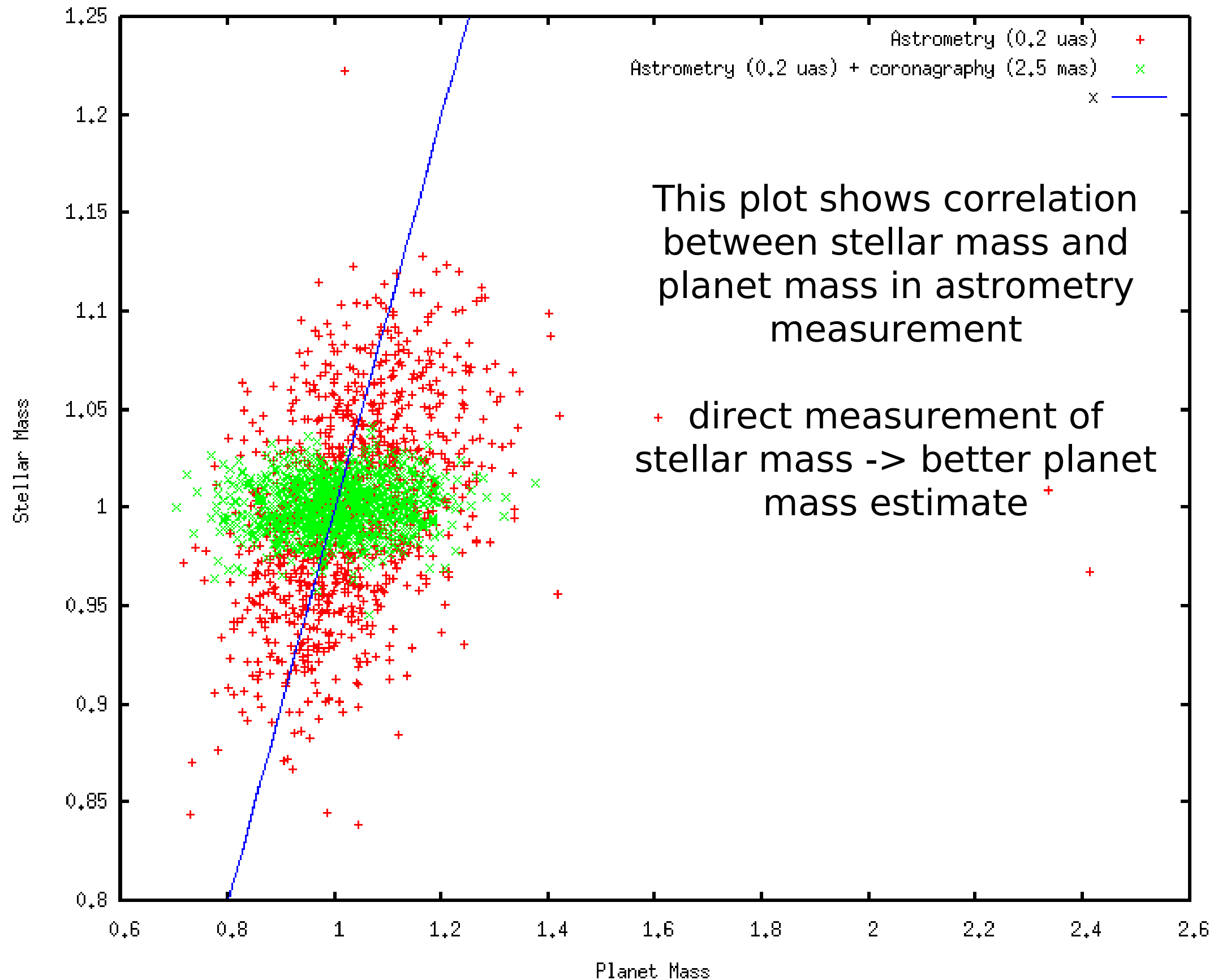
Combined solution for simultaneous coronagraphy + astrometry is very accurate for orbital parameters measurement



Better estimate of orbital parameters -> better planet mass estimate



Better estimate of stellar mass -> better planet mass estimate



Combined solution for simultaneous coronagraphy + astrometry

	Standard deviation	
	Astrometry only	Astrometry + coronagraphy
parallax	0.037 μas	0.035 μas
x proper motion	0.017 $\mu\text{as/yr}$	0.012 $\mu\text{as/yr}$
y proper motion	0.020 $\mu\text{as/yr}$	0.013 $\mu\text{as/yr}$
Planet mass	0.132 ME	0.098 ME
Semi-major axis	0.0228 AU	0.0052 AU
orbital phase	0.653 rad	0.039 rad
orbit inclination	0.0968 rad	0.0065 rad
sma projected PA on sky	0.1110 rad	0.0040 rad
orbit ellipticity	0.098	0.0035
PA of perihelion on orbit plane (w)	0.648 rad	0.0034 rad
stellar mass	0.050 M_{Sun}	0.013 M_{Sun}

~10x better
estimate on
orbital
parameters

Direct stellar
mass
measurement

Benefits of simultaneous coronagraphy + astrometry

Coronagraph images provide an accurate measurement of the orbital parameters (more precise than astrometry), but no mass measurement.

For a 1 M_{Earth} planet on a 200mas radius orbit around a Sun-like star, a 5mas position measurement accuracy in the coronagraphic image ($\sim 1/10 \lambda/D$ in the blue channel of PECO) = $1/40$ orbit radius is equivalent to 0.015 uas astrometric precision.

Note: Position measurement in the coronagraphic image is unlikely to be much better than $\sim 5\text{mas}$ (even with $\gg 100$ photon) due to unknown residual speckle field and exozodi structures.

Solving for planet orbit and mass using the combined astrometry + coronagraphy measurements is scientifically very powerful:

- **Reduces confusion with multiple planets.** Outer massive planets (curve in the astrometric measurement) will be seen by the coronagraph.
- Astrometry will **separate planets from exozodi clumps.**
- Astrometric knowledge allows to **extract fainter planets from the images, especially close to IWA**, where the coronagraph detections are marginal.
- Mitigates the **1yr period problem** for astrometry (see next slide).

Simultaneous coronagraphic imaging + astrometry mitigates the 1-yr period problem

Problem:

Astrometric signal of a planet in a yr period orbit is absorbed in the parallax term. With astrometry only, the mass estimate error grows as the planet period becomes closer to 1yr.

The width of this “blind spot” is reduced with a longer mission life.

Example:

1 Earth mass planet at 1.01 AU from a Sun mass star (period = 1.015 yr) at ecliptic pole. Star distance is 6pc. Assuming circular orbits (for both the Earth and the target planet). Planet orbit phase = Earth orbit phase + 1 radian, orbit is face-on.

32 observations over 5 yr, regularly spaced

Astrometry only (0.3 uas error / per measurement):

Mass estimate (unit = Earth) = 3.25485 ± 4.17483 -> Planet is not detected

Astrometry (0.3 uas error / measurement) + imaging (5 mas / measurement):

Mass estimate (unit = Earth) = 1.01314 ± 0.161752

Detailed error budget analysis and simulations

Error terms

Error terms can be grouped in 4 categories:

1. Astrophysical noise

Includes stellar activity on the central star and astrometric wobble of background reference stars.

2. Fundamental measurement noise

Measurement noise due to the primary design parameters such as telescope diameter, pixel sampling and wavelength. This would be equal to the total instrument noise in the absence of defects in the detector or optical train.

Includes photon noise contribution from background stars and zodi background.

3. Static astrometric error terms

Contribution of all static defects, such as poorly calibrated detector response or manufacturing errors in the optical surfaces.

Even perfectly static defects produce astrometric errors, as the trajectories of the background stars on the focal plane are slightly different between observations (proper motion, parallax).

4. Dynamic astrometric error terms

Errors due to changes of the telescope and instrument between observations.

Includes variations in the shape of optics surfaces, variations in detector geometry (detector pixels move between observations) and variations in detector sensitivity.

Dynamic errors are not fully calibrated by the spikes (spikes have a limited SNR, and do not fully sample the field of view). Dynamic errors can also create errors in the measurement of the spikes positions.

	Noise term	Description	Impact
Astrophysical noise	Sunspots and stellar activity	The central star photocenter moves due to stellar activity and sunspots, creating an astrometric signal	Small to moderate
	Astrometric signal of background reference stars.	Several background stars have astrometric motions due to multiplicity and planets	Small thanks to large number of background stars (averaging). Background stars are also distant and low metallicity (Halo stars)
Fundamental measurement noise	Photon noise on background stars	Photon noise limits the position measurement accuracy on faint stars. The faintest stars are below the zodiacal light level.	Dominant on faint stars
	Photon noise due to zodiacal light		
	Detector finite sampling of a polychromatic PSF	The position measurement error is somewhat larger than the photon-noise limit.	Small for Nyquist sampled image
	Detector readout noise		Small if exposure time is properly chosen
Static astrometric errors	Detector flat field, and sensitivity variations within pixels	These unknown errors produce errors in the position measurement of background stars. Thanks to their roll anticorrelation, they average down quickly with roll.	Small thanks to roll averaging
	Static astrometric distortion due to optics surface figure	Between observations, the trajectory of background stars moves slightly on the focal plane due to proper motion and parallax of the central star. This transforms static distortions into a small time-variable astrometric error.	Moderate to strong Can be mitigated by increasing total light in spikes, which allow (1) smaller spacing between spikes in focal plane, and (2) reduced impact of spike photon noise on the astrometric calibration
	Static astrometric distortion due to unknown detector geometry		
Dynamic astrometric errors	Dynamic astrometric distortion due to change in optics surface figure	Mirror shapes change between observations, and this distortion is not perfectly removed by the astrometric calibration using diffraction spikes	
	Dynamic astrometric distortion due to change in detector geometry	The large focal plane array is likely made of many individual chips which can move and deform. This distortion is not perfectly removed by the astrometric calibration using diffraction spikes.	
	Dynamic astrometric distortion due to change in detector response	Unknown changes in detector response are misidentified as a motion of the spikes, creating a change in the astrometric calibration	Significant if > 1%
	Dynamic astrometric distortion due to spots moving on mirror	Spots move on the PM between observations, creating a differential motion between spikes and background stars	Small ?

Approach

Baseline: 1.4-m telescope (PECO), with 0.25 sq deg FOV (0.5 x 0.5 deg)

The FOV is chosen to reach performance goals in a sufficiently stable system. Photon noise limited performance for this FOV is 0.044 μ as single measurement at galactic pole, but actual performance is significantly lower (larger error) due to distortions and detector limits.

When detailed simulations are required, a smaller FOV system is used (0.1 deg radius = 0.03 sq deg FOV) to ease computations (16k x 16k images).

	Value in simulations	Value for mission	Rationale for flight instrument value	Impact on astrometric accuracy
Telescope diameter (D)		1.4 m	PECO sized, cost constrained	Astrometric accuracy goes as D^{-2} , thanks to larger collecting area and smaller PSF size (assuming constant FOV)
Detector pixel size		44 mas	Nyquist at 600 nm	Little impact as long as sampling is close to or finer than Nyquist
Field of view (FOV)	0.03 sq deg (0.1 deg radius)	0.25 sq deg (0.5 deg X 0.5 deg)	low WF error across field, 1.6 Gpix detector	Astrometric accuracy goes as $FOV^{-0.5}$
Single measurement time		48 hr	Typical single observation duration for coronagraph	Astrometric accuracy goes as $t^{-0.5}$
Dot coverage on PM (area)	1%	8%	Keeps throughput loss moderate in coronagraph	Larger dot coverage allows observation of fainter sources.
Flat field error after calibration, static (high spatial frequency)		1.02% RMS, 6% peak	Conservative estimate for modern detector after calibration	Negligible effect on background PSF measurement (well averaged with roll)
Flat field error, dynamic		1e-4 RMS per pixel, uncorrelated spatially and temporally between observations	1e-4 loss in sensitivity for each pixel over 48 hrs = 2% per year = 10% over 5 yrs	Negligible effect on background PSF measurement, but significant effect on measurement of spikes locations
Telescope roll		1.0 rad (+/- 0.5 rad)	Manageable sunshielding	Larger telescope roll leads to better averaging of detector errors
Uncalibrated change in optics surface between observations for M2 & M3		40 pm	Wavefront measurement repeatability (optical element removed / reinserted) obtained when testing similar sized optics on ground	Larger change in optics surface reduces astrometric accuracy
Static optics surface error (M3 mirror)		1.5 nm	WF error and PSD taken from similar existing optical element	Small impact on performance, as background PSFs are almost fixed between observations
<i>Astrometric accuracy, single measurement, single axis, $m_v=3.7$, galactic pole</i>	<i>0.58 μas</i>	<i>0.20 μas</i>	<i>0.2 μas is required to achieve science goals</i>	

Simulation description

Simulation details available on:

<http://www.naoj.org/staff/guyon/04research.web/30astrometry.web/conter>

(60 slides describing next chart)

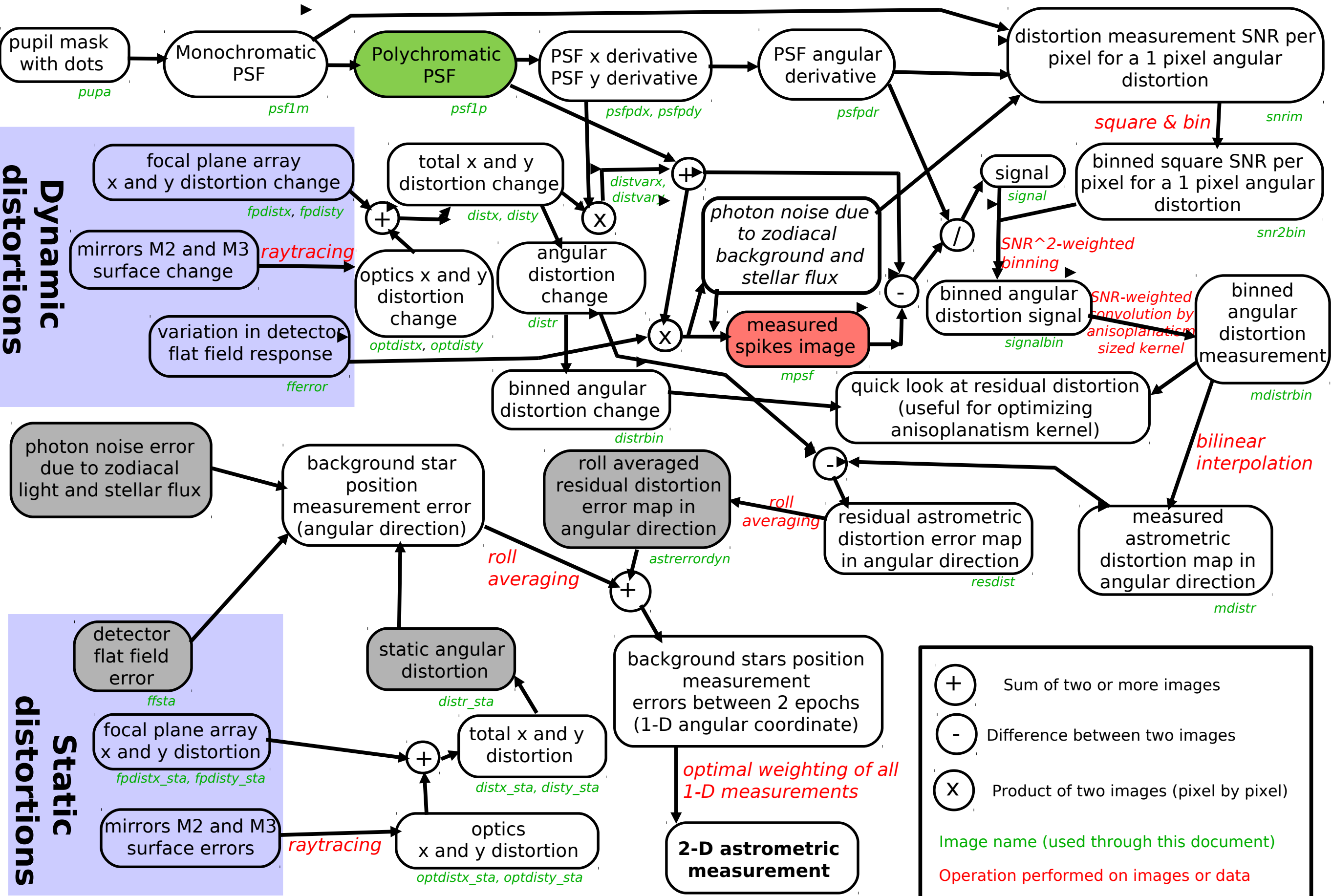
Simulation assumes:

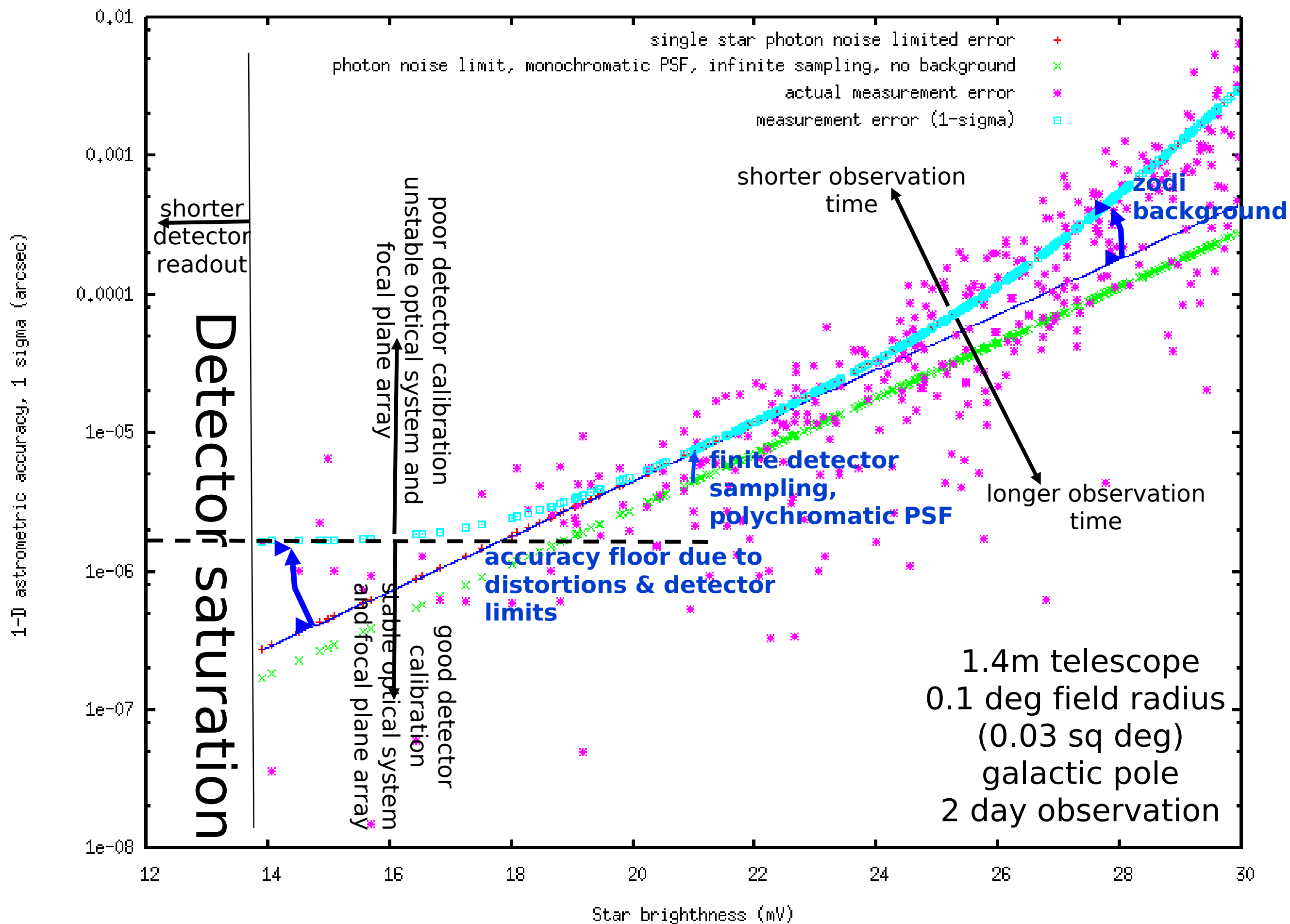
- 1.4m telescope TMA (Woodruff design)
- 1.5nm surface (3nm WF) optics for M2 and M3, PSD provided by Tinsley
- Circular field of view, 0.2 deg diam (0.03 sq deg)
- Galactic pole observation (worst case scenario)
- central star is $m_v=3.7$ (faintest of the 7 PECO targets for which an Earth can be imaged in <6hr, 14th brightest target in the 20 high priority targets list)
- 90% detector peak QE, 80% optical throughput (0.96^3 for optics reflectivity x 0.92 due to dots on PM)
- Nyquist sampled detector at 0.6 micron = 44 mas pixels
- Telescope roll = 1 rad (larger angle = better averaging, but more difficult to maintain stability)
- Single epoch observation = 2 day

Distortions in the system are computed with 3D raytracing (code written in C, agreement with Code V results from Woodruff has been checked)

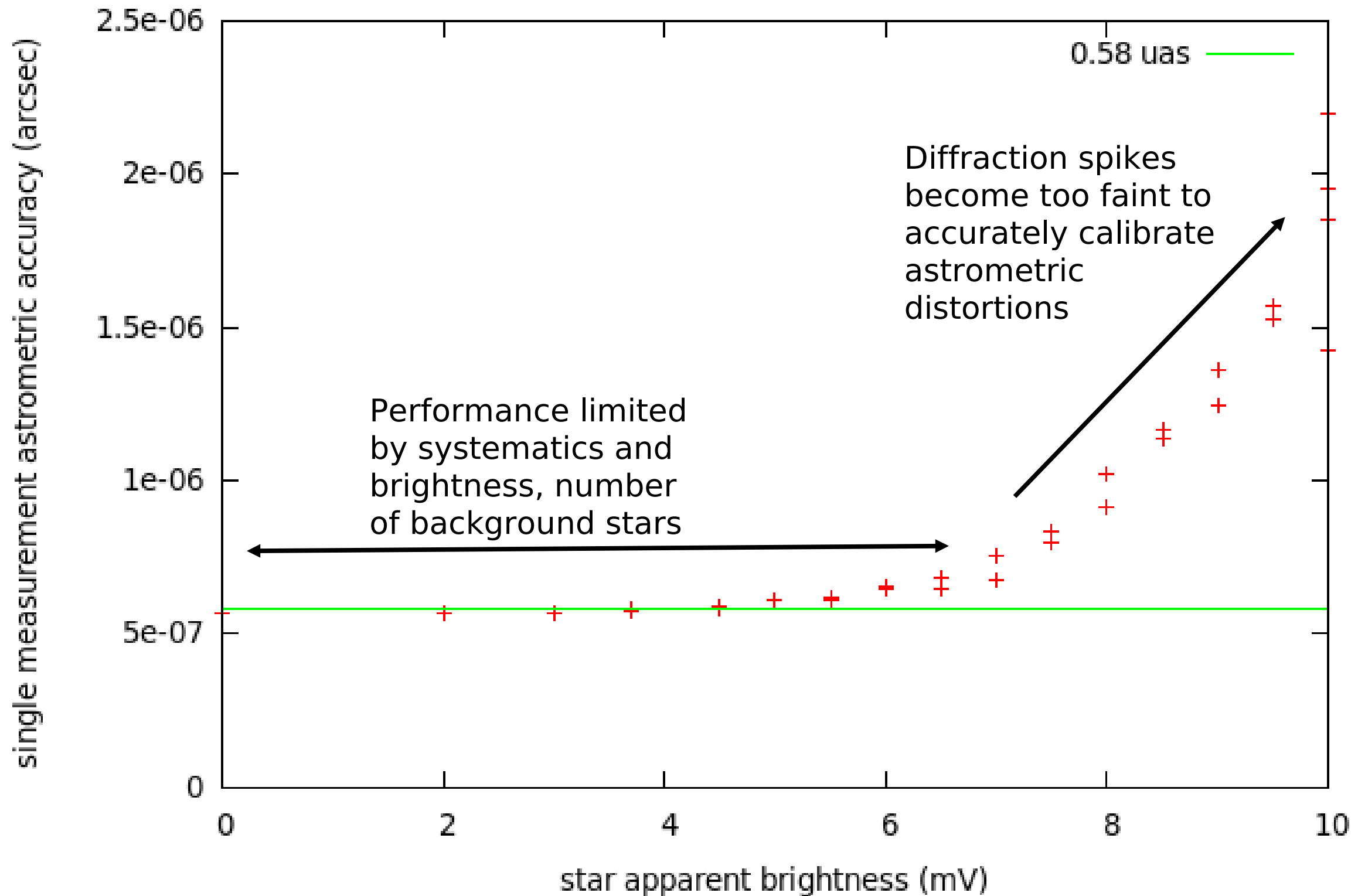
Images produced by Fourier transform, and then distorted according to geometrical optics. Image sizes are 16k x 16k.

Numerical simulation approach





Performance as a function of star brightness



8 % area coverage on PM
 $m_v = 3.7$ target
 Galactic pole observation
 2 day per observation

Larger telescope diameter :
 - more light in spikes (D^2), finer spikes ($1/D$) → spike calibration accuracy goes as D^{-2}
 - more light in background stars (D^2), and smaller PSF ($1/D$) → position measurement goes as D^{-2}

Astrometric accuracy goes as $D^{-2} \text{FOV}^{-0.5}$
 Number of pixels goes as $D^{-2} \text{FOV}$
 At fixed number of pixels, larger D is better

But: mean surface brightness of spikes gets fainter as FOV increases

	FOV = 0.03 sq deg	FOV = 0.1 sq deg	FOV = 0.25 sq deg	FOV = 0.5 sq deg	FOV = 1.0 sq deg
D = 1.4 m	0.58 μ as	0.31 μ as	0.20 μ as	0.14 μ as	0.11 μ as
D = 2.0 m	0.28 μ as	0.15 μ as	0.10 μ as	0.07 μ as	0.05 μ as
D = 3.0 m	0.13 μ as	0.067 μ as	0.044 μ as	0.030 μ as	0.024 μ as
D = 4.0 m	0.071 μ as	0.038 μ as	0.025 μ as	0.017 μ as	0.013 μ as

Technological challenges and future work

1.4-m off-axis TMA, diffraction limited in visible

1.5 Gpix focal plane array (1.5 x GAIA) → CMOS for compactness ?

Dots on PM → lithography on large curved surface

Pointing to 10 mas → easier than required for coronagraph

Optics stability → more relaxed than for coronagraph, but over longer periods of time

Future work:

Lots of modeling required to refine error budget, explore calibration strategies

Need for more realistic model of radiation damage on detector, and evolution of astrometric distortions as a function of time during the 5yr mission

Data reduction algorithm, pre-launch and on-orbit calibrations

Lab demonstration, including test with coronagraph

A stable platform for several instruments

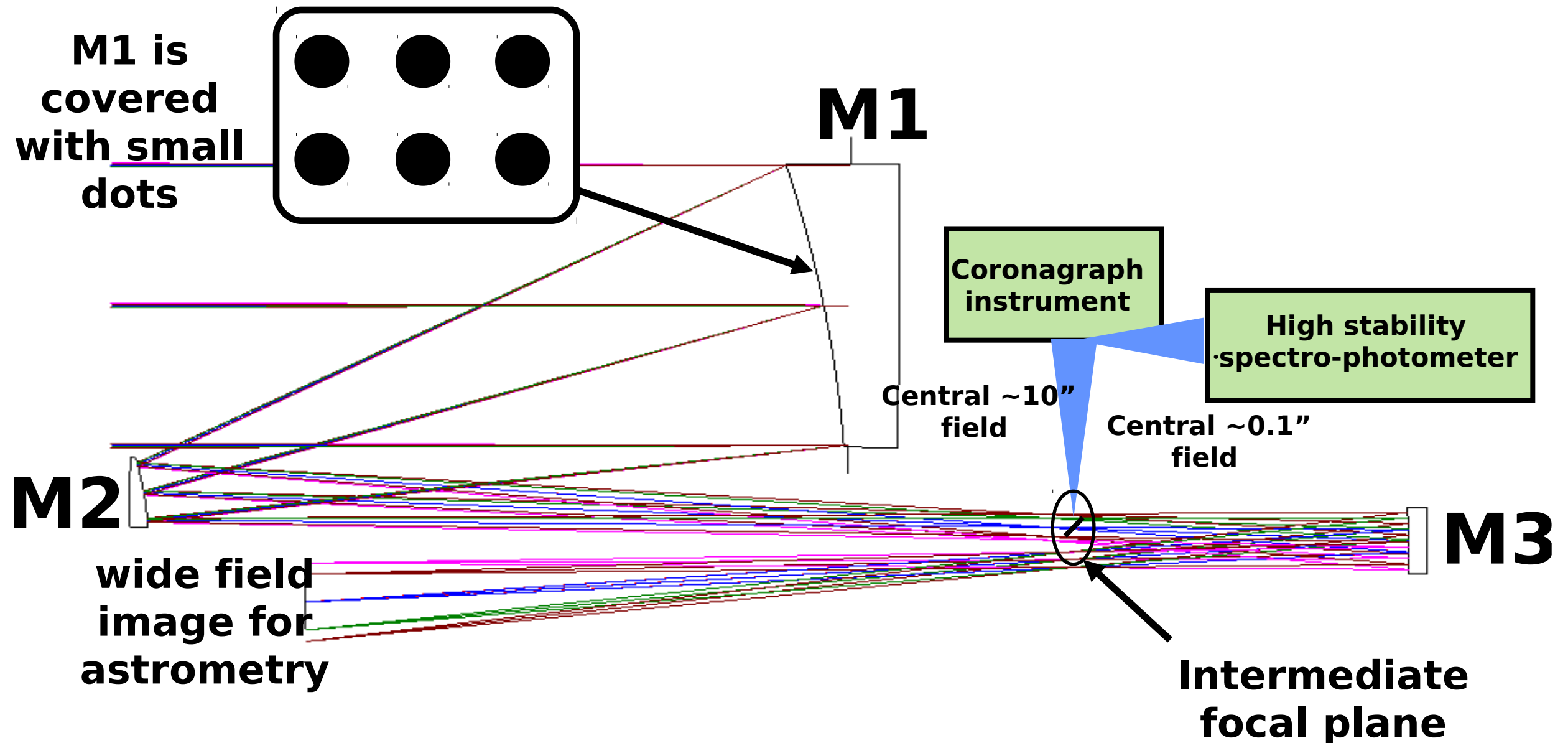
Highly stable and quiet telescope, well suited for:

coronagraphy

astrometry + stellar spectra + imaging of outer disk + (transit by outer disk ?)

+ **general astrophysics** (large FOV, highly stable diffraction-limited PSF)

transit spectroscopy (coronagraph does not use central light or near-IR light)



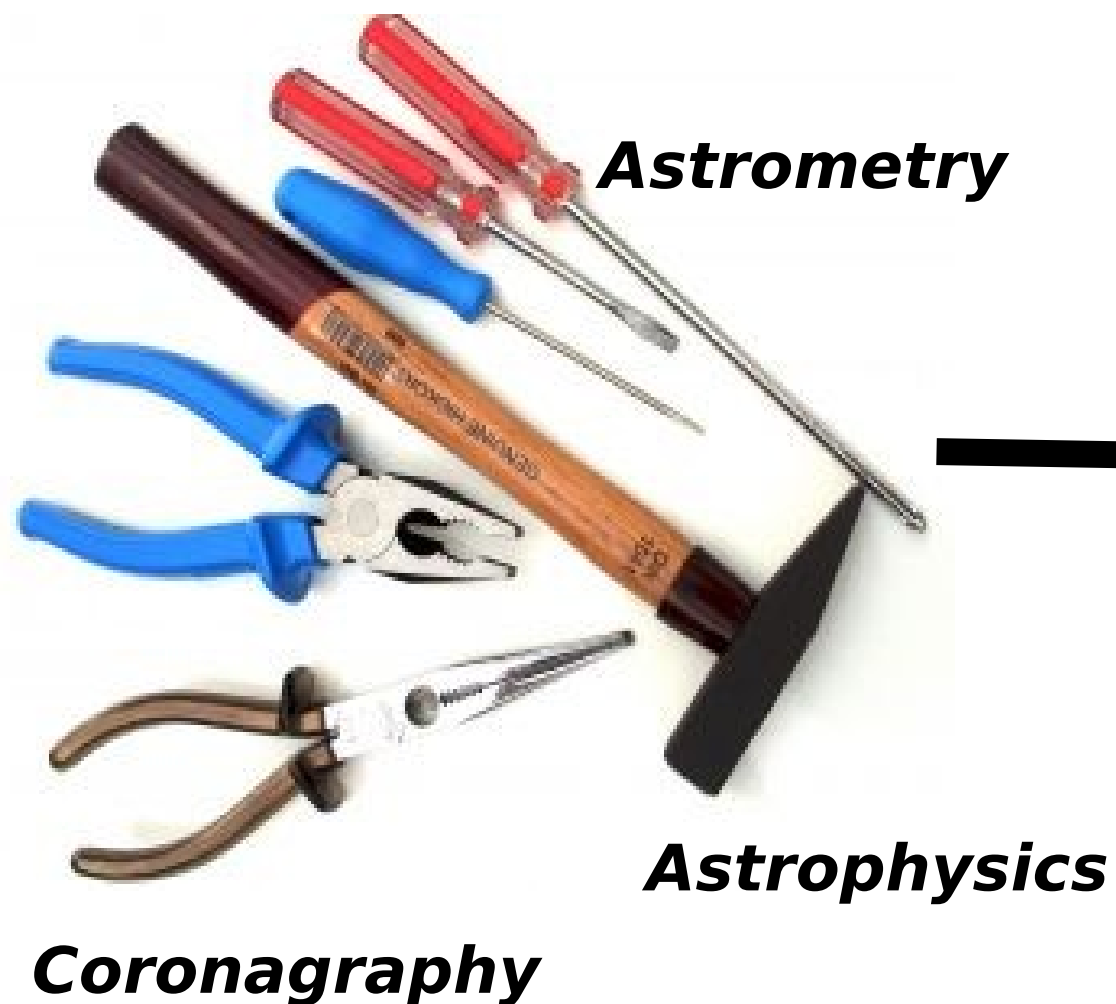
Conclusions

For more info:

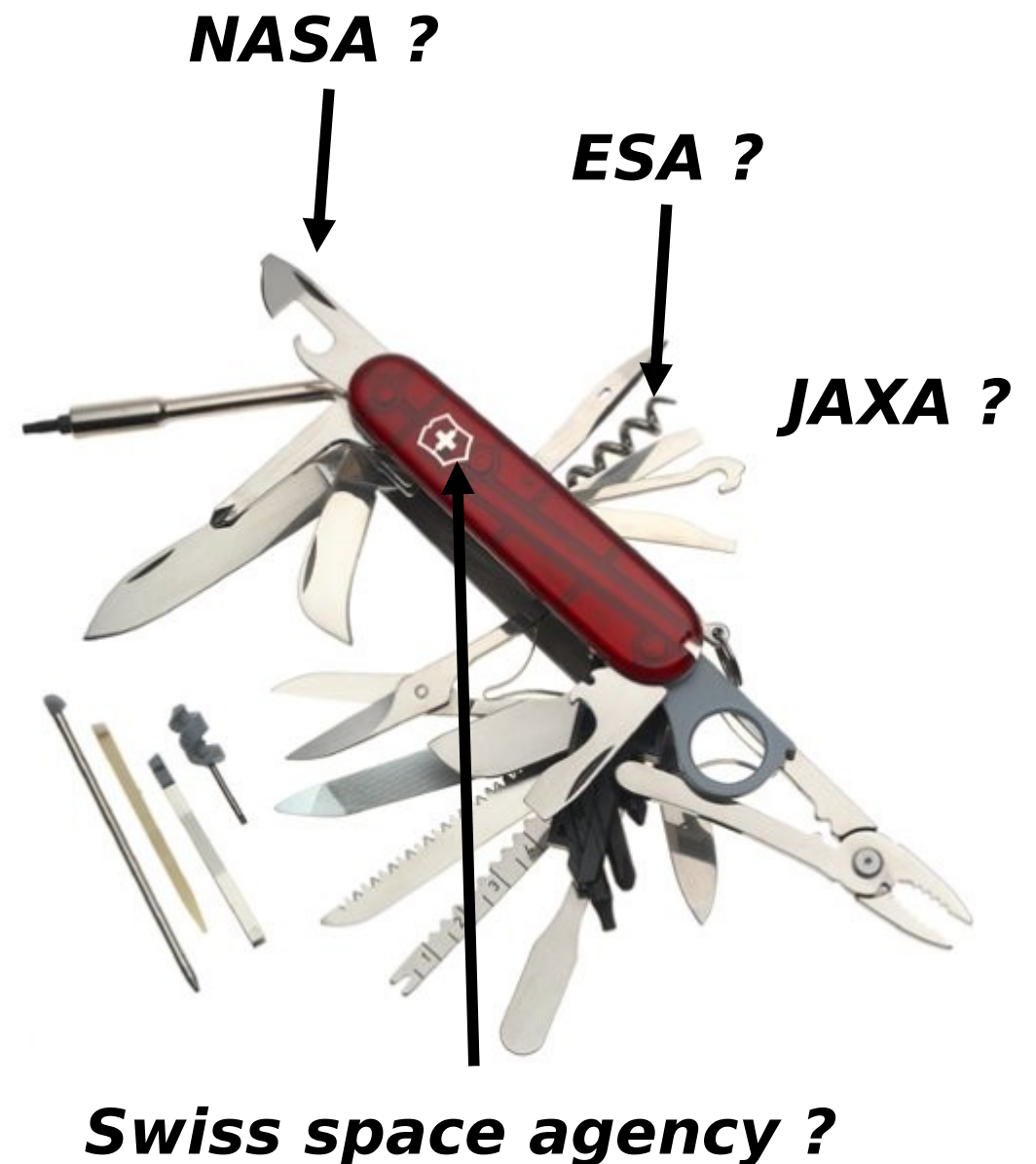
<http://www.naoj.org/staff/guyon/04research.web/30astrometry.web/content.html>

Join our team ! We need and welcome help

Transit (& non-transit) spectroscopy



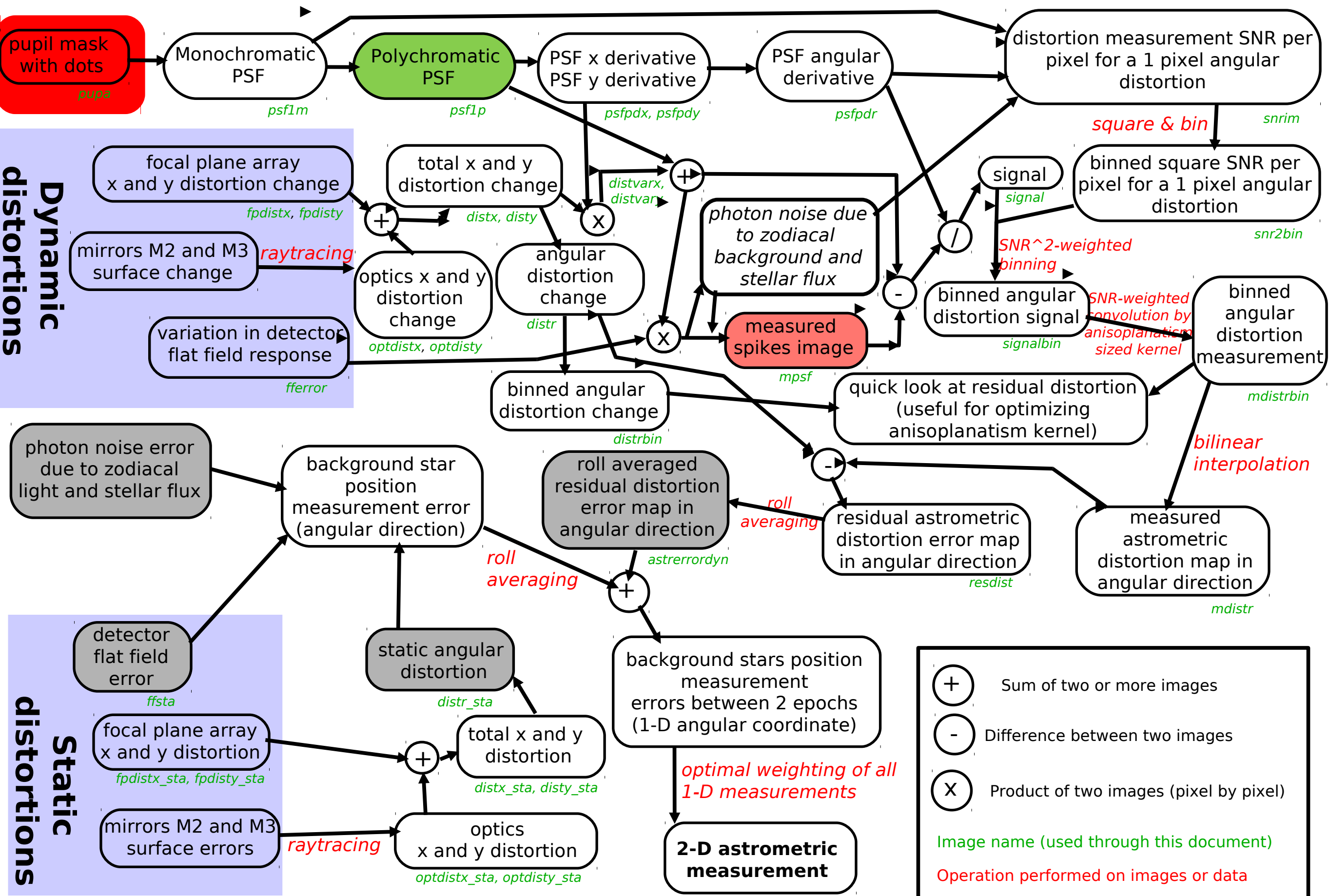
?



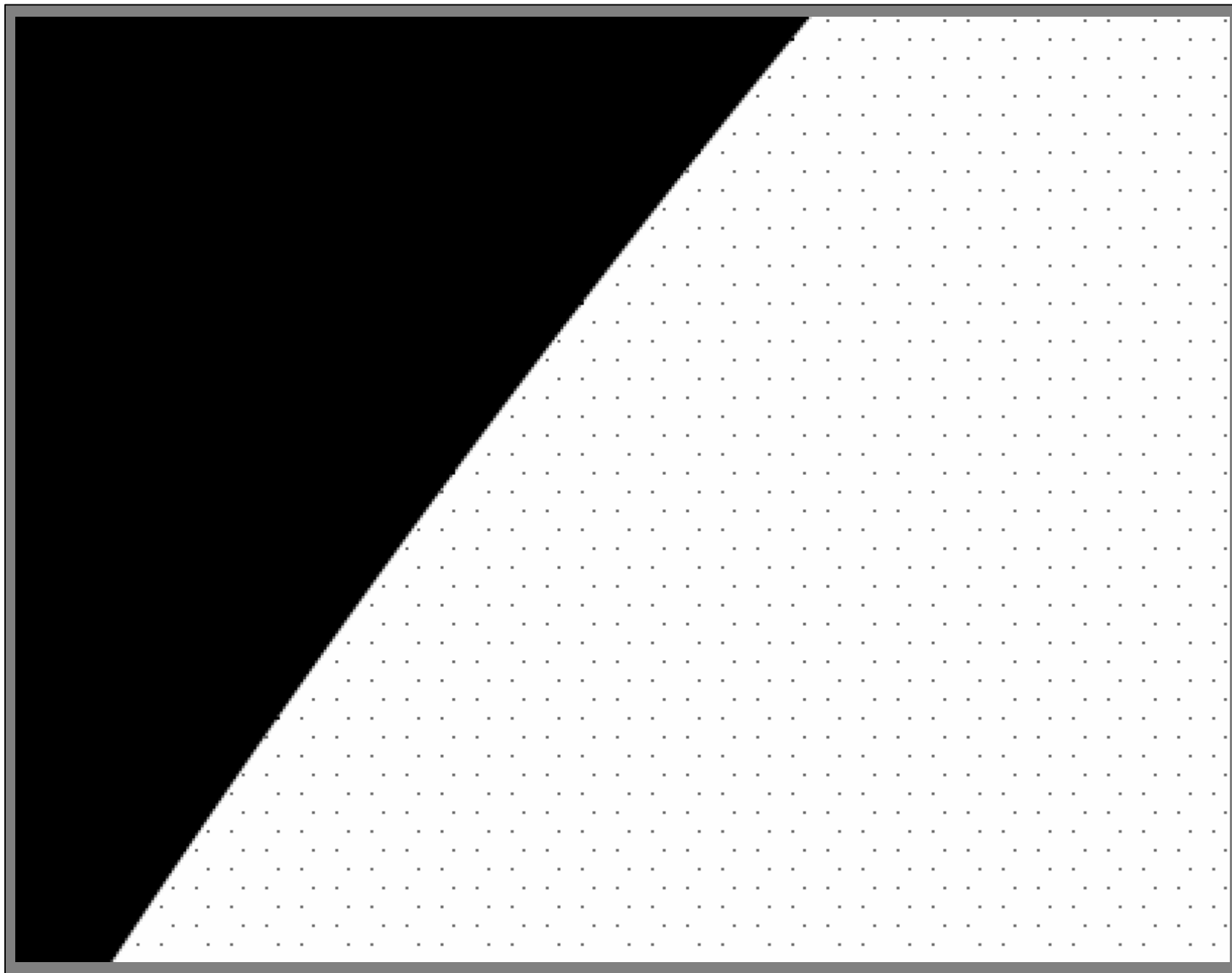
Backup slides

- simulation details**
- lab experiment**

Numerical simulation approach



PM mask



Hexagonal pattern dots. Dots cover 1% of PM surface. Dots are assumed to be perfectly placed, all with same size.

$\frac{1}{2}$ diameter of hexagon = 2.8 mm = distance between closest dots.

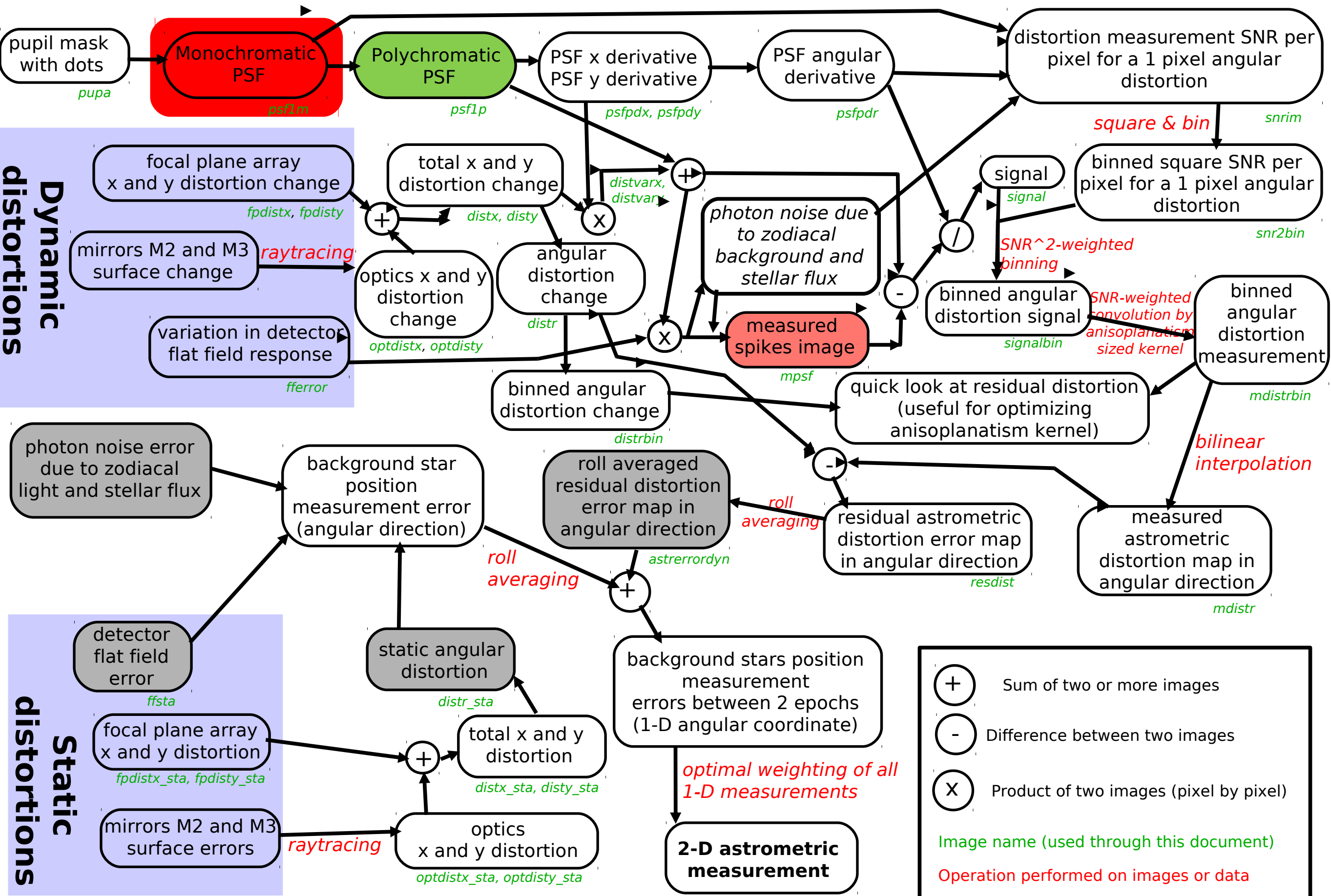
Dot diameter = 180 μm

[note: for mission, dot diameter = 72 μm ; spacing = 0.5 mm]

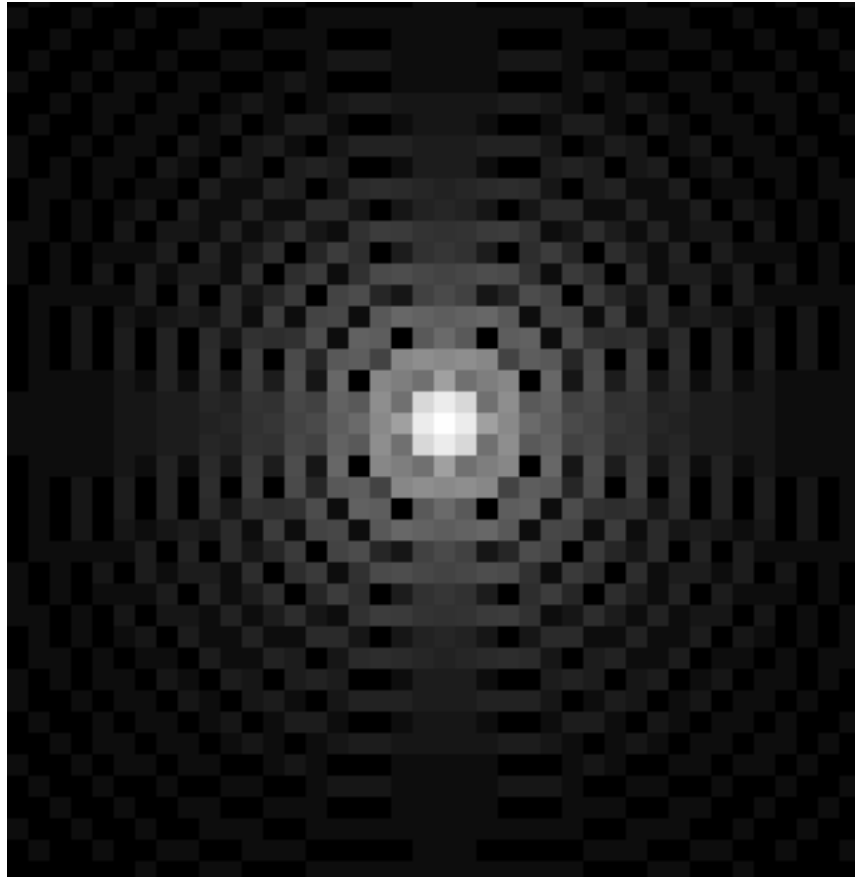
Dots are assumed to be totally black.

Dots do not affect coronagraph if they are regularly spaced (no low spatial frequency)

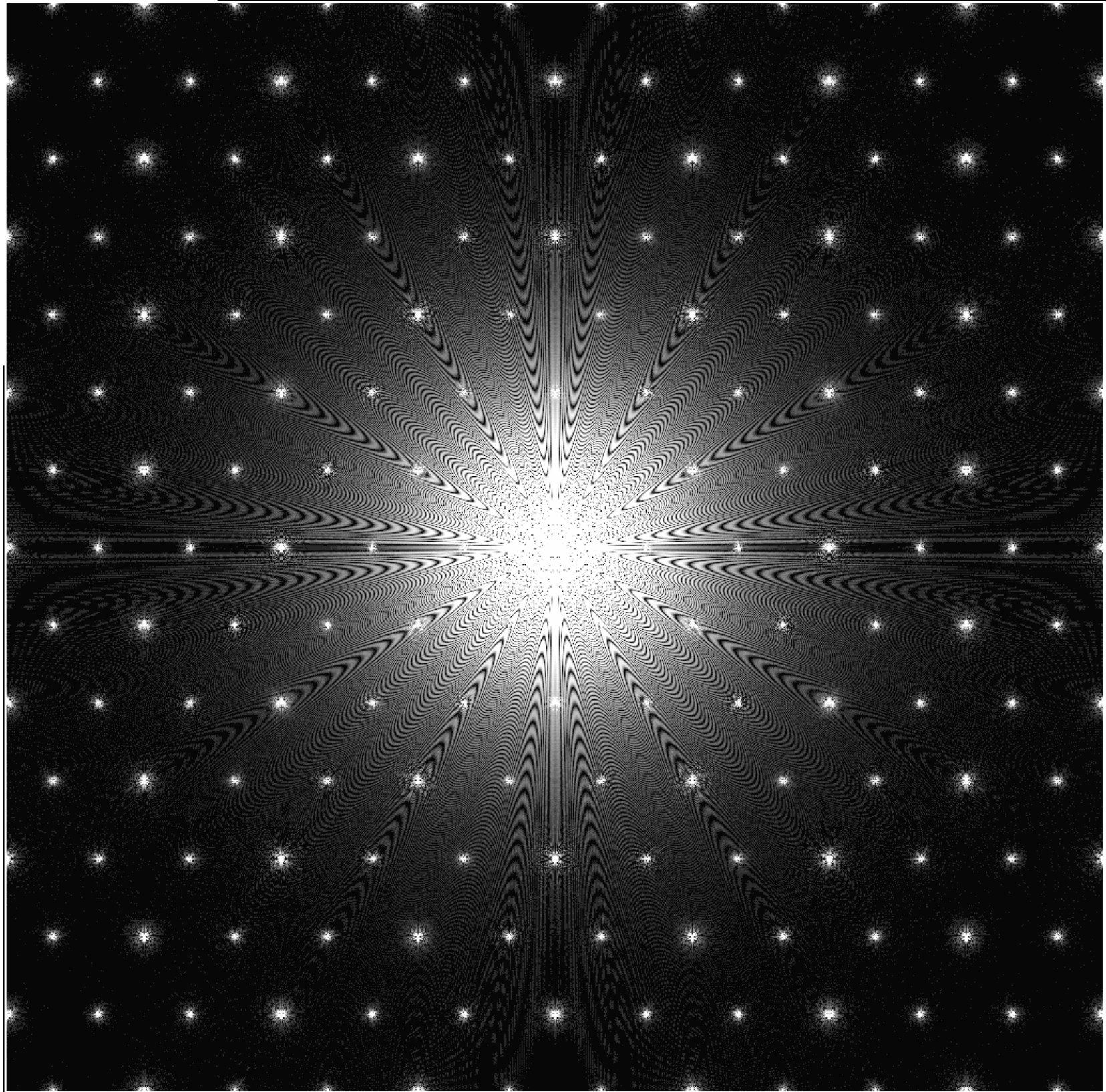
Numerical simulation approach



Monochromatic PSF

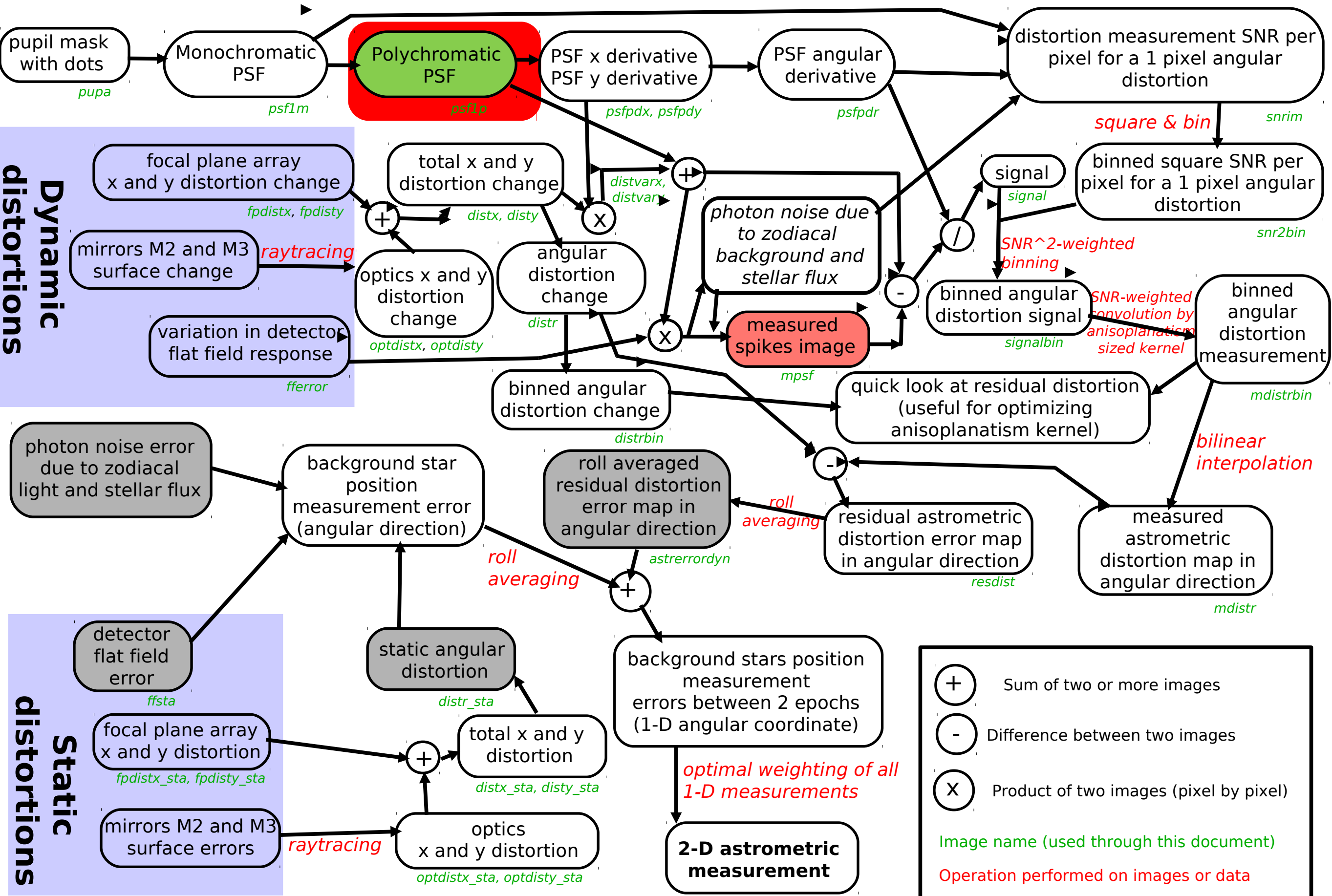


Central part of PSF is not
disturbed by dots



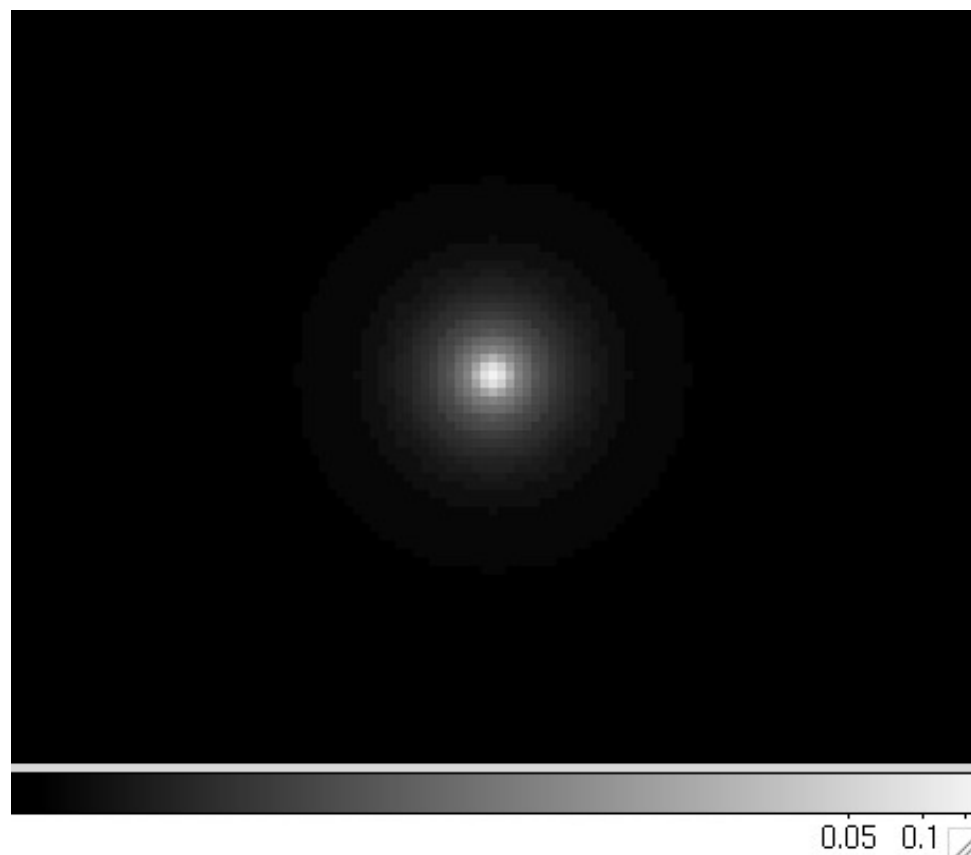
Full field PSF (0.2 deg on a side)
shows 2D grid of diffraction orders

Numerical simulation approach

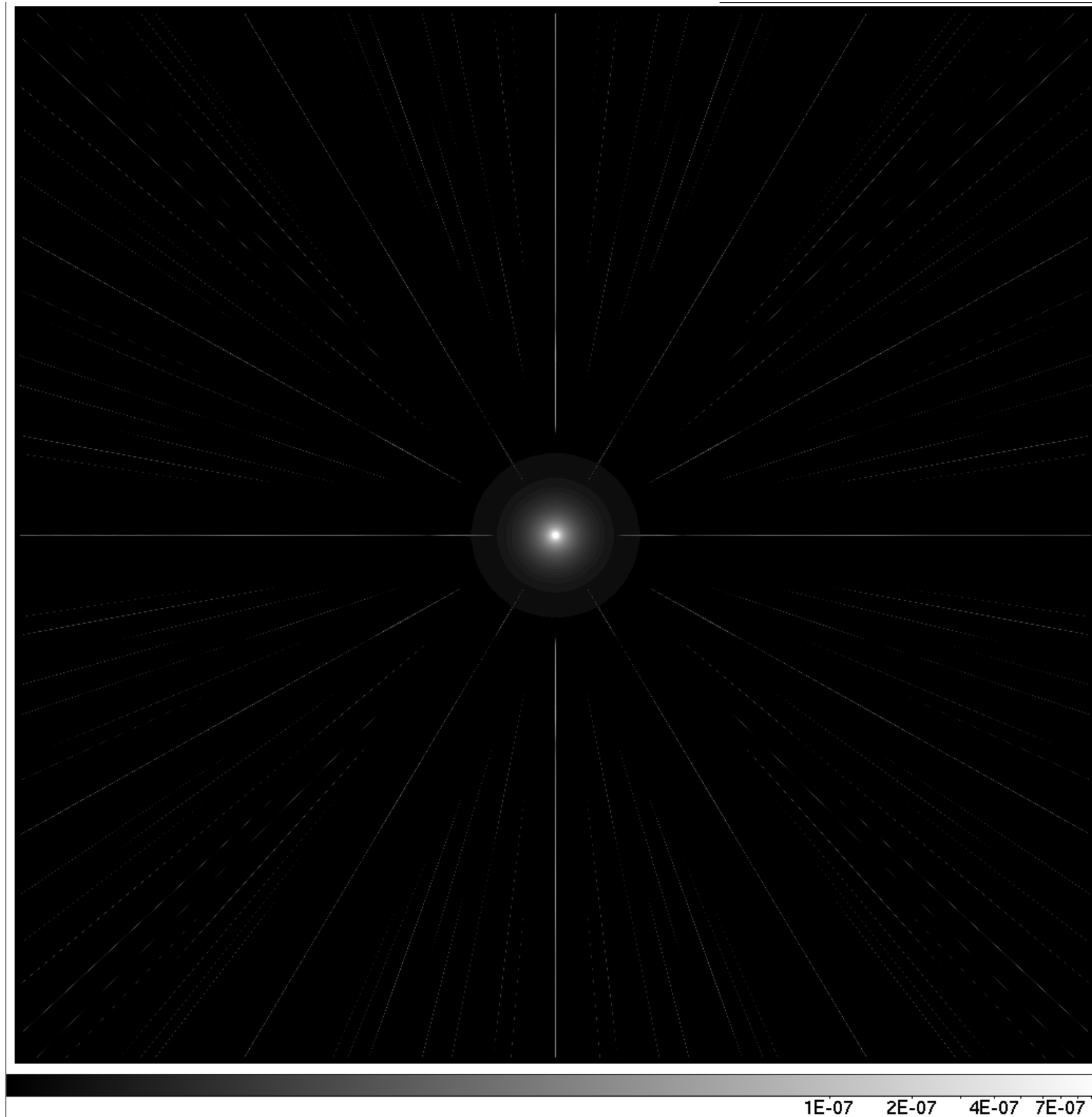


Polychromatic PSF

Computed as incoherent
sum of 5000
monochromatic PSFs: 50
individual FFTs x 100
radial stretch steps



Central part of PSF



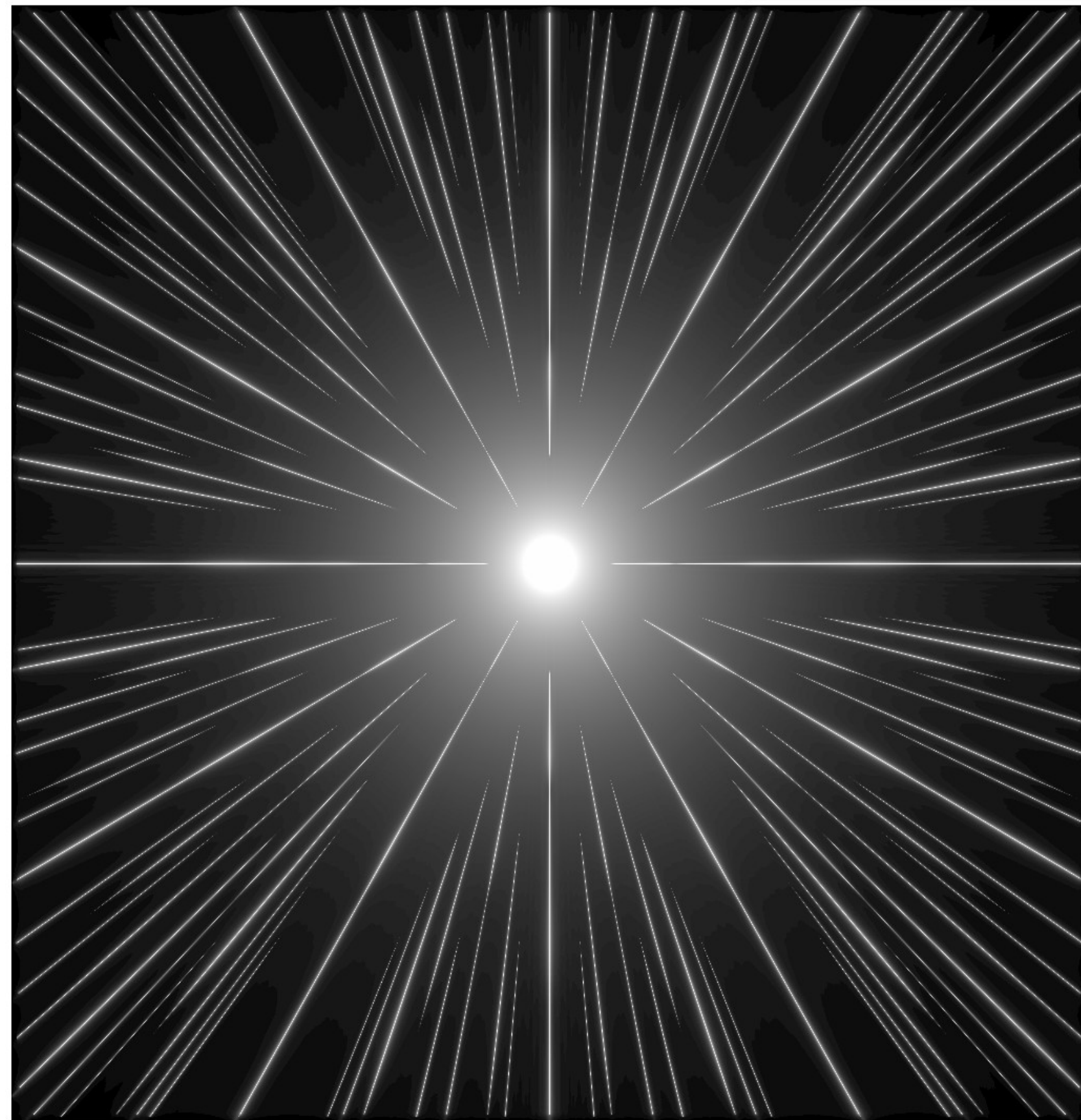
**Full field PSF (0.2 deg on a side)
shows thin narrow spikes**

Polychromatic PSF

Brightest part of spikes is $\sim 10^{-7}$ of central PSF peak
Over most of the field, surface brightness is dominated by zodiacal light, not by spikes.

Scattering by PM surface roughness is much fainter than the spikes, as spikes diffract $\sim 1\%$ of starlight.

Central pixel has 17% of total flux



1E-10 2E-10 4E-10 7E-10

0.2 deg field PSF, log scale

Static distortions

Definition: *Any error static through the mission lifetime.*

Why do purely static errors matter ?

Background PSFs follow different trajectories during the telescope roll for different observation epochs. The trajectories are close (\sim arcsecond level), so what matters is the differential astrometric distortion over a $\sim 1''$ distance.

Main errors:

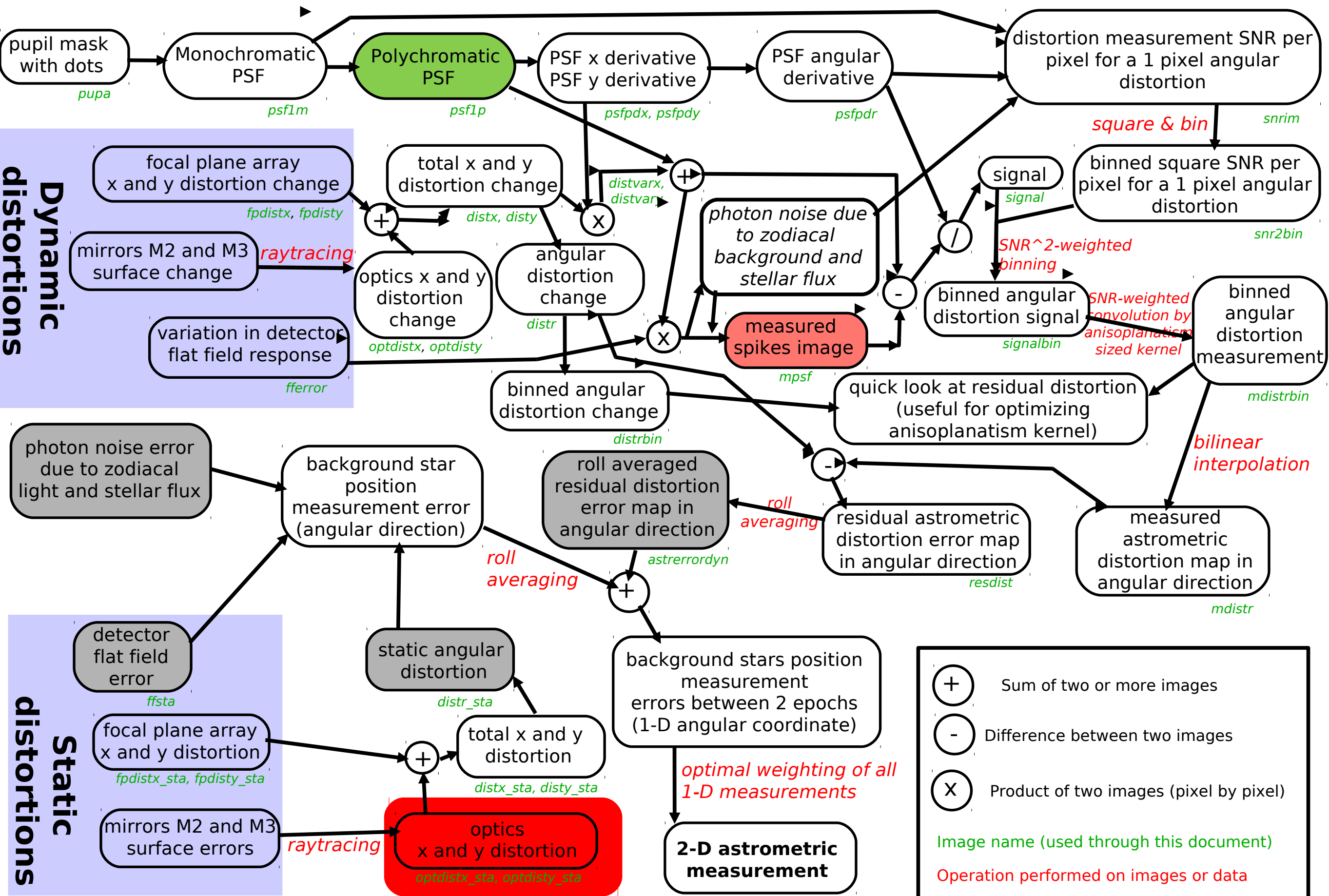
- Distortions due to optical figure of mirrors M2 and M3
- Focal plane array geometry: position of individual detector chip & variations in pixel size across the detector
- Non-calibrated flat field errors

Impact and mitigation:

Static errors are not calibrated by the diffraction spikes:

- lack of absolute reference for spikes makes it impossible to calibrate static errors (where should the spikes be in a perfect system ?)
- spikes can only calibrate low order distortions, but relevant static errors are small scale errors

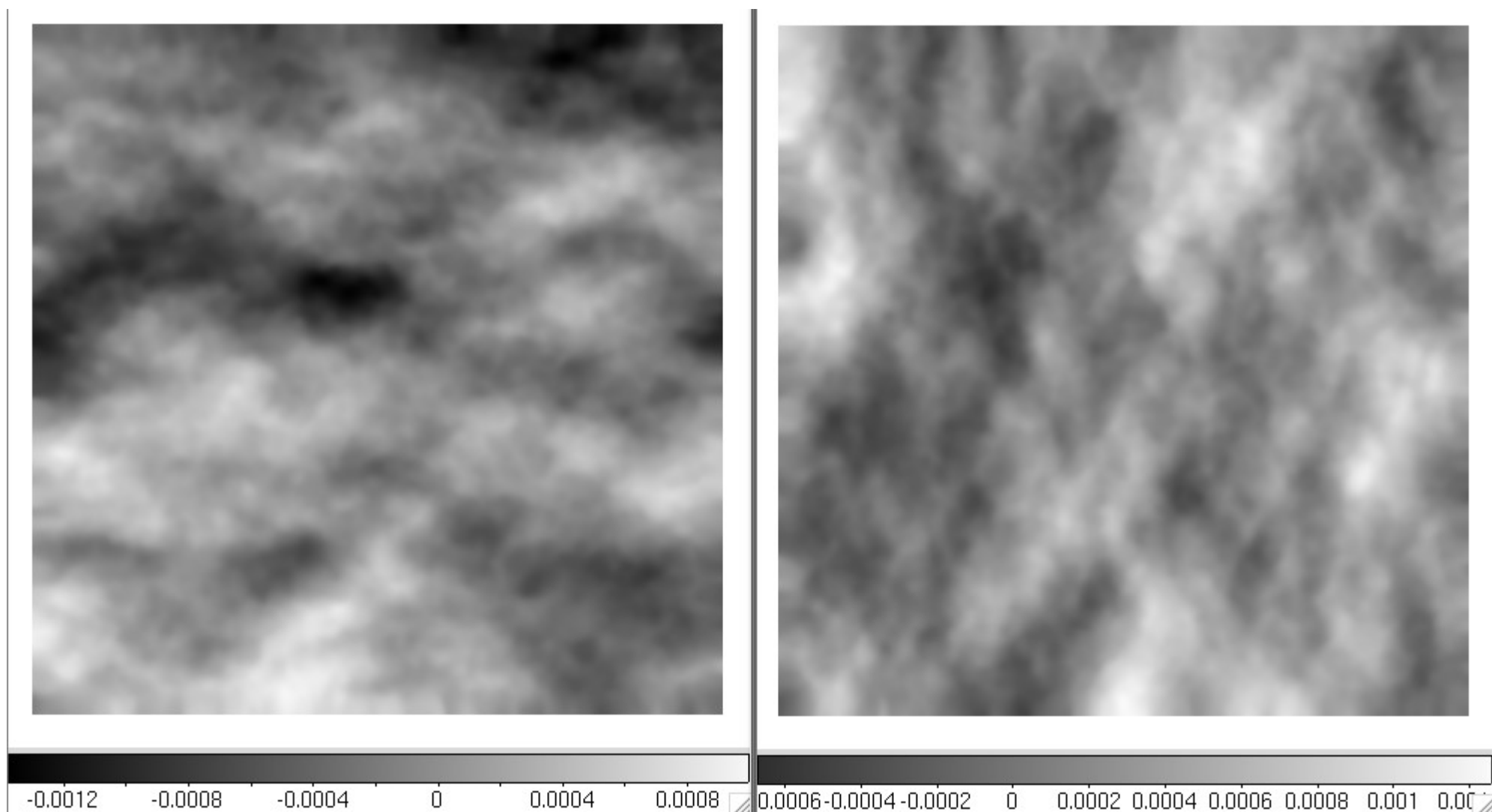
Numerical simulation approach



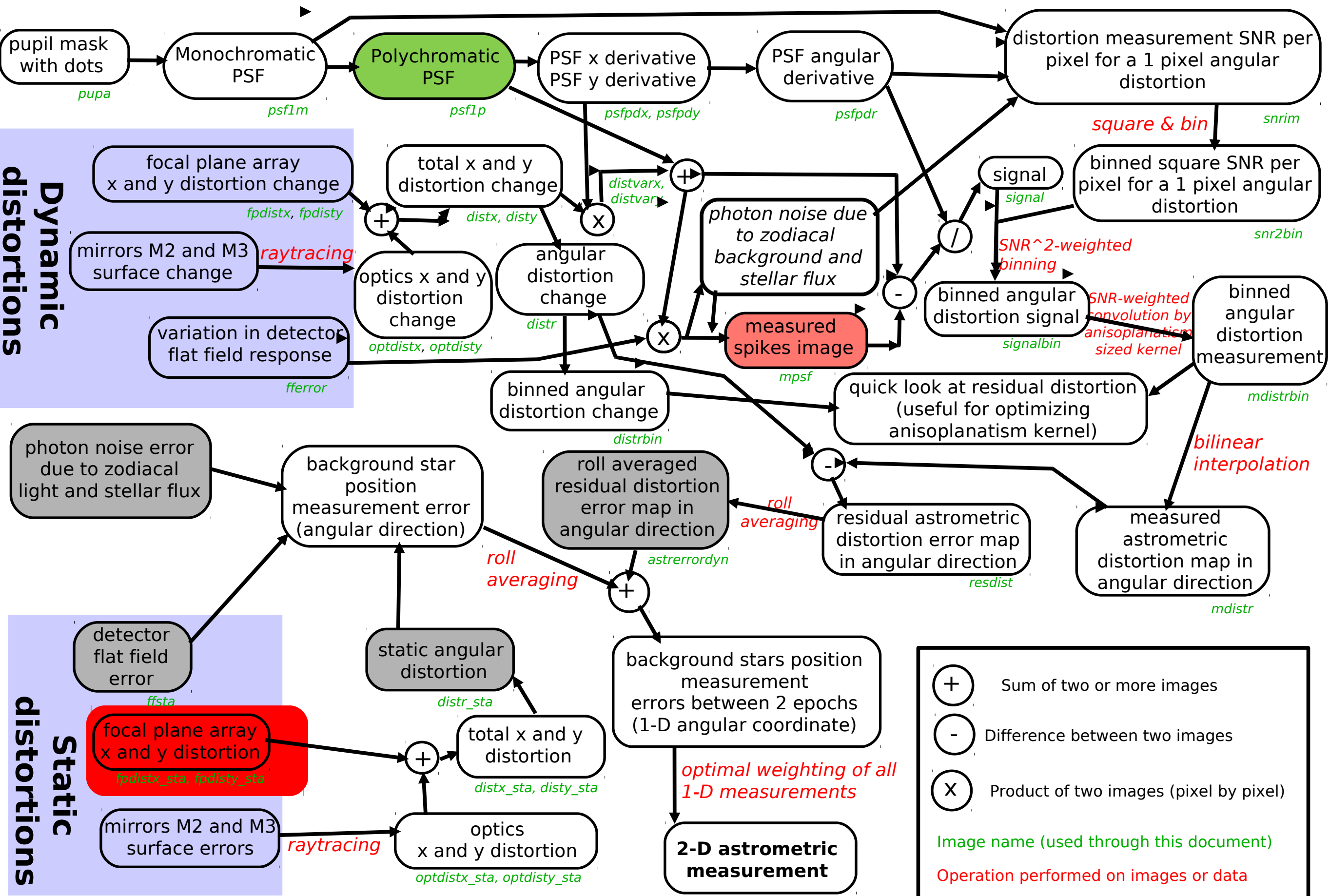
Static distortion map due to M2 & M3 optical surfaces

Distortion maps shown below is for 0.46×0.46 deg field. Unit is arcsec; left map is x, right map is y. Distortion is computed at 120000 positions on the sky, then interpolation is used to compute the full map.

Distortion amplitude is ~ 1 mas, dominated by low order modes. The differential distortion over $\sim 1''$ is much smaller.



Numerical simulation approach

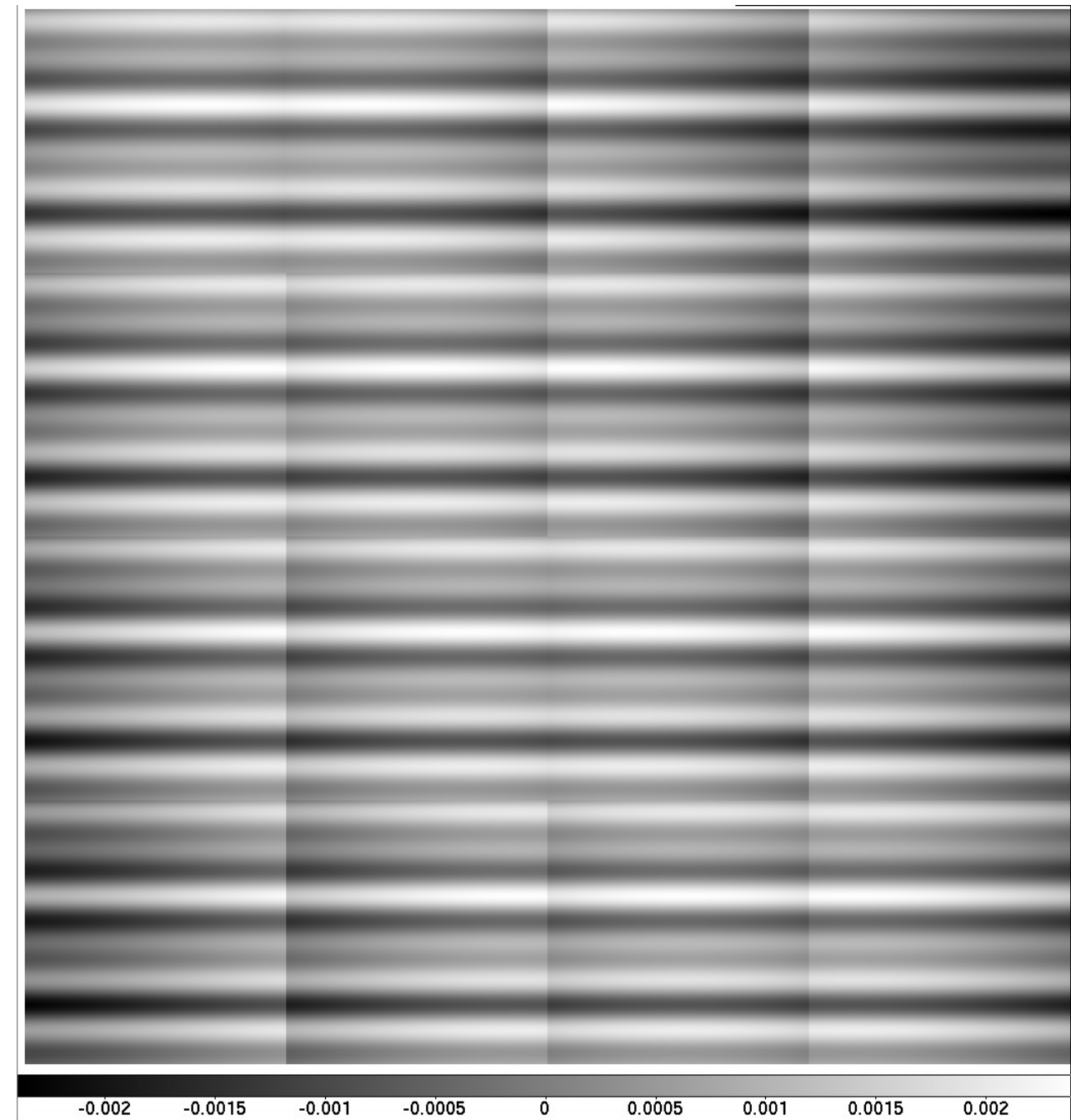
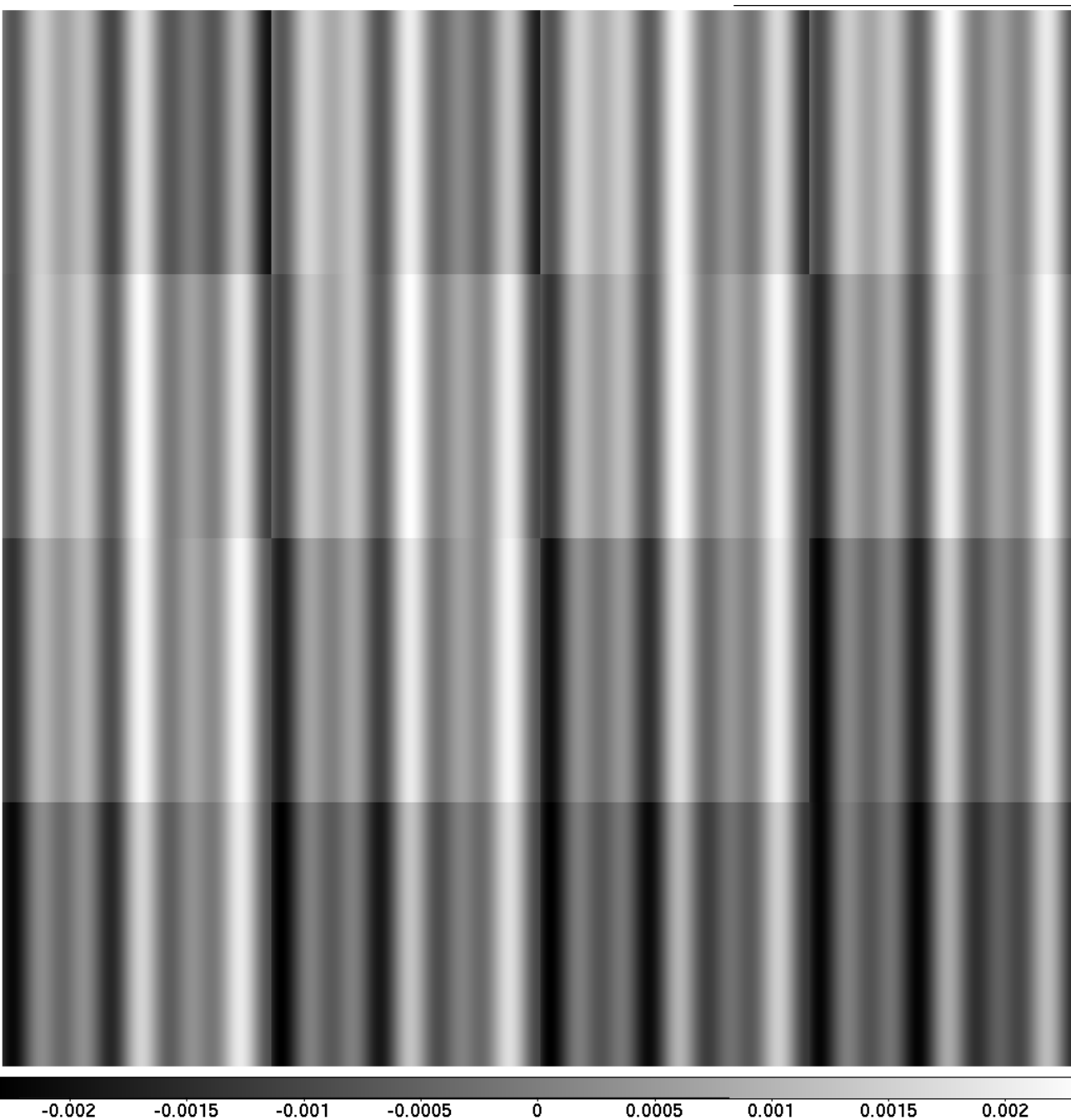


Static distortion map due to focal plane array

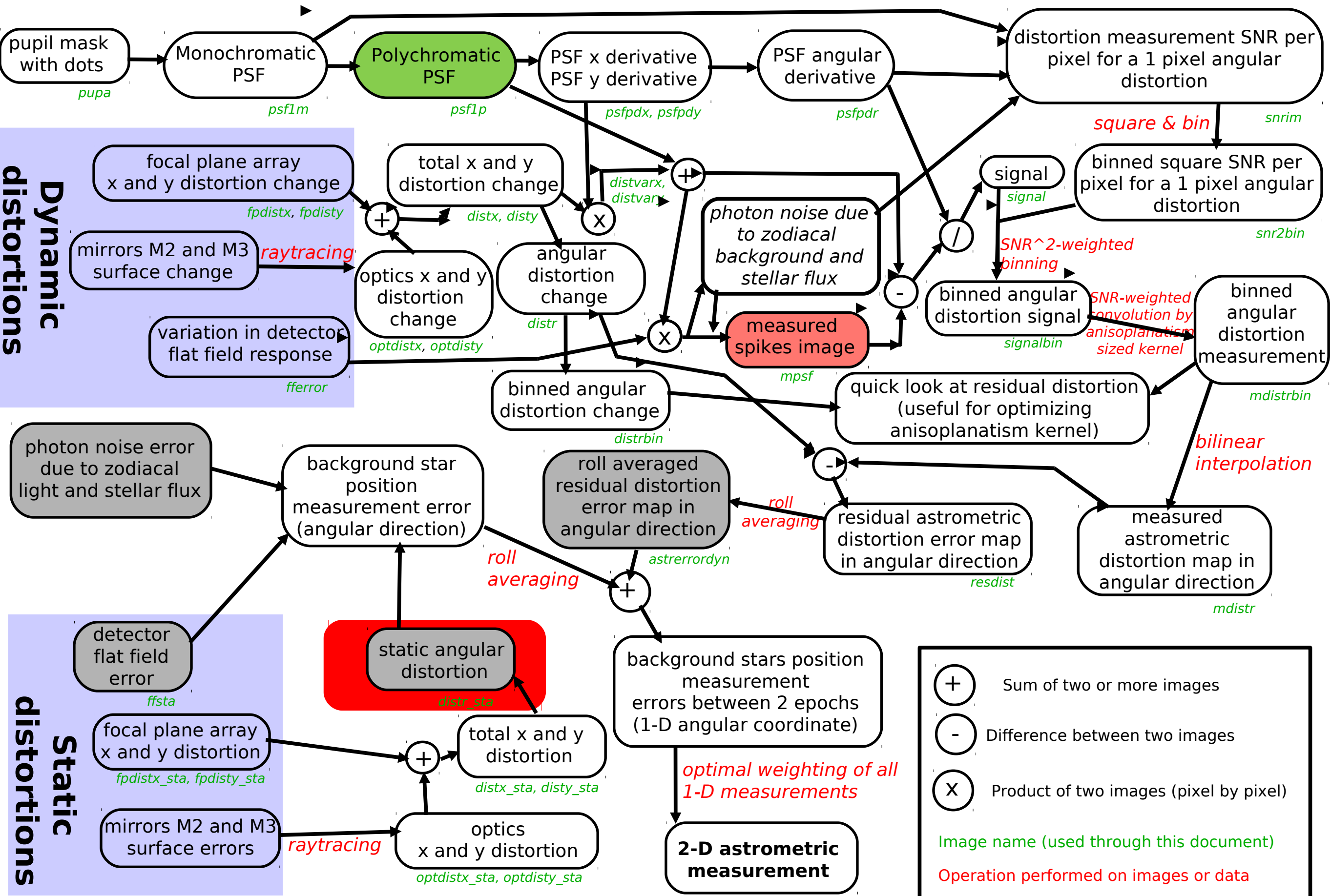
Distortion maps shown for 0.2×0.2 deg. Due to pixel size non-uniformity residual after ground/in orbit calibration of detector. Spatial frequencies chosen here put most power in between spikes and at \sim arcsec separation (worst case)

$\sim 2/1000$ pixel amplitude = 90 μ as

left: x, right: y. Unit = pixel (44mas)



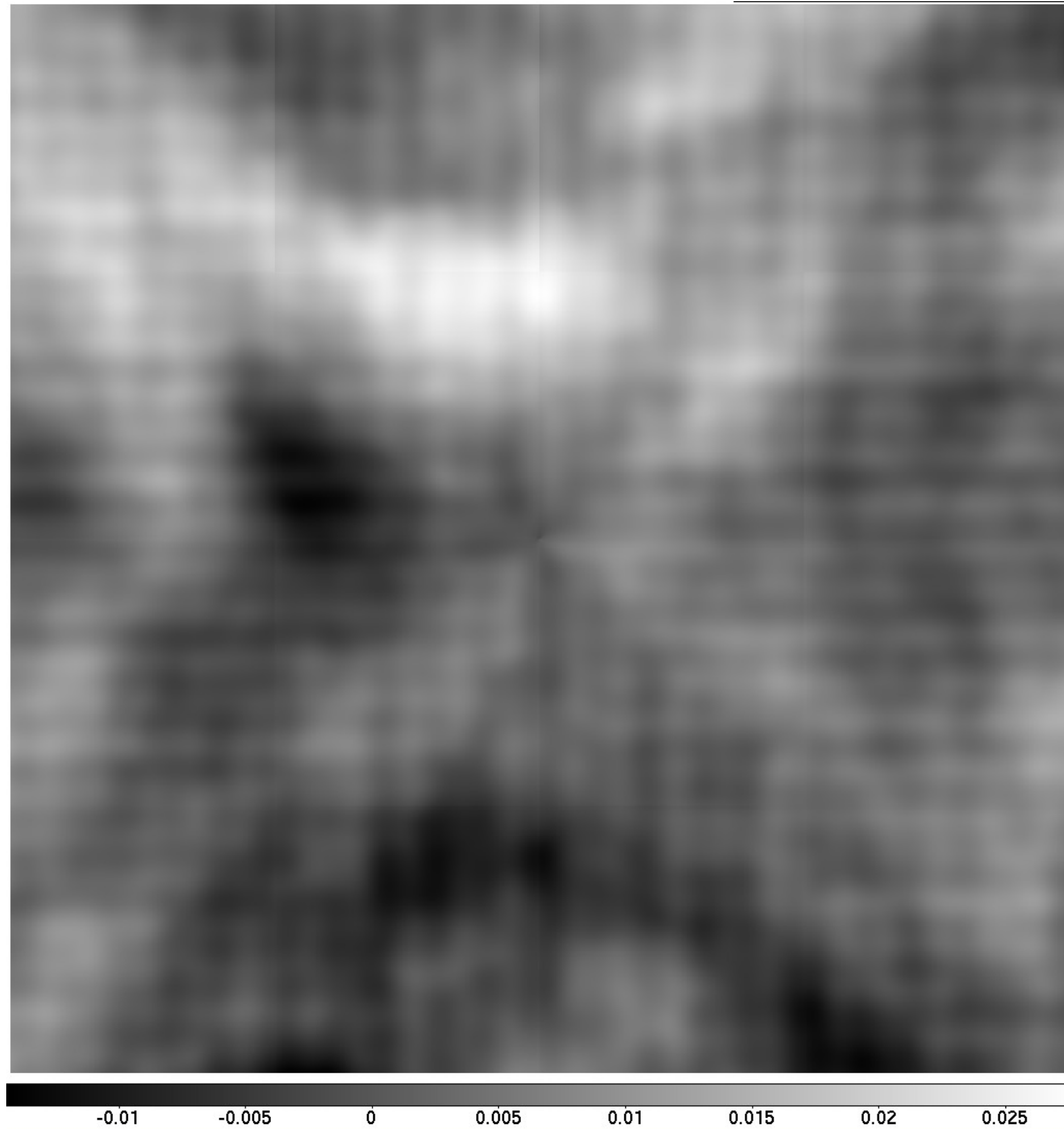
Numerical simulation approach



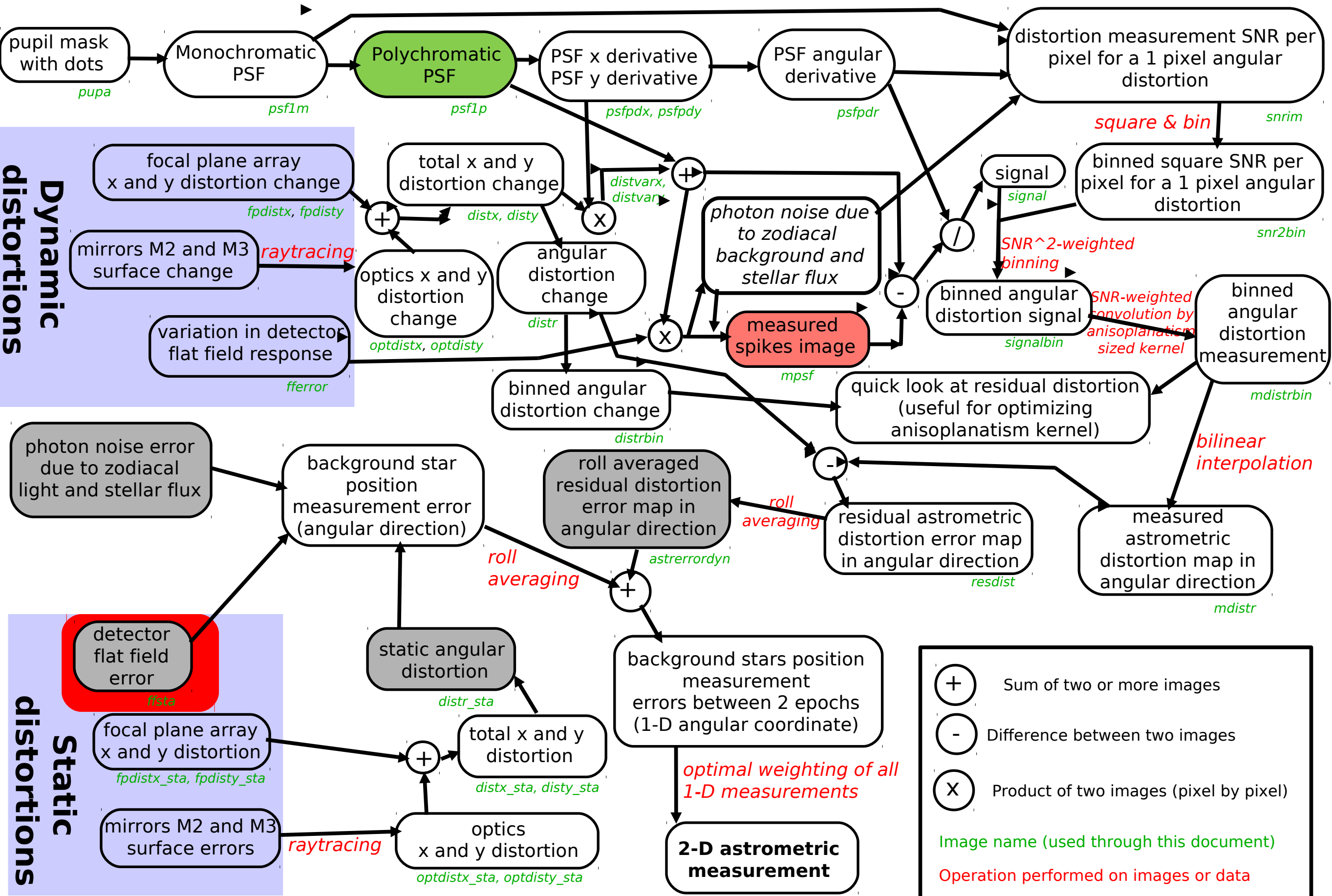
Total static distortion map

Angular coordinate
distortion
(perp. to spikes)
map shown for 0.2×0.2
deg.
Unit = pixel (44mas)

distortion is ± 1 mas
approximately



Numerical simulation approach



Static uncalibrated flat field error

1% random error + lines and columns errors

error is +/-6% peak, 1.02% RMS

full frame

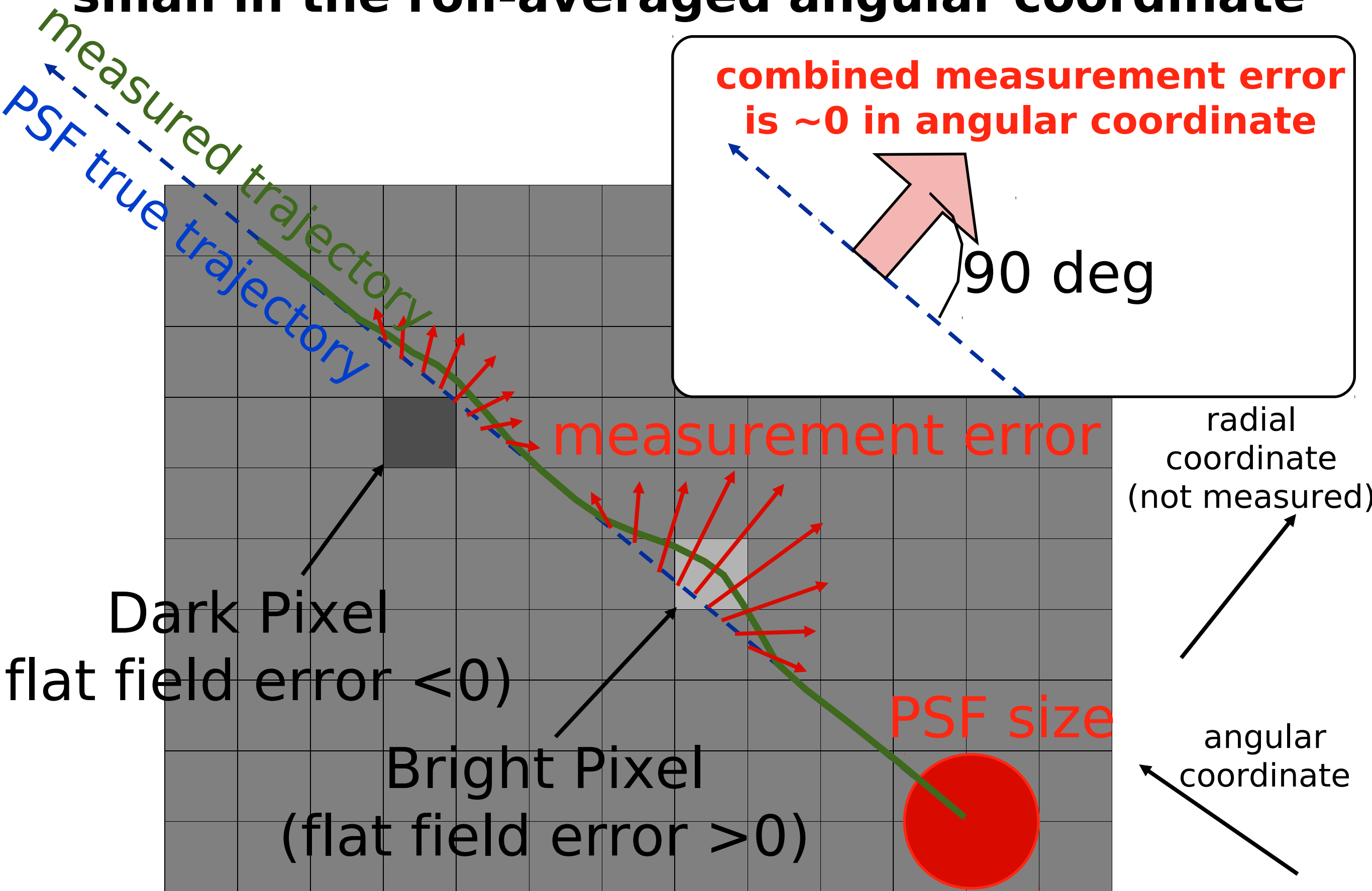
detail



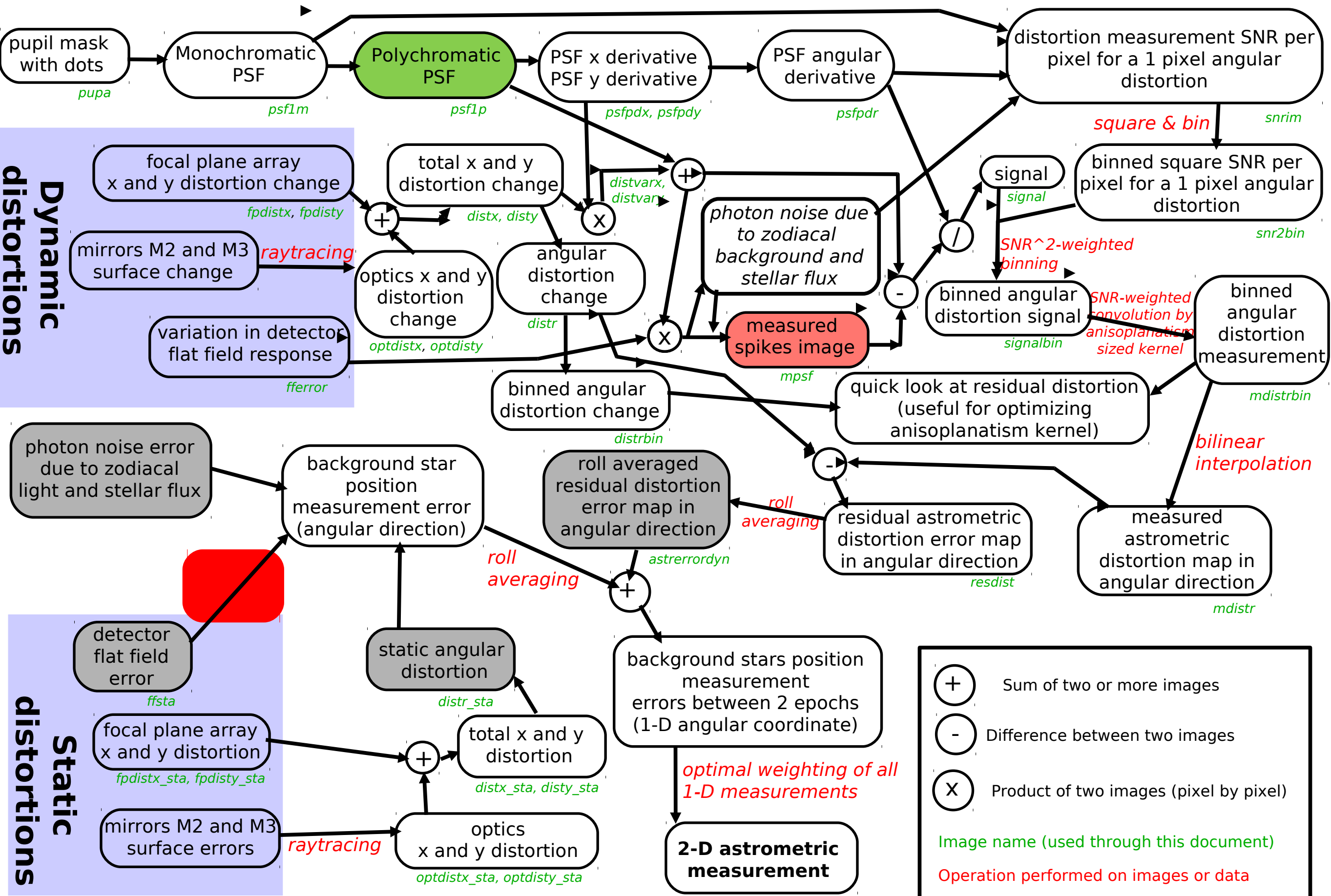
Flat field knowledge requirement

- With 0.2 deg diam, 1 rad roll, measurement is done over ~ 100 stars x 3000 independent positions (separated by more than $1/D$) on the detector = $3e5$ measurements
- $0.2 \text{ uas} = 1/200000 \text{ pixel} \rightarrow$ allowed error (if not correlation) is $< 1/500 \text{ pixel} \sim 1\%$ error on flat field at small scales (pixel to pixel)
- Astrometric error due to pixel-to-pixel flat field errors is strongly anticorrelated along the PSF track on the detector \rightarrow averages closer to $1/N$ than $1/\sqrt{N}$ \rightarrow flat field knowledge errors of a few % should be OK (see next slides)

Detector static errors are expected to be very small in the roll-averaged angular coordinate



Numerical simulation approach



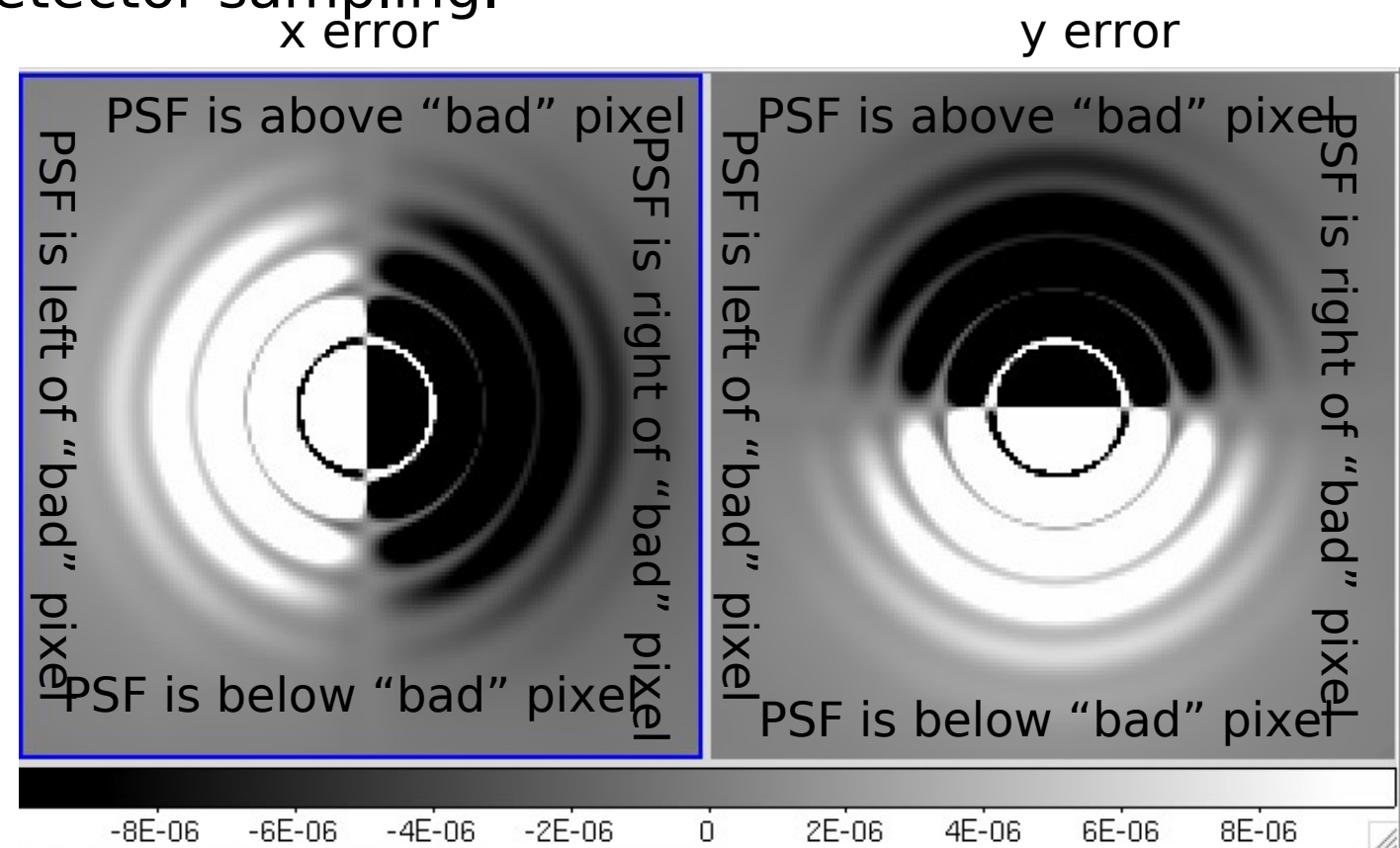
Numerical simulation of astrometric error due to flat field errors

Step 1: pre-compute how a single pixel sensitivity error “pulls” the estimated PSF position (= astrometric error kernel for a single pixel error).

This is done at 0.1 I/D step size, over 10 I/D radius: for each 2-D offset (within 10 I/D radius, with 0.1 I/D step) between the PSF center location and the “bad” pixel, compute the error in PSF position measurement in x and y. Computation uses finely sampled PSFs binned down to the detector sampling.

Maps on the right show how a sensitivity error in a single pixel affects the PSF position measurement.

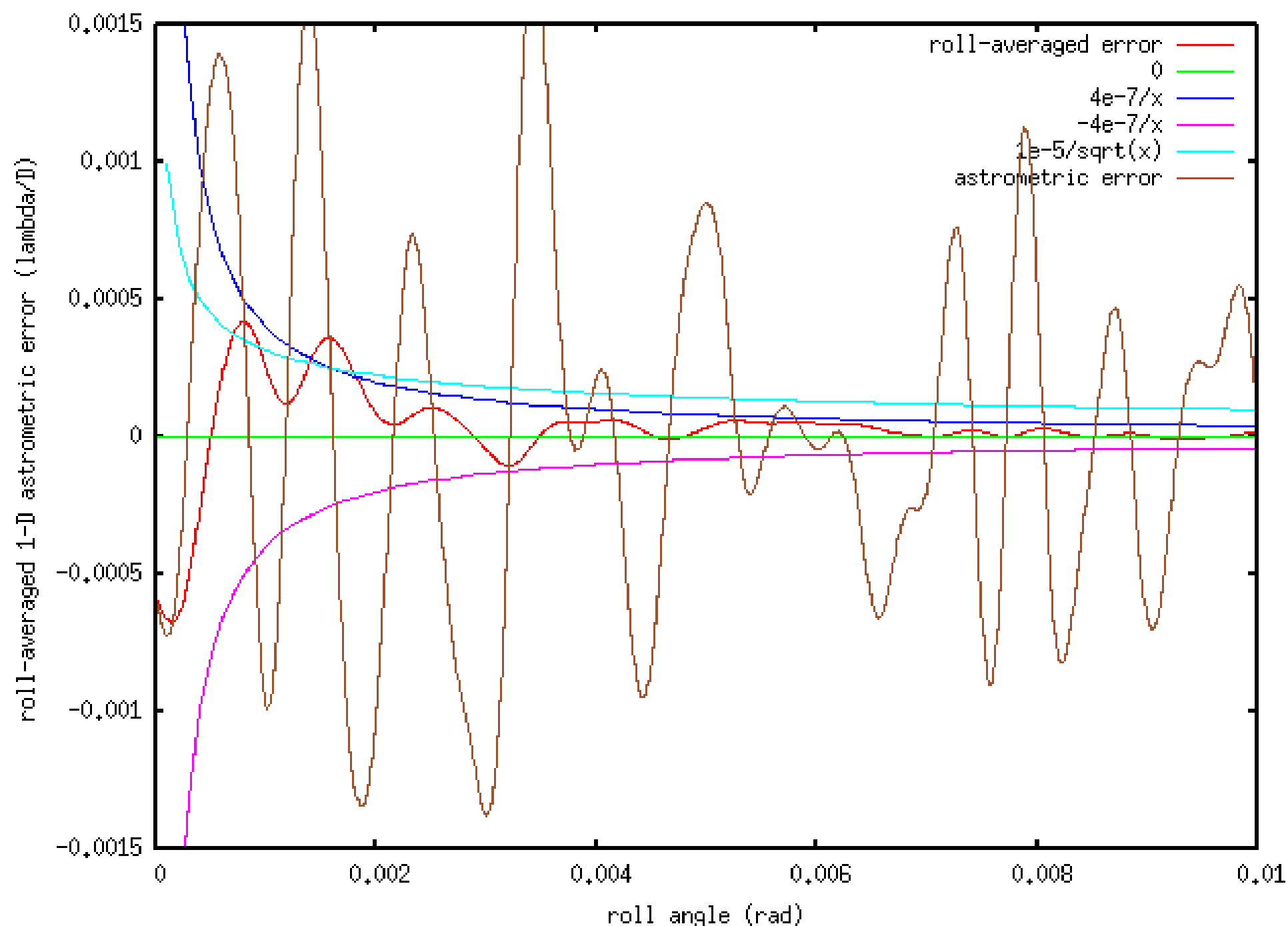
Maps are normalized to the relative pixel sensitivity error. Unit is I/D. Peak value is 0.05: a 1% sensitivity error can move the PSF measured position by $0.0005 \text{ I/D} = 44 \text{ uas}$

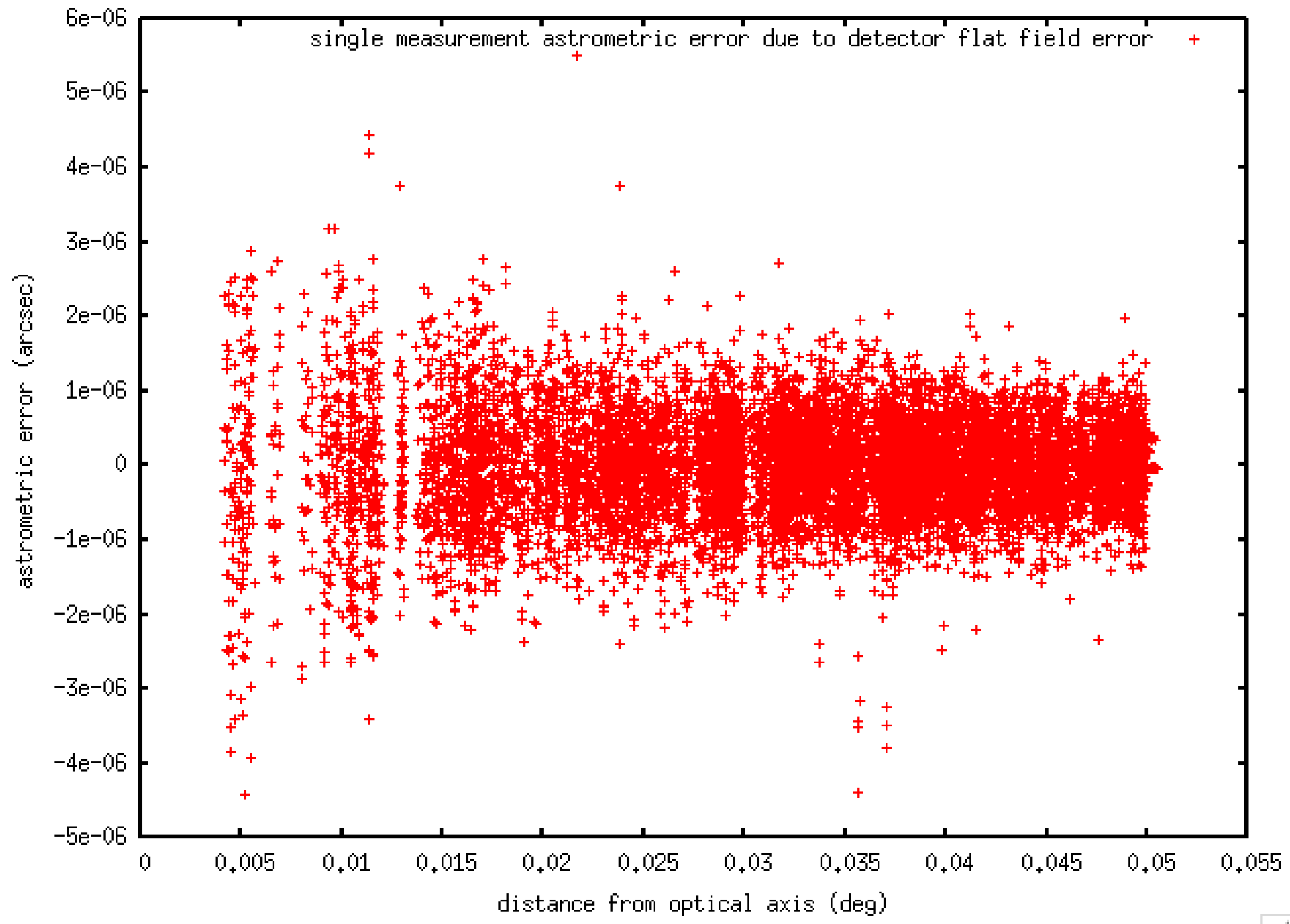


Step 2: For each roll angle and star, compute 2-D PSF position error by summing all errors due to pixels sensitivity errors within a 10 I/D radius of actual PSF position. This computation uses the maps shown above: for each pixel, the fractional offset between the pixel and the PSF is computed, and the corresponding error values (x and y) are derived from bilinear interpolation of the maps computed in step 1.

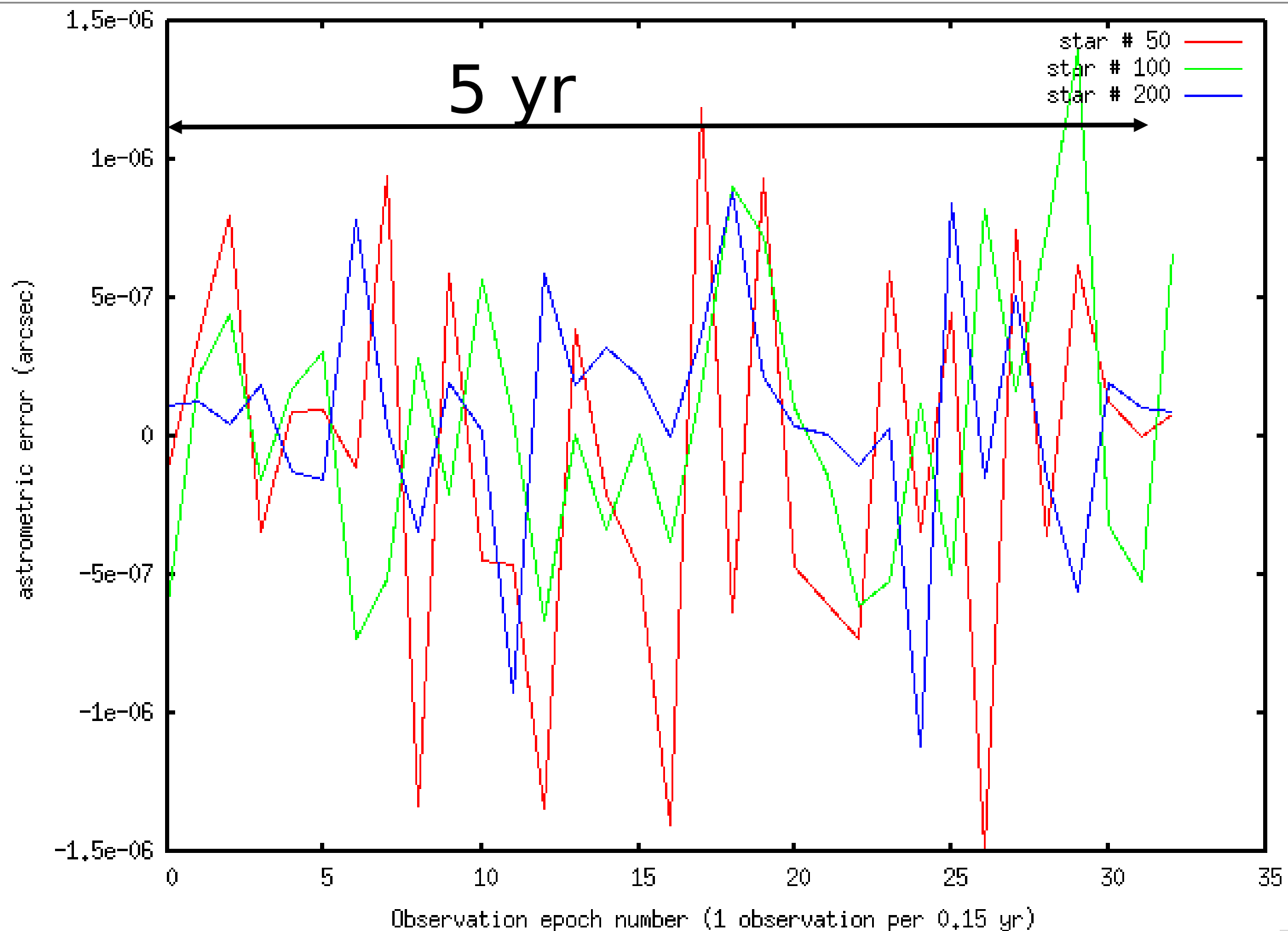
Flat field errors are strongly anticorrelated with roll angle -> they average as $1/N$ instead of $1/\sqrt{N}$

Figure on the left shows 1-D astrometric error for a single star as a function of roll angle. The raw error (brown) is $\sim 10^{-3}$ I/D RMS (~ 0.1 mas). The roll-averaged error (red) goes as $1/\text{roll angle}$.





Astrometric error due to flat field errors is ~ 0.5 uas per star for a 1 rad roll.
Error is stronger for stars closer to the optical axis (less roll averaging)



Single star astrometric error due to flat field errors shows no obvious time correlation in this example (1 arcsec / yr proper motion). With smaller proper motion and more distant stars (small parallax), correlation is expected over two timescales : time for proper motion to move star by 1 pixel, and 1 year period due to parallax.

Intra-pixel sensitivity errors are captured in this analysis

Unknown variations of sensitivity within a pixel show the same anti-correlation behavior, and are captured in this analysis.

Example: top half of a pixel less sensitive than bottom half

If PSF is below the pixel, PSF position error is positive

If PSF is above the pixel, PSF position error is negative

A small error in sensitivity between pixels is similar to a larger error within a pixel.

Intra-pixel sensitivity errors can be simulated by the same analysis as shown here, but with a finer sampling.

Dynamic distortions

Definition: Any change between observations epochs

These changes introduce errors in the measured position of background stars or on the distortion change measured by the spikes image.

Description of main error terms:

- Variation in the optical shape of mirrors M2 and M3 due to thermal and mechanical stresses introduces astrometric distortions that change between the observation epochs
- Rigid body motion of optics (telescope alignment)
- Focal plane array geometry: motion and distortion of individual detector chip due to temperature fluctuation and mechanical stress
- Variations in the flat field response of the detector

Impact and mitigation:

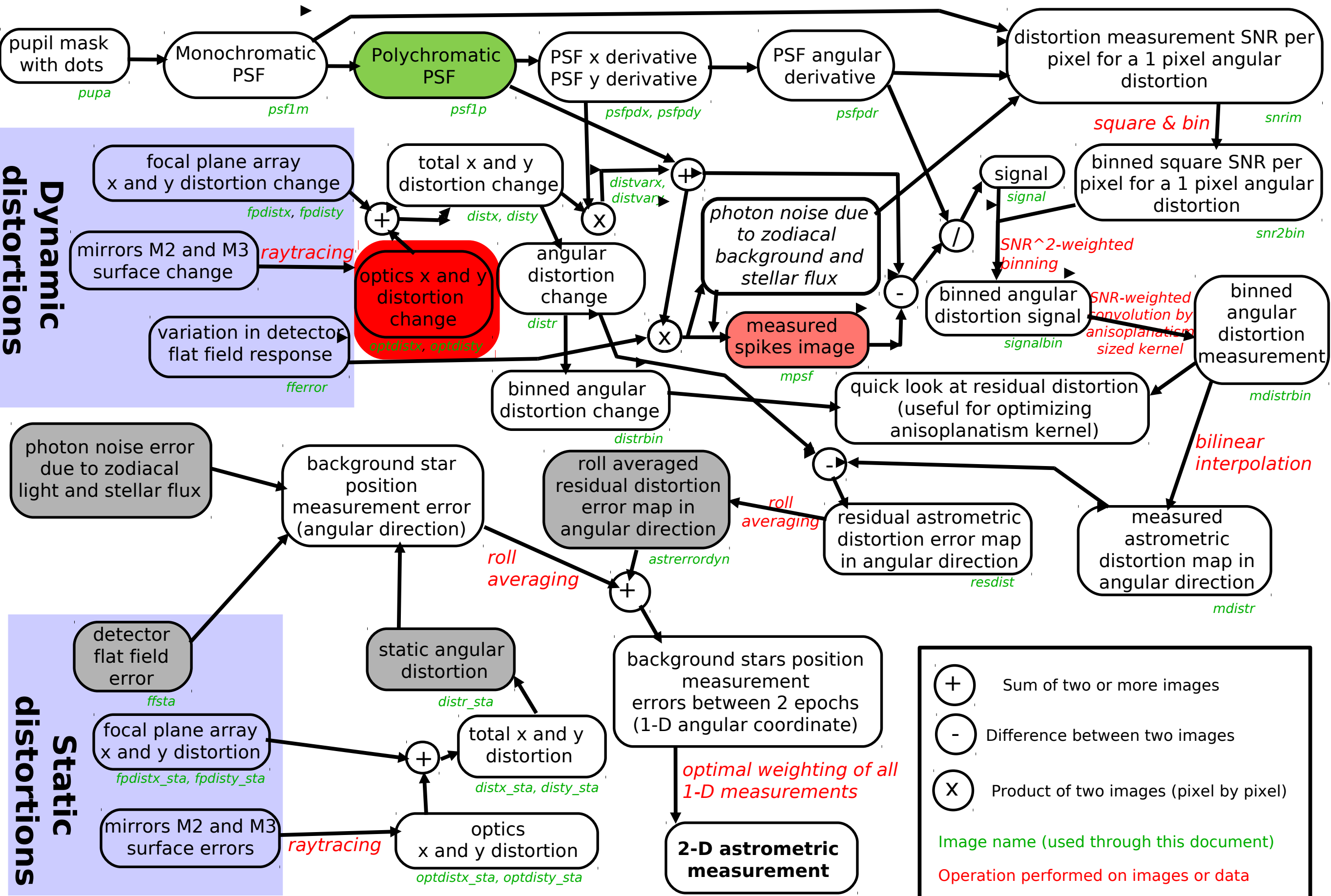
Low order components of dynamic errors are calibrated by the diffraction spikes. To measure how distortions change between observations, the motion of the spikes is measured by comparison of the spike images between the different observation epochs.

Errors in this estimate come from

- photon noise (spikes, zodi)
- changes in the pixel response between the 2 epochs
- interpolation between spikes (no signal between spikes)

Time-variable distortions are not perfectly estimated by the spikes -> astrometric error

Numerical simulation approach



Time-variable distortions: M2 and M3

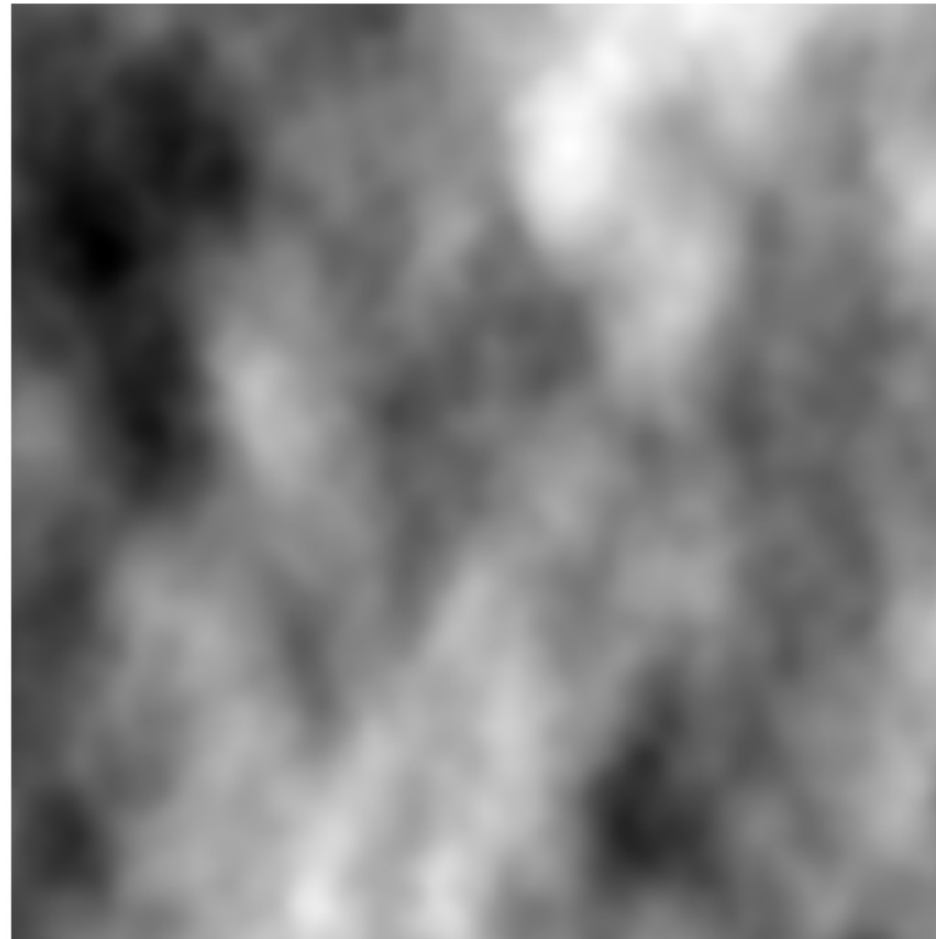
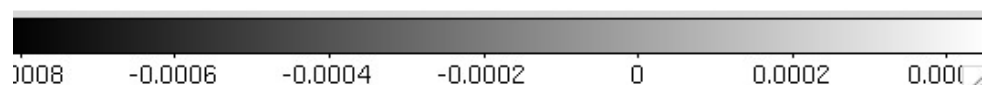
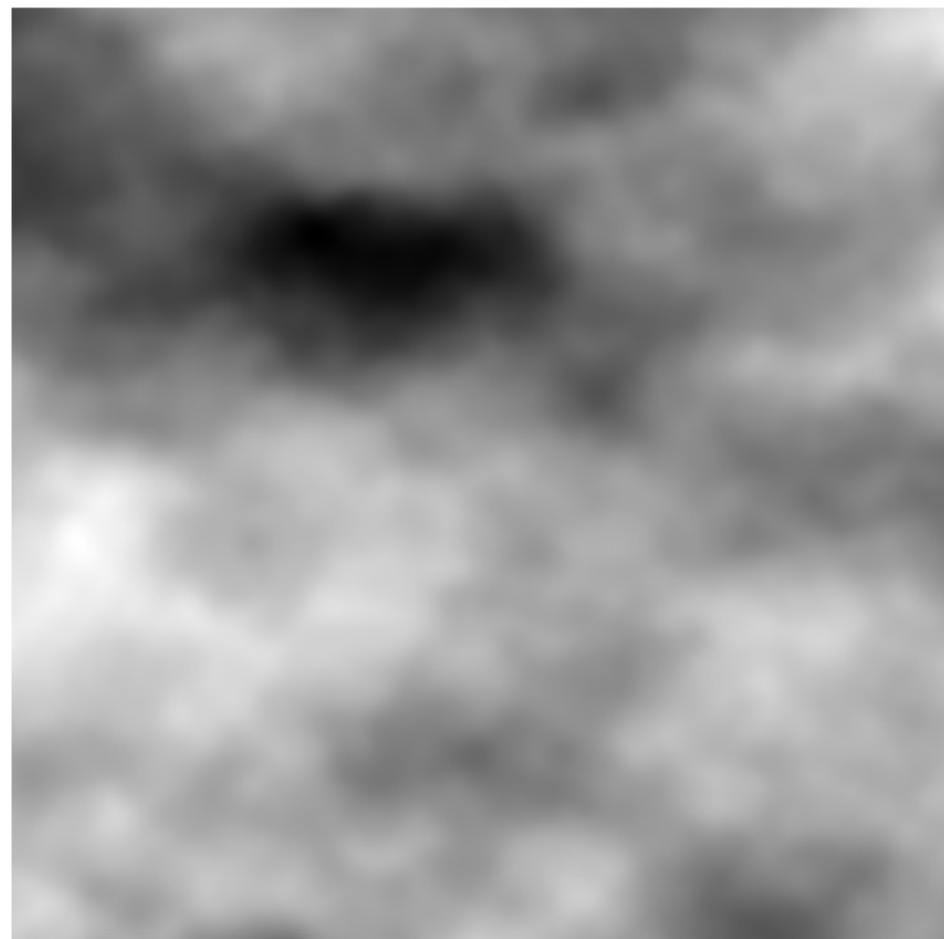
Thermal variations in substrate + mirror mounting:

On 150-350mm apertures, better than 0.1nm RMS wavefront insertion repeatability with 0.25 C temperature stability. (Jay Daniel, L-3 Tinsley, private communication)

Assuming 100mK temperature stability-> 40 pm RMS stability

Material creep :

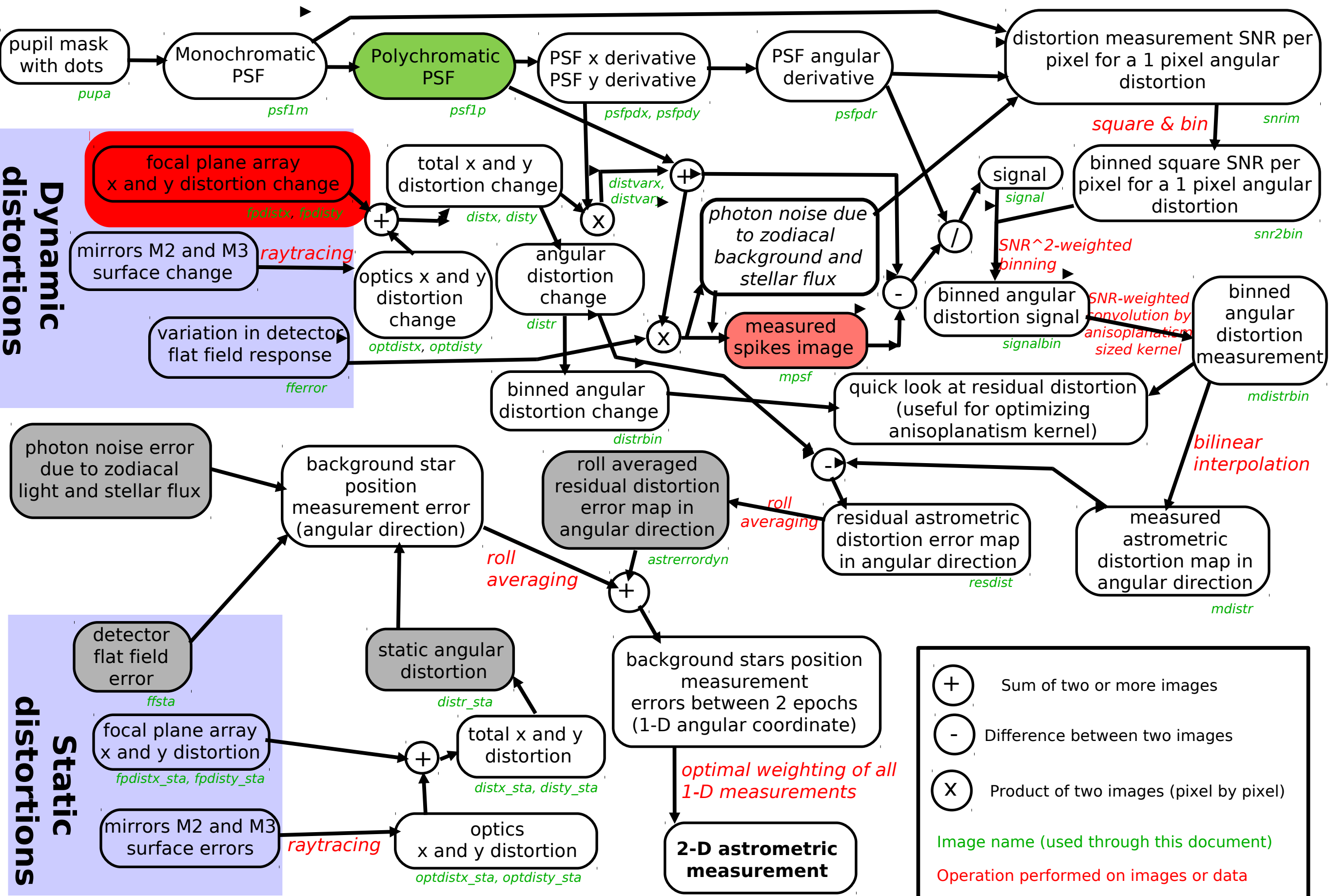
probably slow process (timescale > single observation) which can be tracked during course of mission by averaging distortions over several consecutive observations. -> not included



x and y astrometric distortions due to change in the shape of optics is shown on the left.

Same as static optical distortions, but scaled by 3%.
Unit = pixel (44 mas)

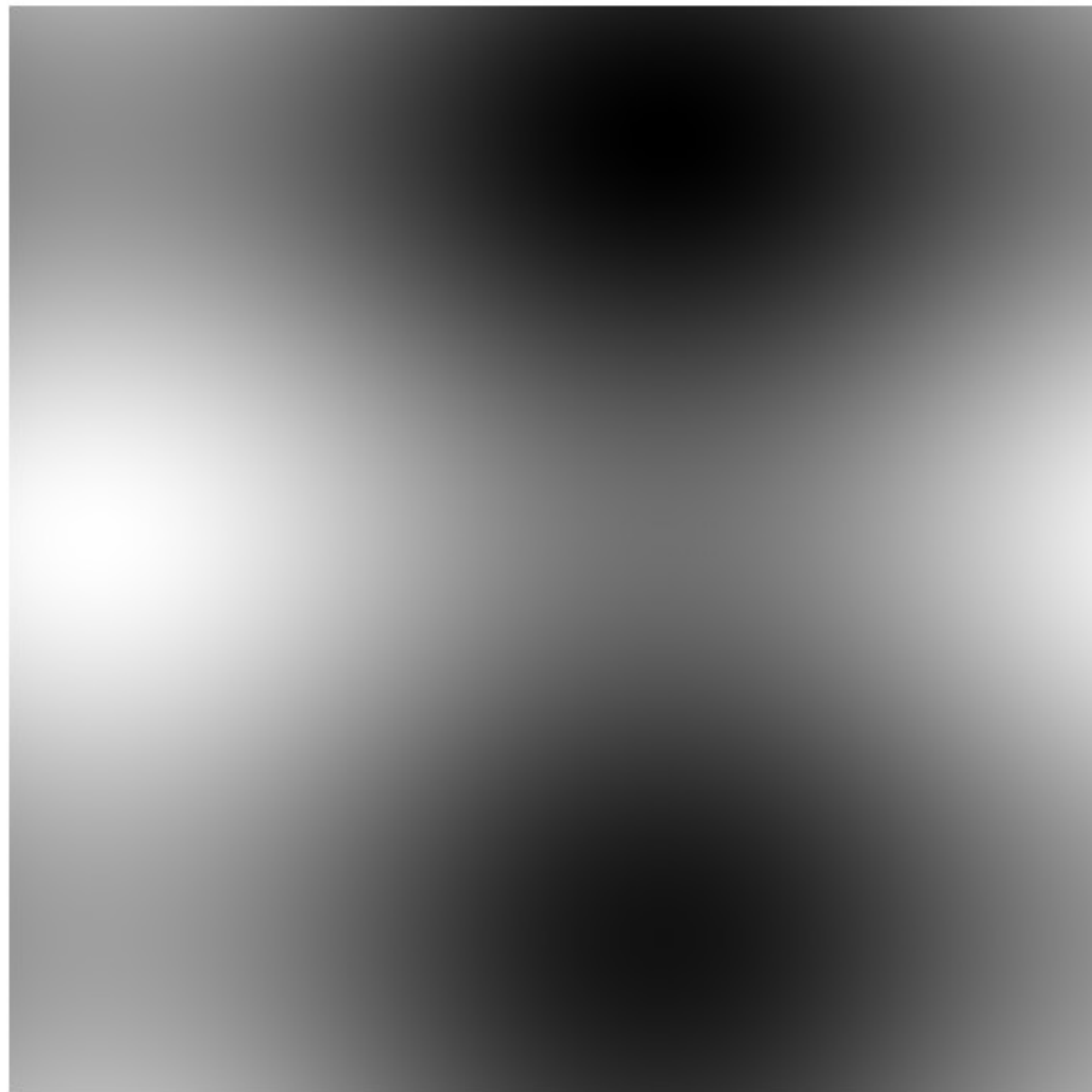
Numerical simulation approach



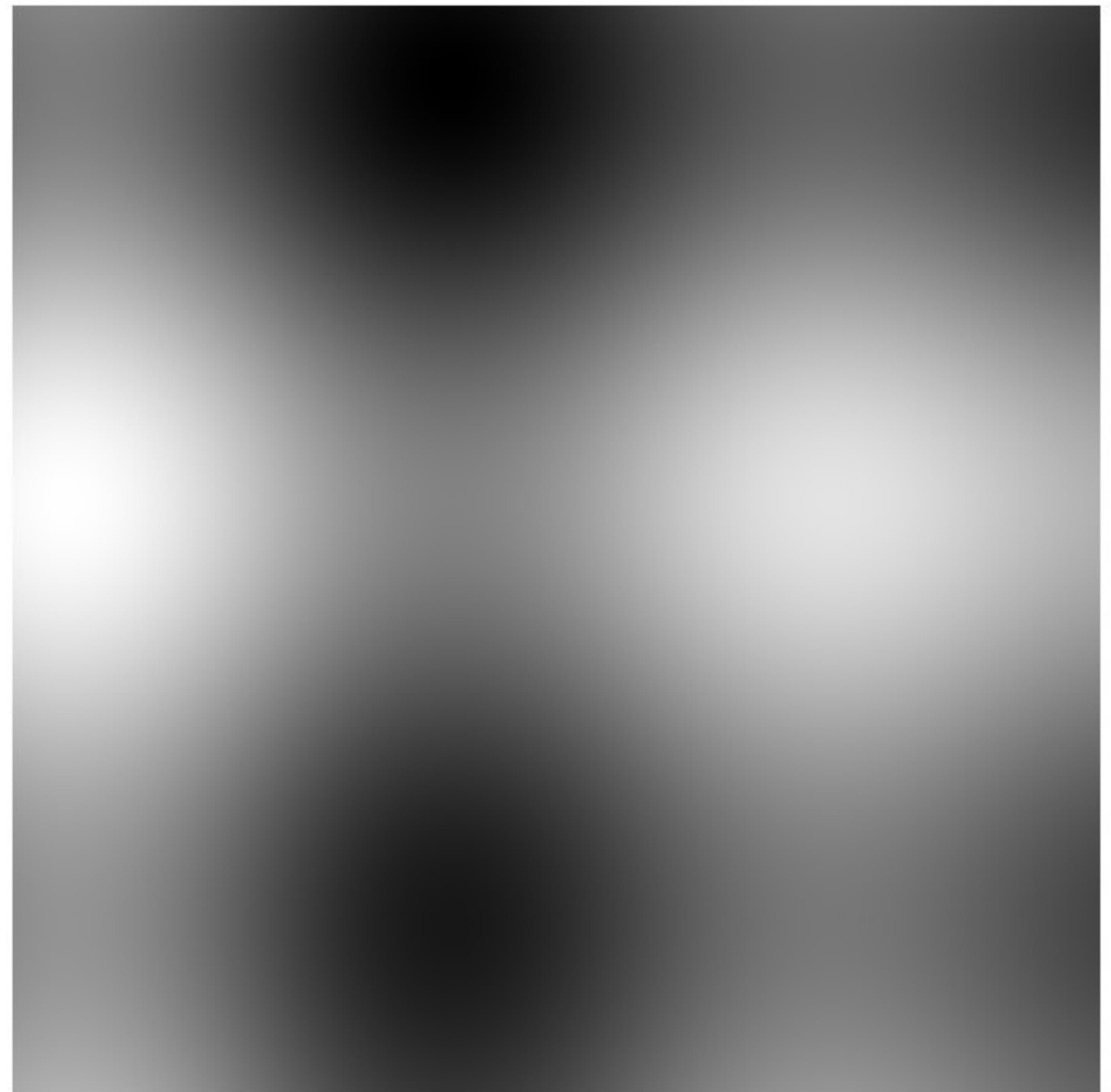
Detector array distortions

A 100 mK temperature change on a 4k detector changes its linear size by 0.00172 pixel, assuming Si (CTE=4.2e-6). This is simulated by a low order term in x distortion with $\pm 1e-3$ pixel and period \sim single 4k detector size. Translation between detector chips not included here - would need to be fitted as a translation for each chip.

Unit = pixel (44 mas)

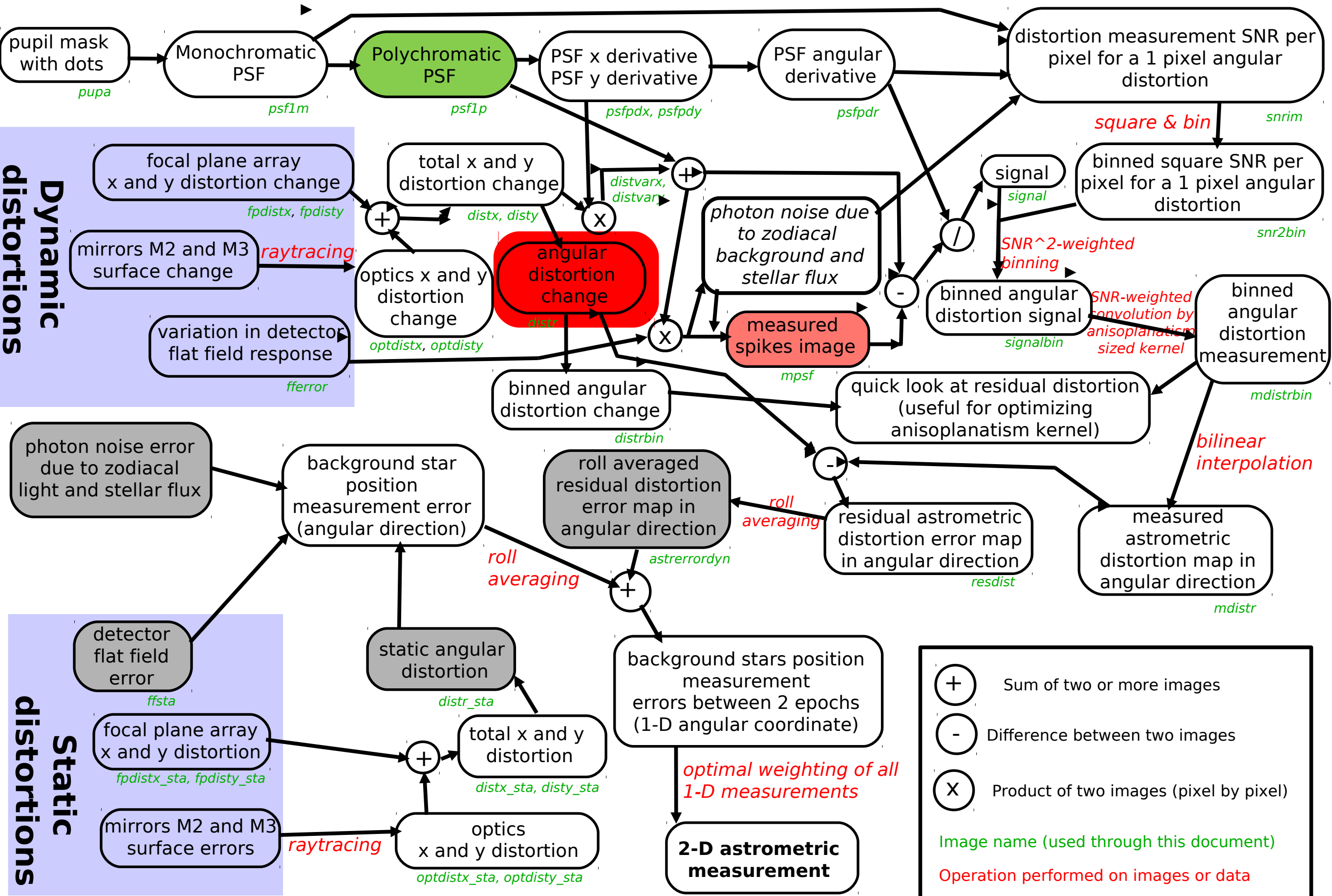


-0.001 -0.0008 -0.0006 -0.0004 -0.0002 0 0.0002 0.0004 0.0006 0.0008 0.001



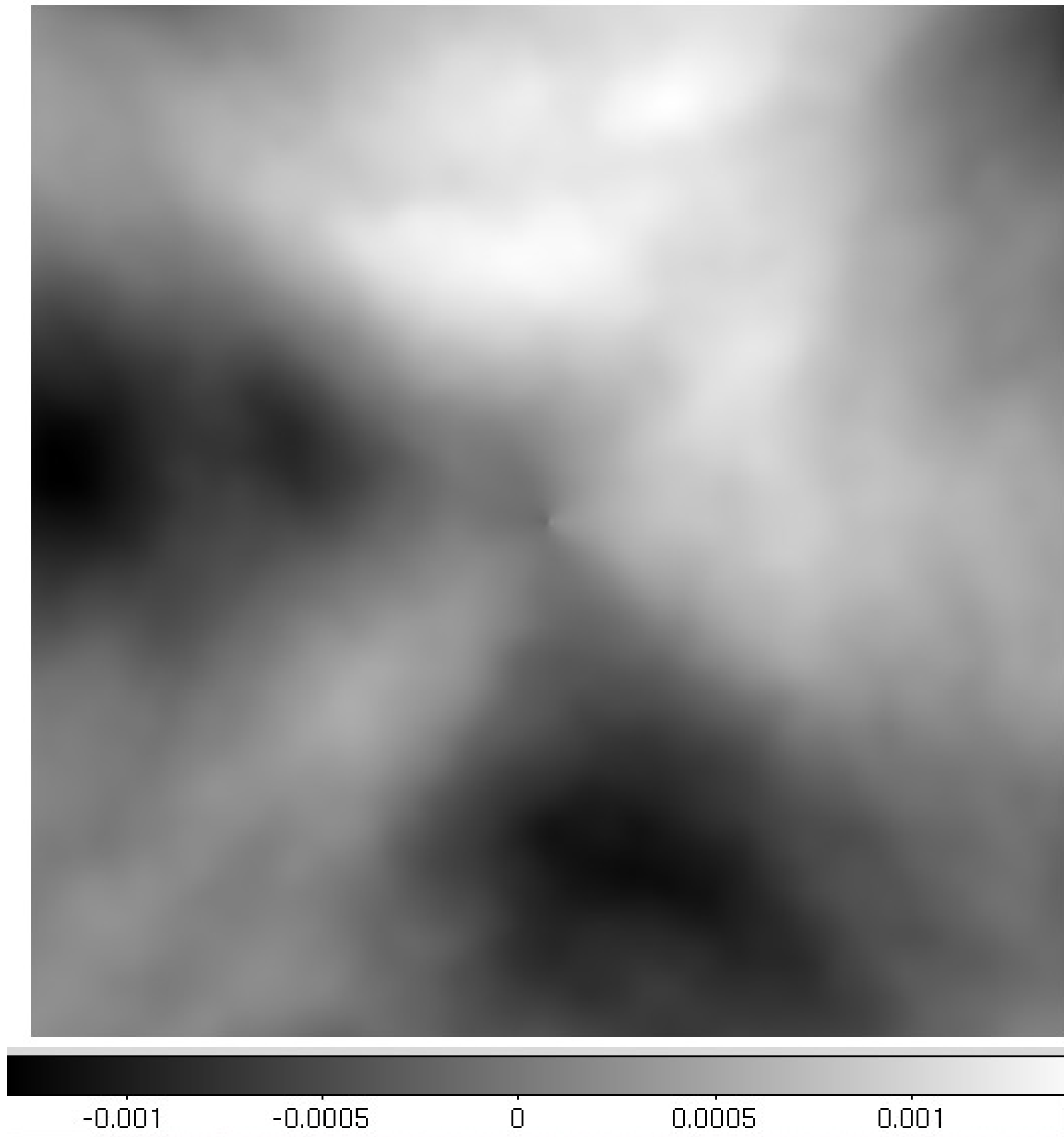
-0.001 -0.0008 -0.0006 -0.0004 -0.0002 0 0.0002 0.0004 0.0006 0.0008 0.001

Numerical simulation approach



Total angular distortion change

Unit = pixel (44 mas)
Amplitude $\sim 1/1000$ pixel (44 uas)



Flat field change between epochs

Detector response map changes between observation by $1e-4$ (RMS)

This will produce an error in the measurement of spikes displacements.

Even if the spikes are steady (no distortion), a distortion will be measured.

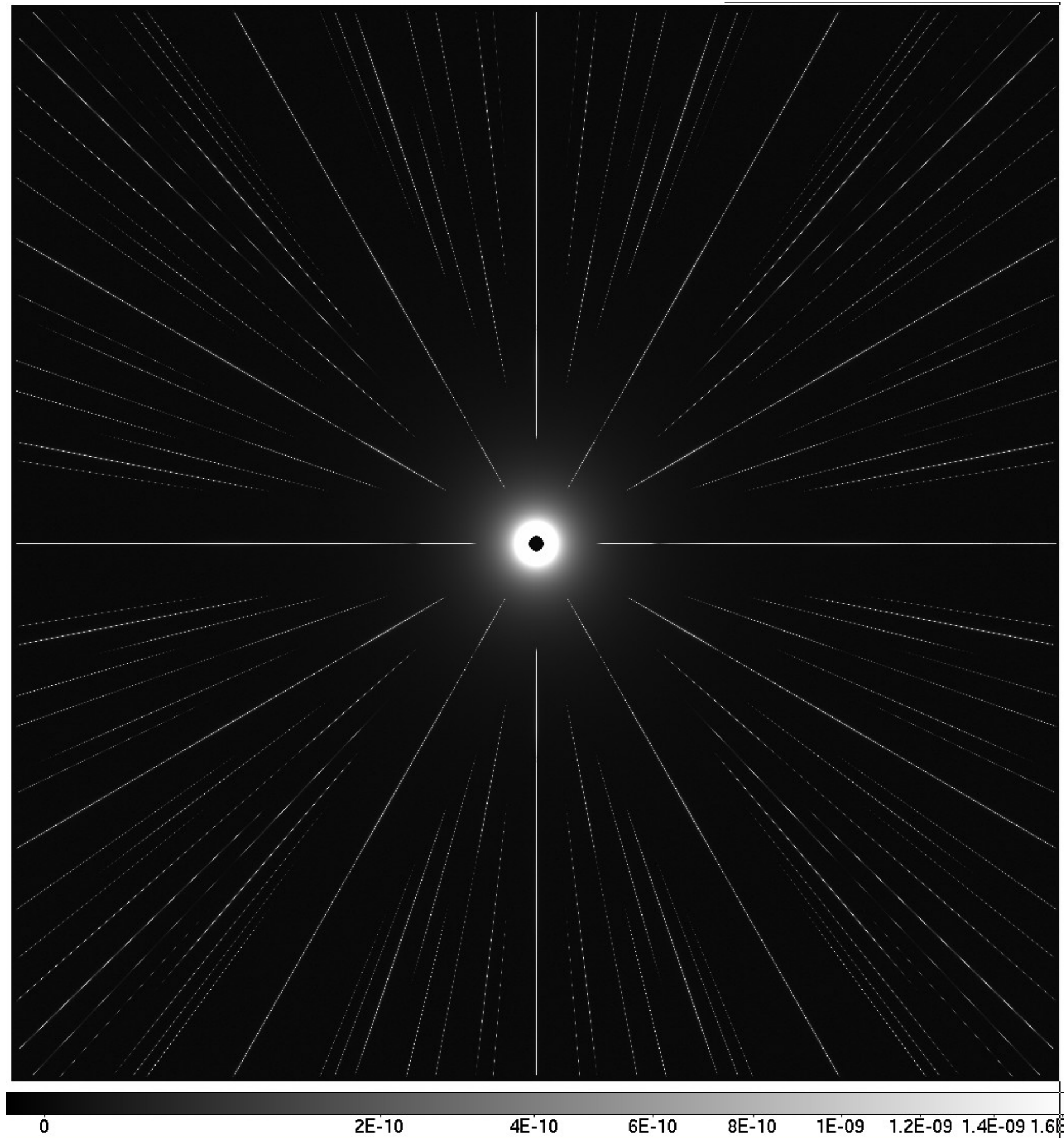
Spikes image, 0.2 deg FOV

Spike image is computed
by:

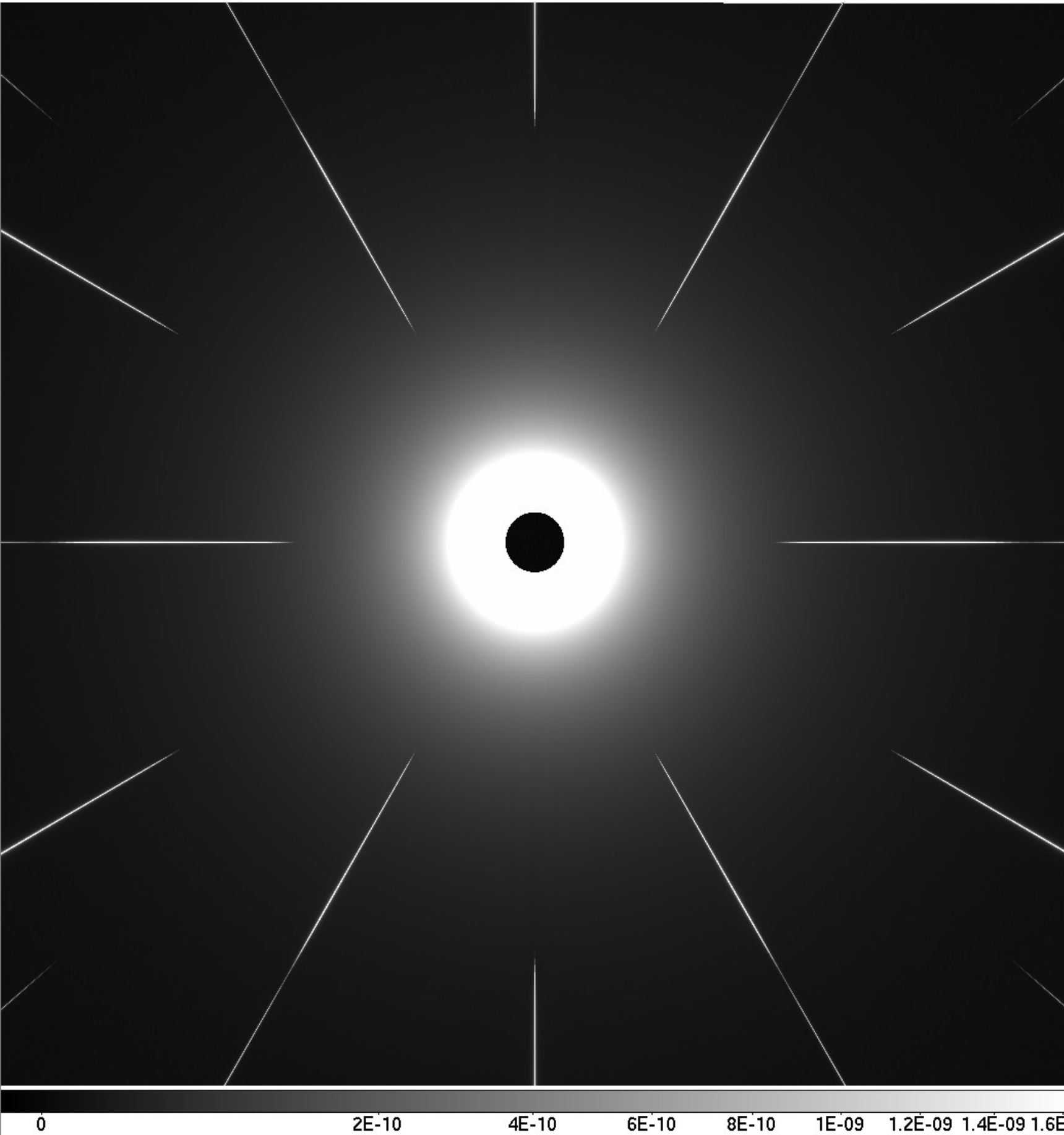
step 1: compute derivative
in x and y for the spikes

step 2: multiply derivative
by x and y distortion maps

step 3: add noise terms
(photon noise, readout
noise, flat field noise)



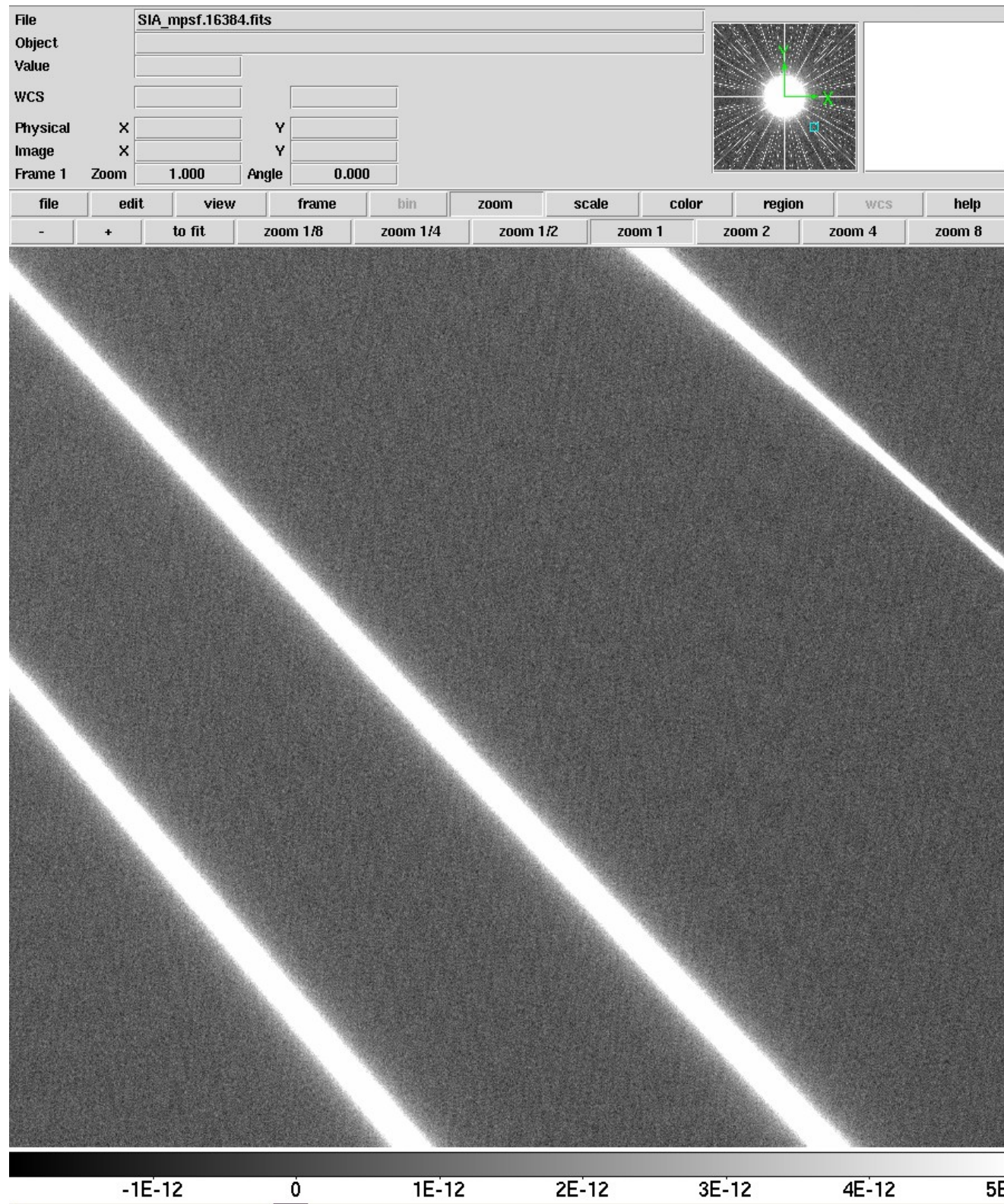
Spikes image (central region, 3'x3')



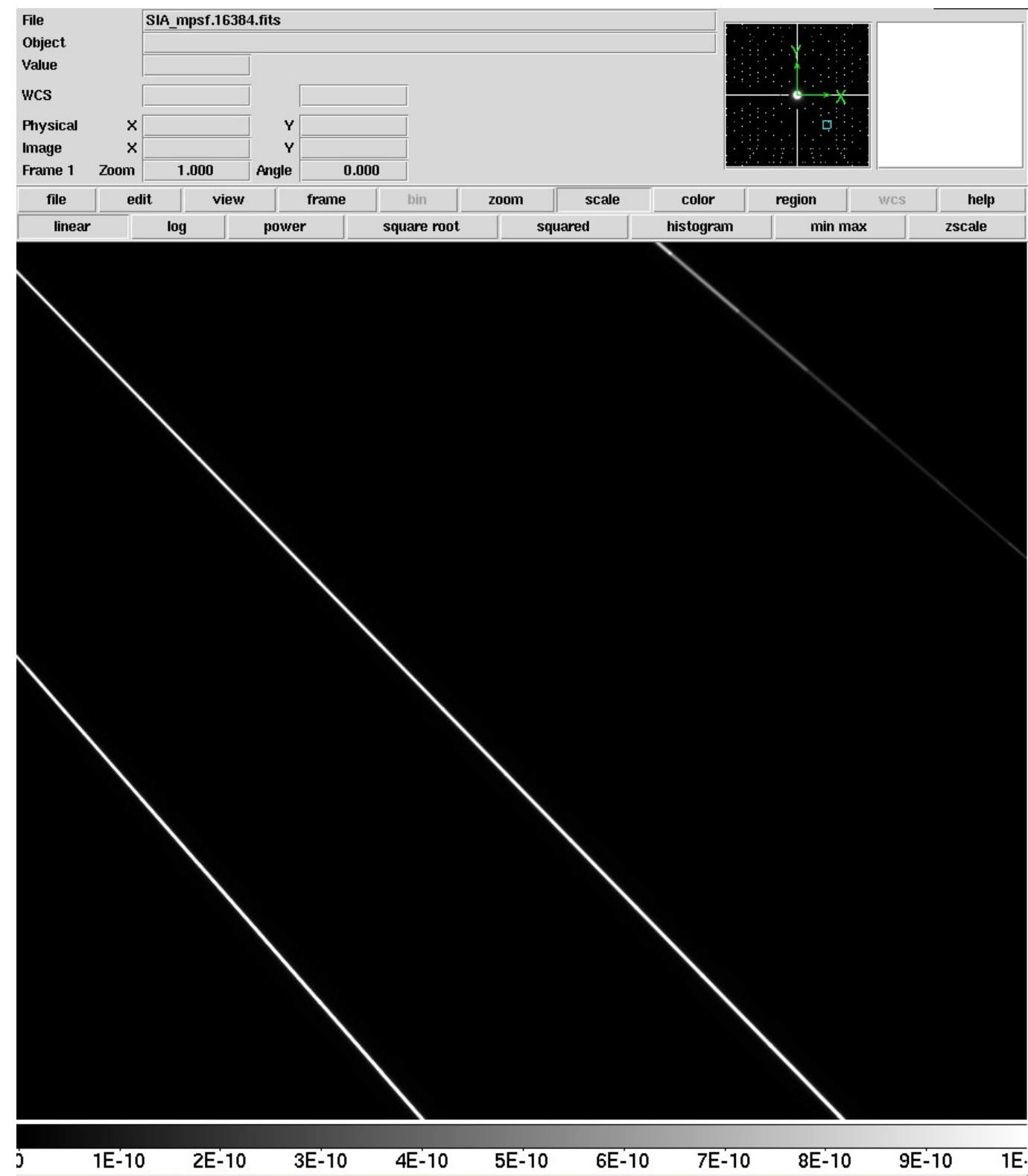
Central part of the field is blocked by the coronagraph pickup mirror.

The spikes do not extend inward to the coronagraphic field.

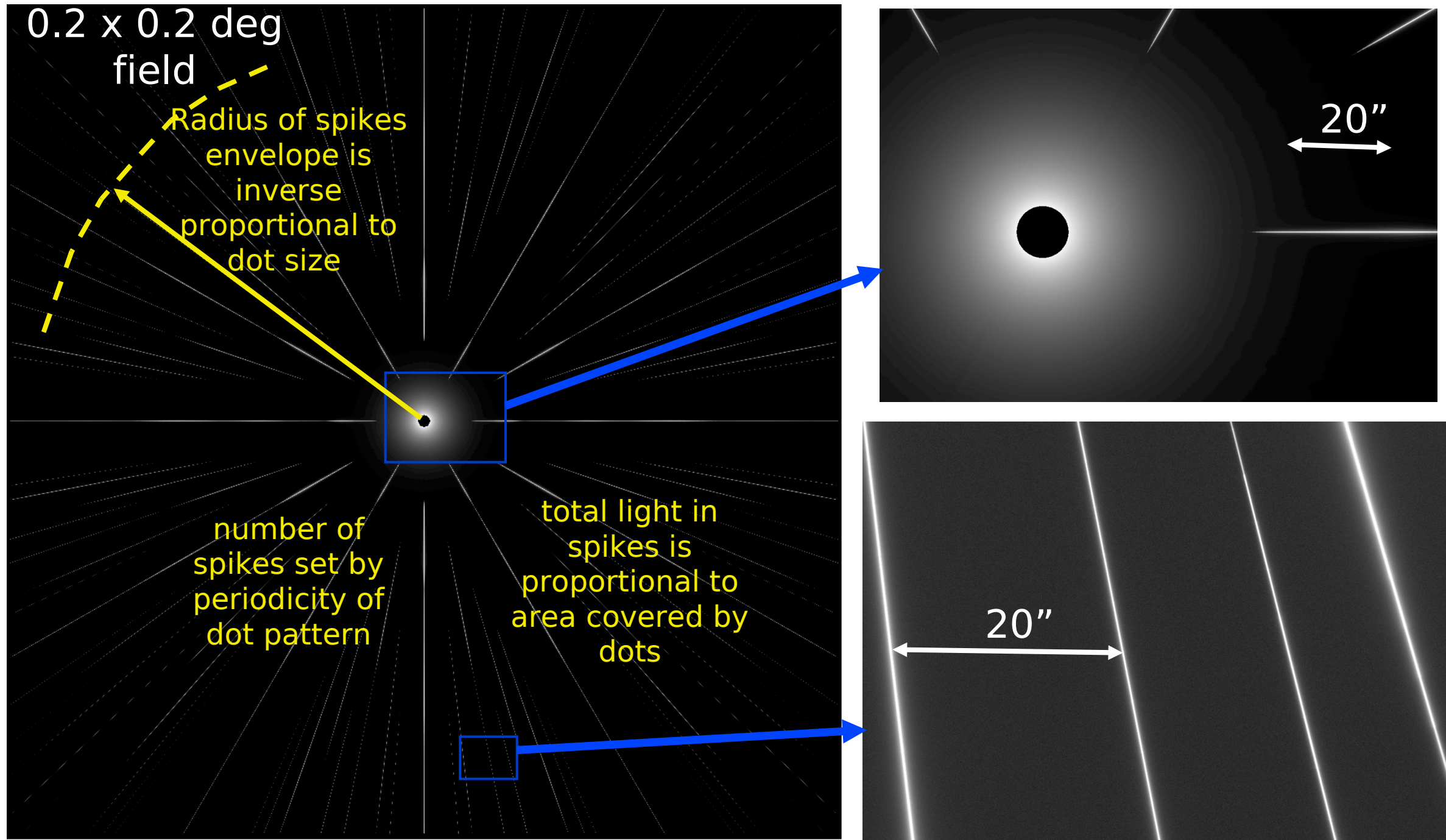
Zodi-subtracted spikes image, no background stars



Photon noise from spikes and zodiacal light are visible in this frame.



Spikes are I/D wide



The overall size of the spike envelope, the spikes density (spacing between spikes) and brightness can be chosen by design of the dot pattern.

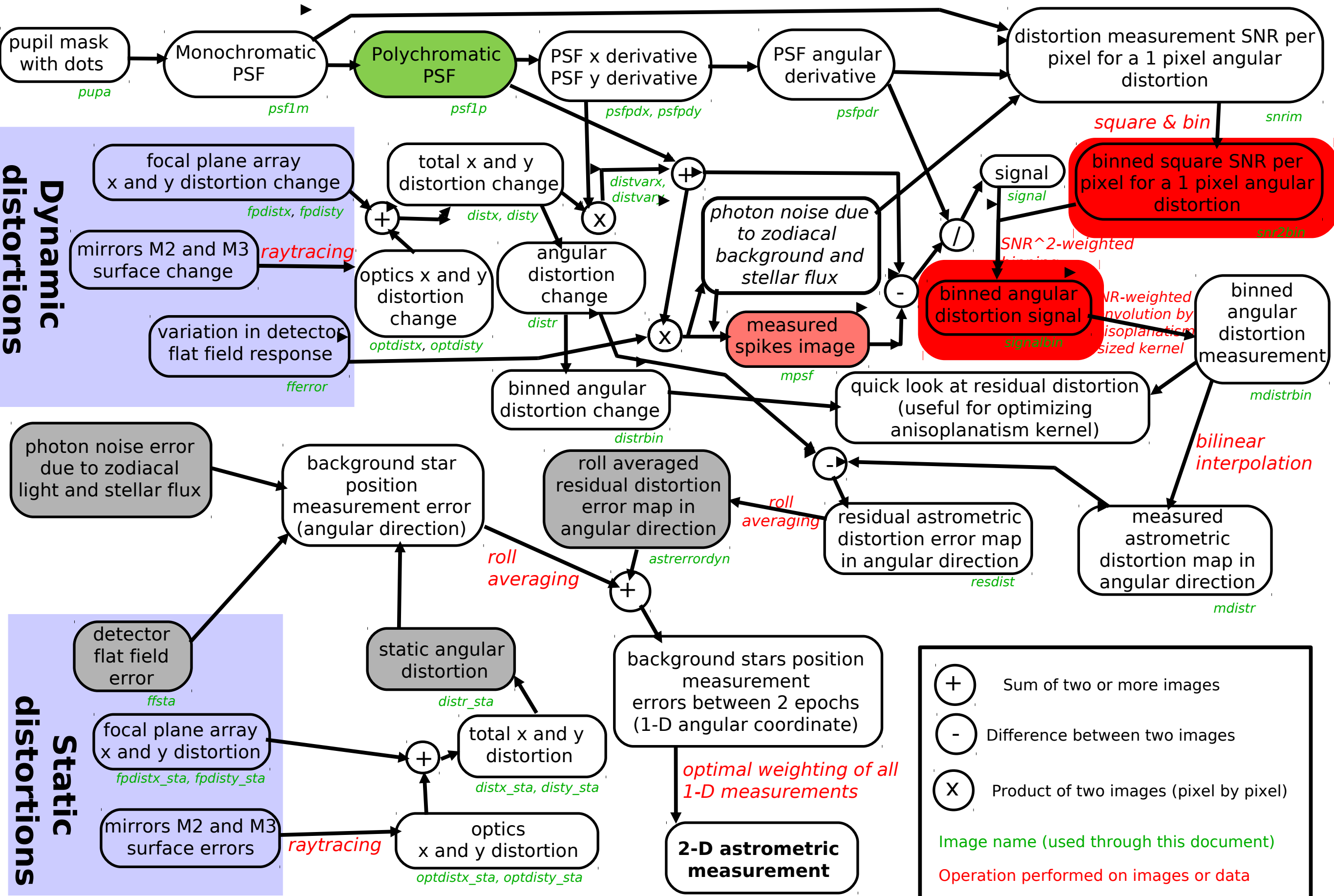
Distortion measurement

Compute SNR for a 1 pixel angular distortion for each pixel -> SNRmap

Compute signal (unit = pixel of angular distortion) for each pixel = difference between ideal spike image and measured spike image, divided by $d\text{Image}/d\text{Distortion}$ -> Signalmap

To speed up computation, Signalmap and SNRmap are binned to lower resolution (with optimal weights derived from SNRmap)

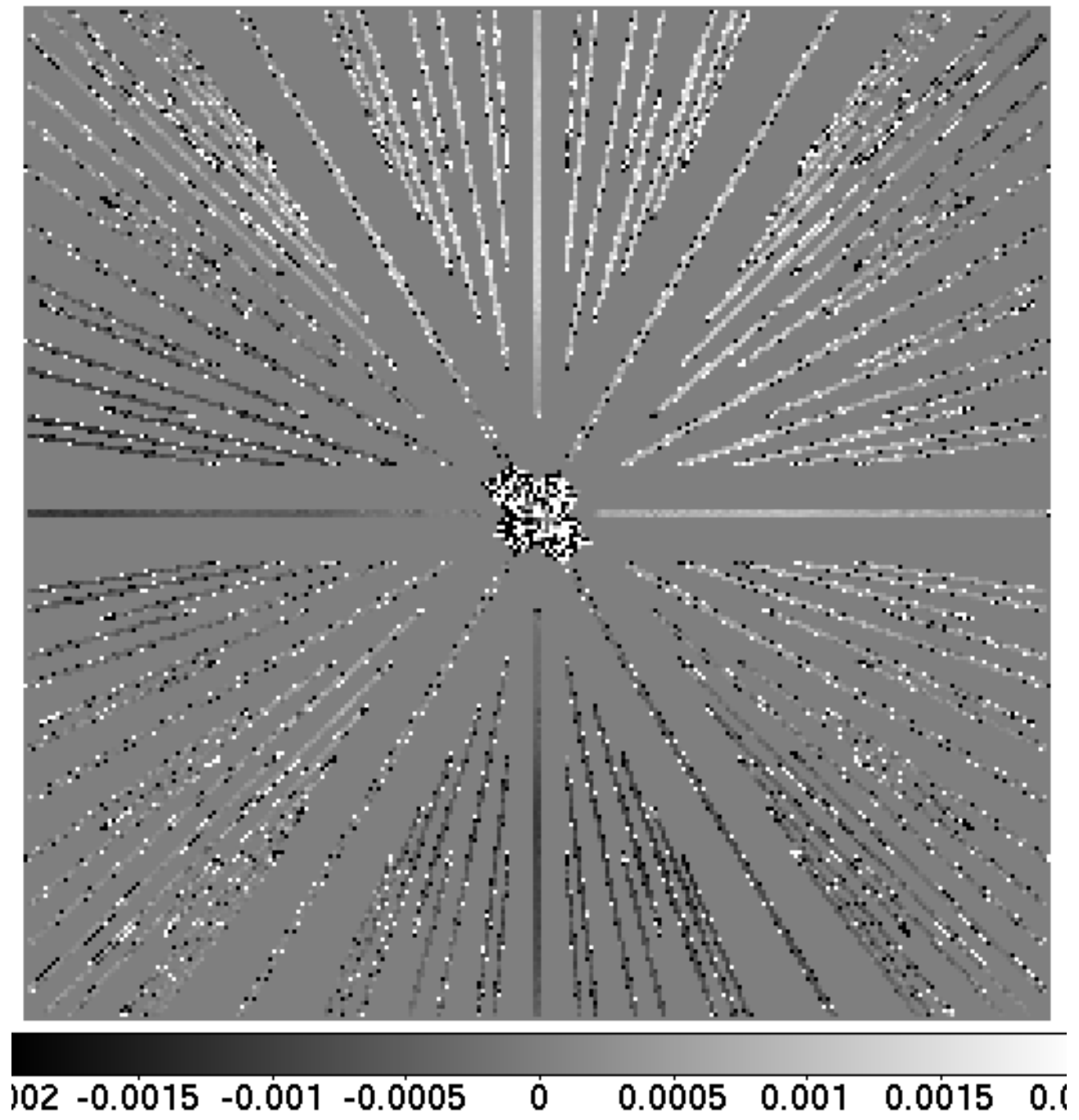
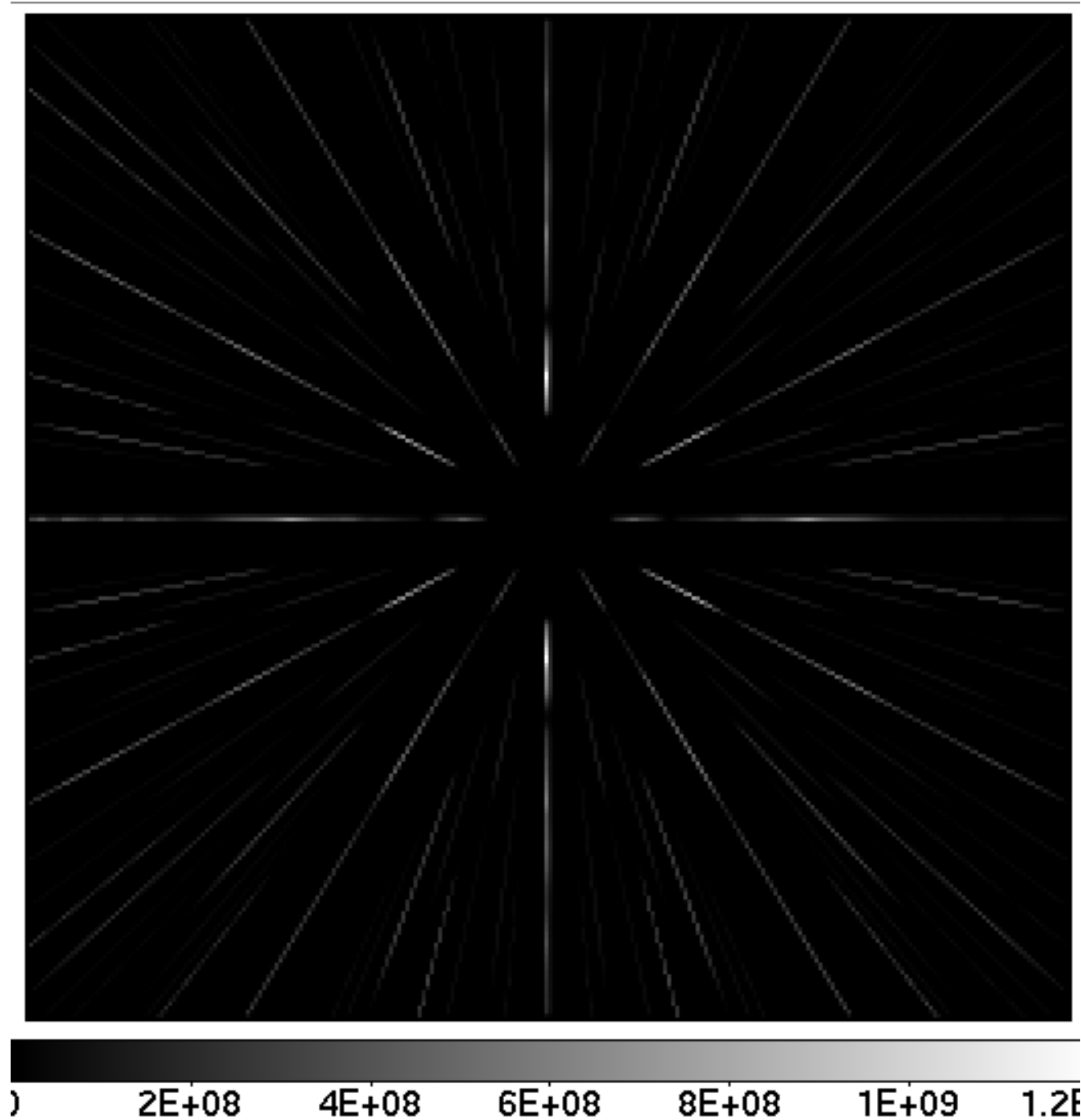
Numerical simulation approach



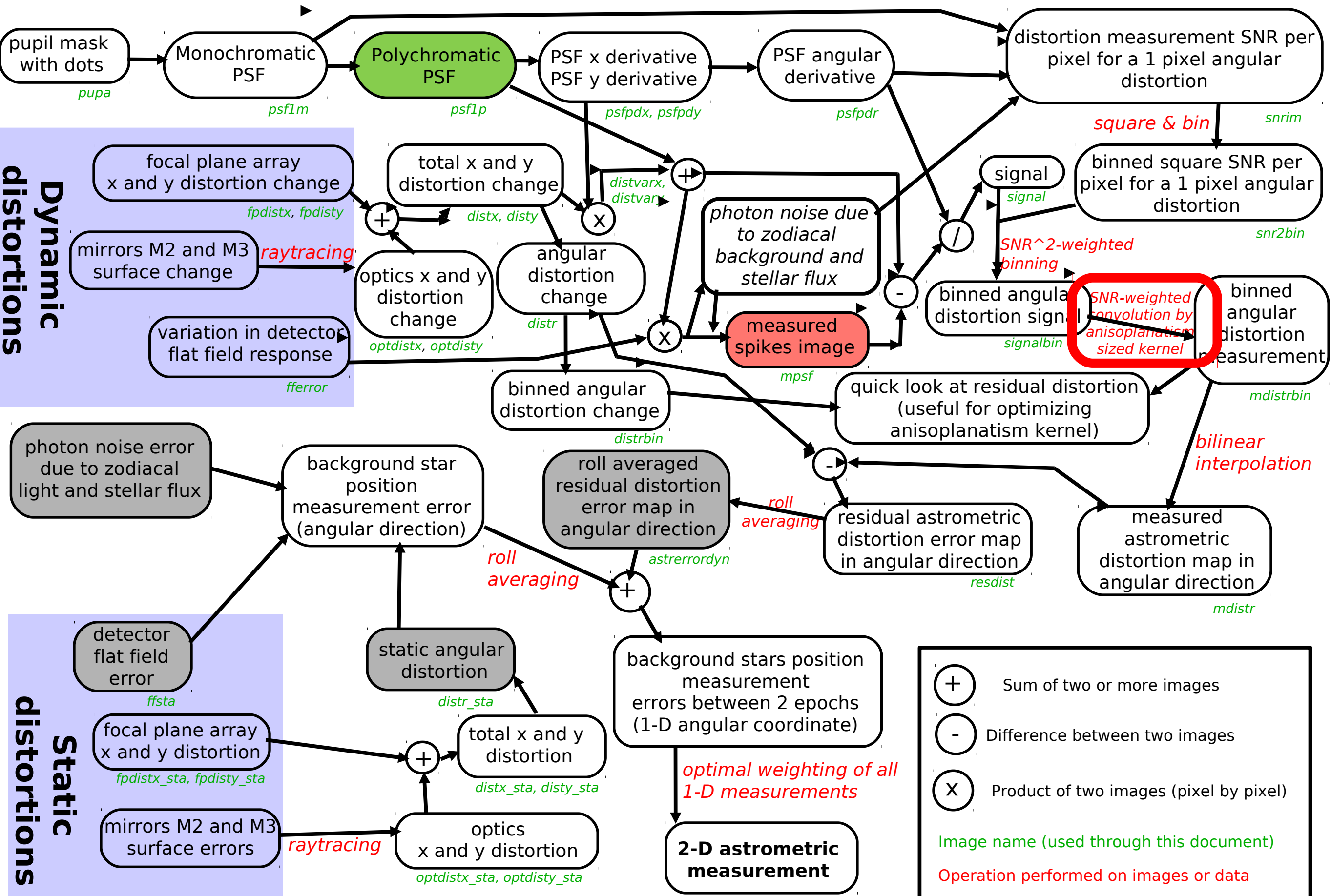
Distortion measurement

SNR^2

binned Signal (using SNR^2 weighting within each bin)
Value set to zero where SNR is below threshold



Numerical simulation approach



Distortion interpolation

Convolve signal $\times \text{SNR}^2$ by gaussian kernel, with sigma of the kernel \sim anisoplanatism patch size

Problem: next to a bright spike, the solution will give a flat value with a sharp jump when moving to the next spike.

Estimate for each pixel the effective centroid of the result (different from the pixel location), and the local slope of the distortion \rightarrow using these 2 quantities, correct for the centroid offset error.

Distortion interpolation

```
for(ii=0;ii<sizeb*sizeb;ii++)  
    distarray[ii] = 0.0;
```

```
for(ii0=0;ii0<sizeb;ii0++)  
    for(jj0=0;jj0<sizeb;jj0++)  
    {
```

```
        v = 0.0;  
        vx = 0.0;  
        vy = 0.0;  
        xt = 0.0;  
        yt = 0.0;  
        vcnt = 0.0;  
        vxcnt = 0.0;  
        vycent = 0.0;
```

```
        for(kk=0;kk<NBpt;kk++)
```

```
        {  
            ii = iarray[kk]-ii0;  
            jj = jarray[kk]-jj0;  
            x = 1.0*ii*SIA_pixscale*binfact; // radian  
            y = 1.0*jj*SIA_pixscale*binfact; // radian  
            r2 = x*x+y*y;  
            r2 /= SIA_corr_aniso_rad*SIA_corr_aniso_rad;  
            if(r2<9.0)
```

```
            {  
                v += varray[kk]*snr2array[kk]*exp(-r2);  
                xt += x*snr2array[kk]*exp(-r2);  
                yt += y*snr2array[kk]*exp(-r2);  
                vcnt += snr2array[kk]*exp(-r2);  
            }
```

```
        }  
        if(vcnt > eps)
```

```
        {  
            v /= vcnt;  
            xt /= vcnt; // effective x  
            yt /= vcnt; // effective y  
        }
```

```
        for(kk=0;kk<NBpt;kk++)
```

```
        {  
            ii = iarray[kk]-ii0;  
            jj = jarray[kk]-jj0;  
            x = 1.0*ii*SIA_pixscale*binfact; // radian  
            y = 1.0*jj*SIA_pixscale*binfact; // radian  
            r2 = x*x+y*y;  
            r2 /= SIA_corr_aniso_rad*SIA_corr_aniso_rad;  
            if(r2<9.0)  
            {  
                vx += (varray[kk]-v)*snr2array[kk]*(x-xt)*exp(-r2);  
                vy += (varray[kk]-v)*snr2array[kk]*(y-yt)*exp(-r2);  
                vxcnt += snr2array[kk]*(x-xt)*(x-xt)*exp(-r2);  
                vycent += snr2array[kk]*(y-yt)*(y-yt)*exp(-r2);  
            }
```

```
        }  
        if(vxcnt>eps)  
            vx /= vxcnt;  
        if(vycent>eps)  
            vy /= vycent;
```

```
        v -= xt*vx;  
        v -= yt*vy;  
        distarray[jj0*sizeb+ii0] = v;  
    }
```

kk is an index to the list of high SNR measurements (5% best pixels)

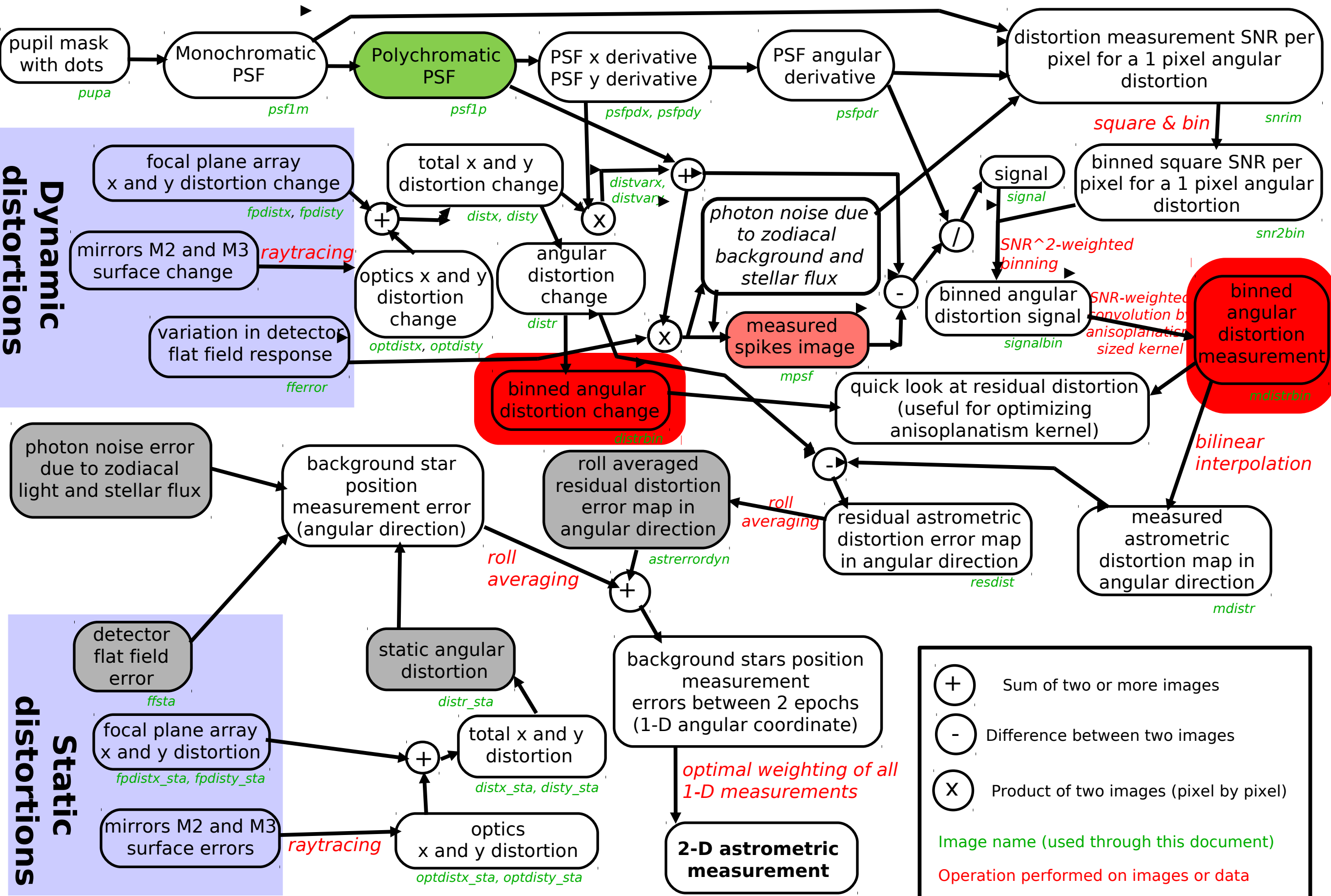
Convolution by kernel

This is the effective centroid to which the computed value corresponds. The centroid gets pulled to bright spikes.

Compute local 2D derivative of the measured distortion

Compensation of error due to centroid offset and local 2D derivative of distortion

Numerical simulation approach

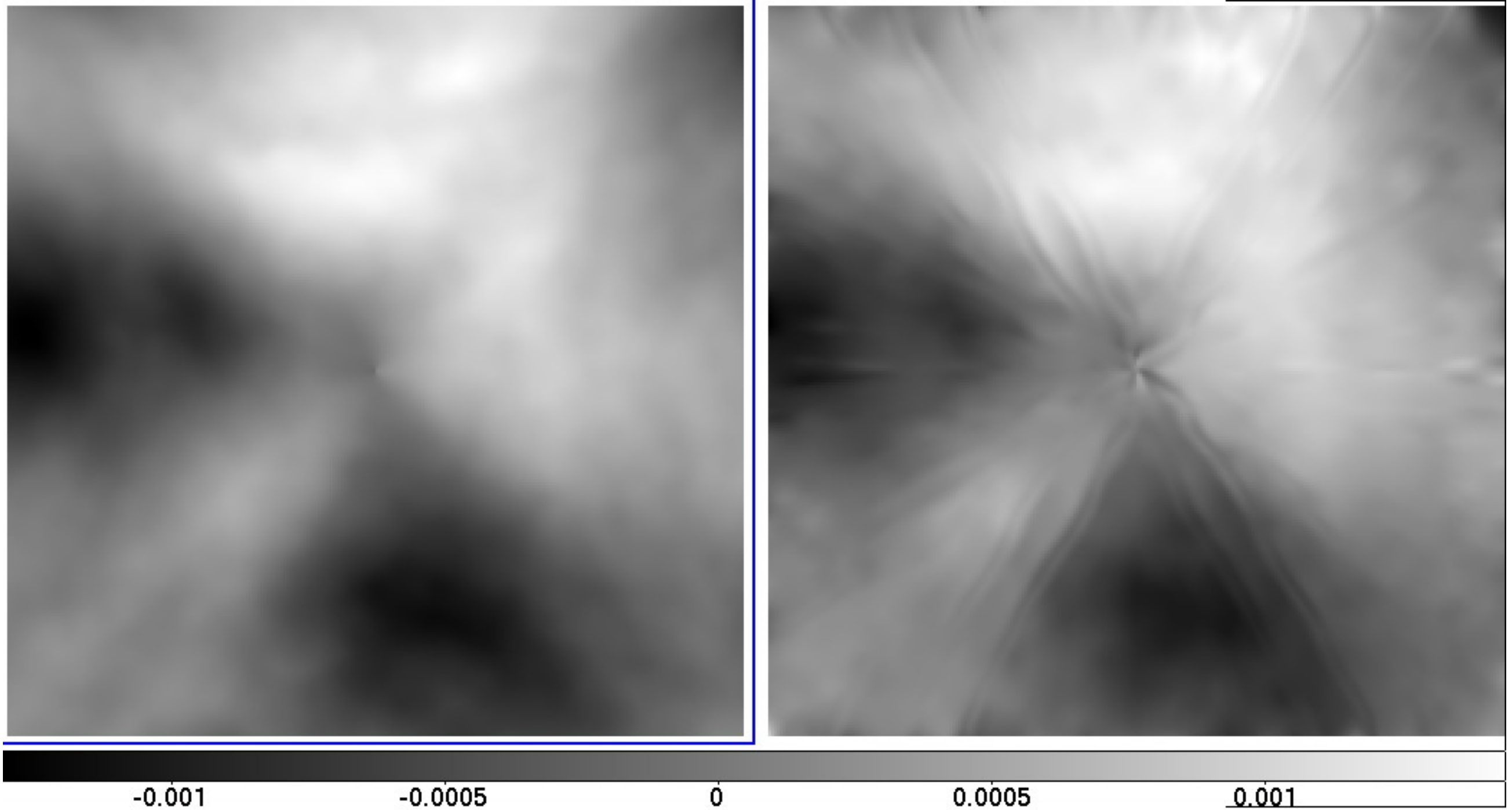


Distortion interpolation

Sigma = 15"

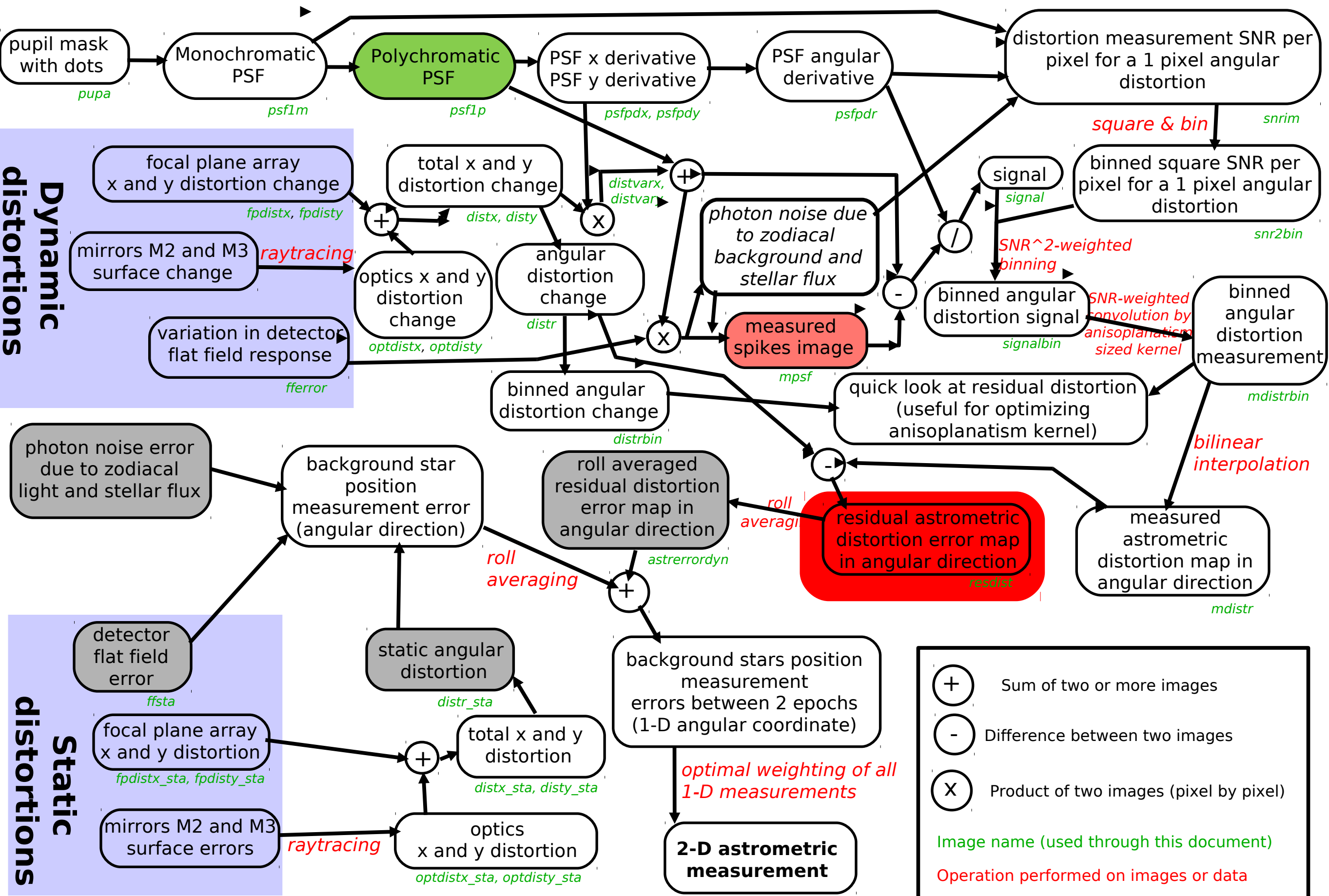
True distortion

Measured distortion



Unit = pixel

Numerical simulation approach

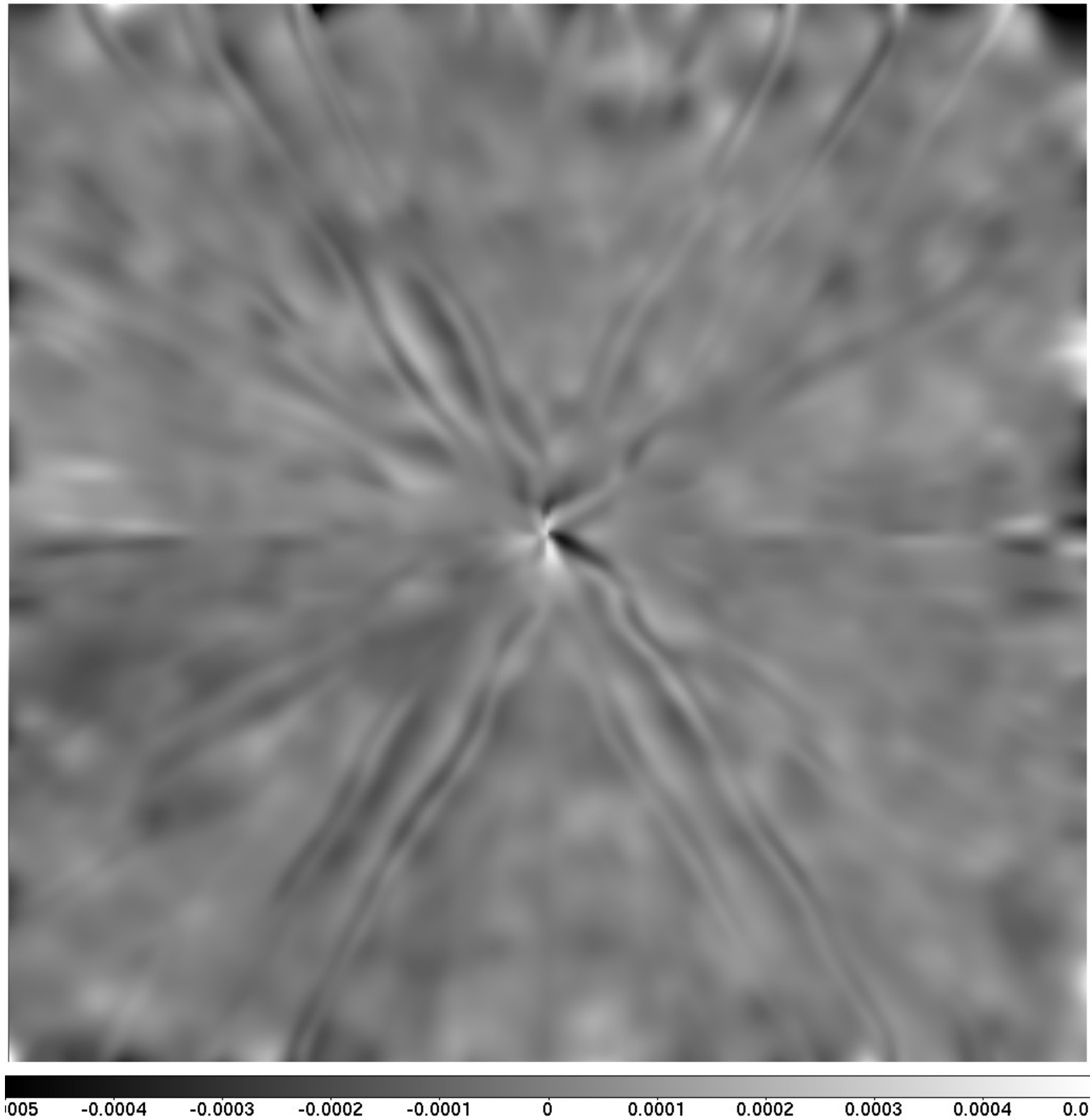


Residual distortion after calibration

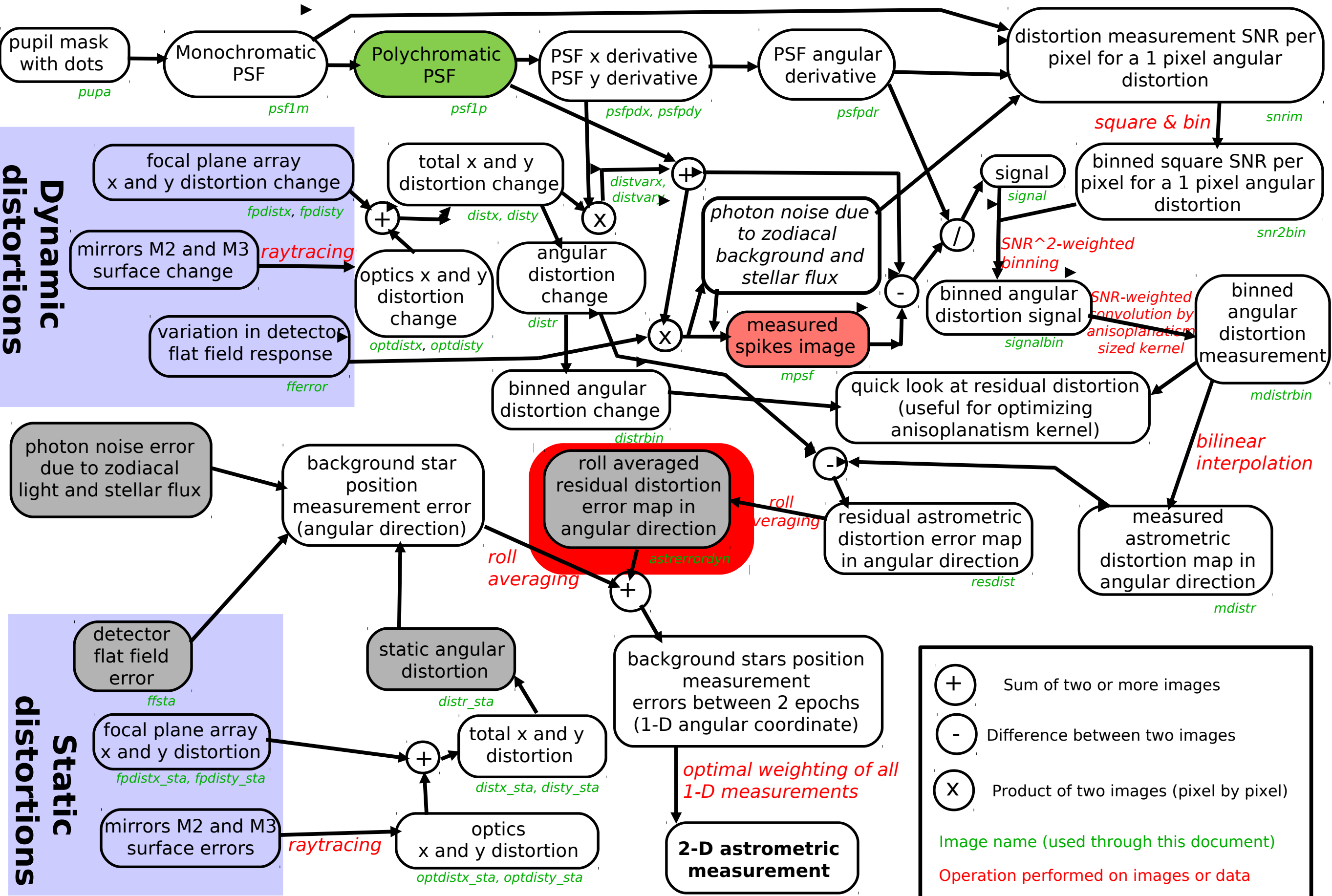
Unit = pixel

Residual distortion after calibration is $\sim 1\text{e-}4$ pix = $4.4\text{ }\mu\text{as}$

This is 10x smaller than original distortion, and residual is mostly free of low order -> will average well with telescope roll.



Numerical simulation approach

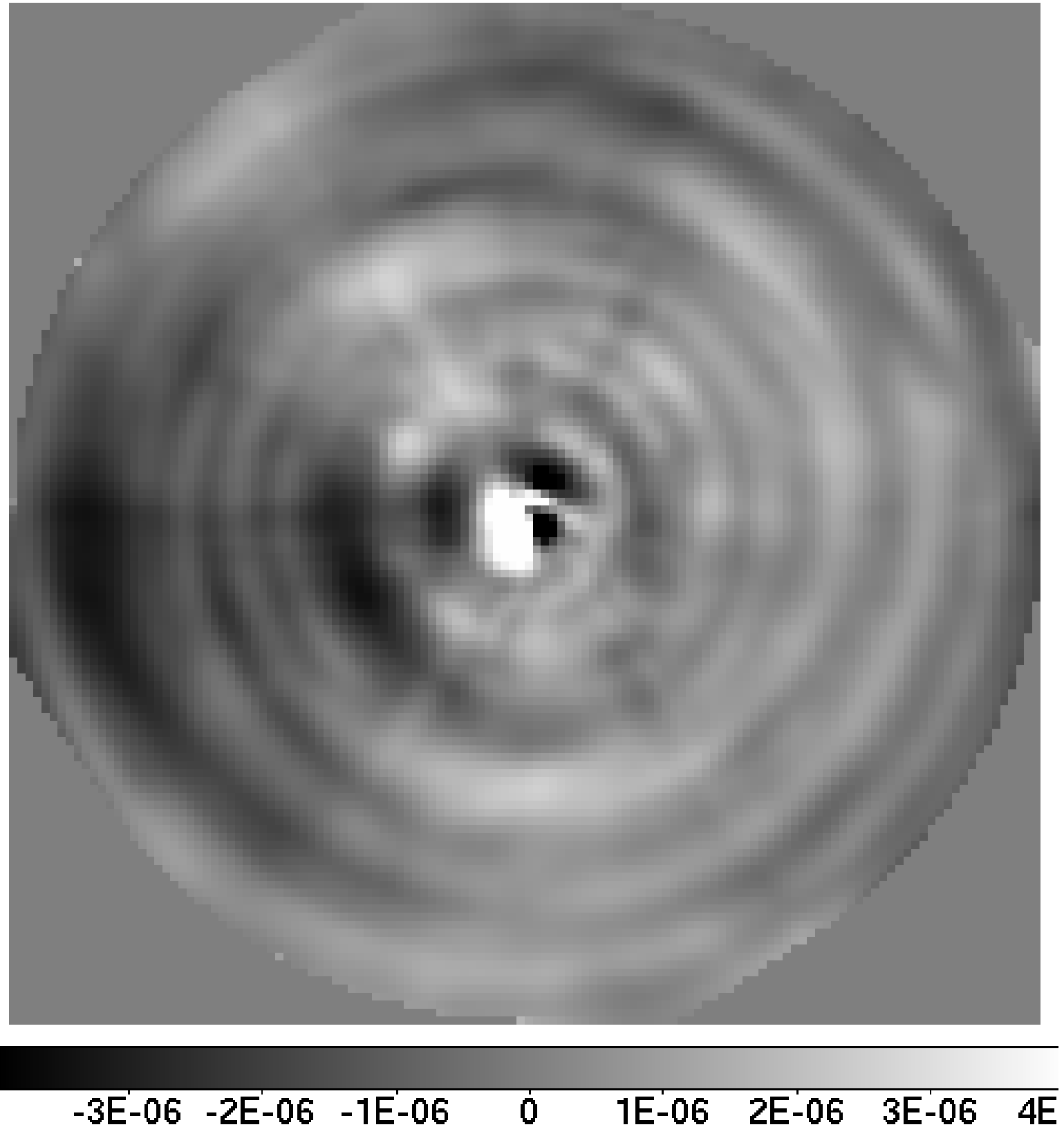


Astrometric error due to distortion changes (after roll)

Unit = arcsec
RMS $\sim \mu\text{as}$

This map is obtained by roll-averaging the distortion map in the previous slide

Error tends to be smaller for stars further out (more averaging thanks to roll)



Final astrometric error

For each star, 1-sigma error is computed as quadratic sum of :

- pixel coordinate error (due to photon noise)
- distortion errors (derived from 2D distortion map)
- flat field error on detector

Then, optimally combine all measurement by weighting according to astrometric SNR^2 for each star.

Final astrometric 1 sigma error in this example :

0.58 μas per axis (1-sigma) for 0.03 sq deg (= 0.1 deg radius circular field)

0.2 μas per axis would require 0.25 sq deg (= 0.5 deg x 0.5 deg)

Note: scaling to larger FOV needs to be done more carefully - this is just a rough estimate

Existing mechanical positioning accuracy

Key issue for coronagraphic performance is placement accuracy of dots and their size uniformity.

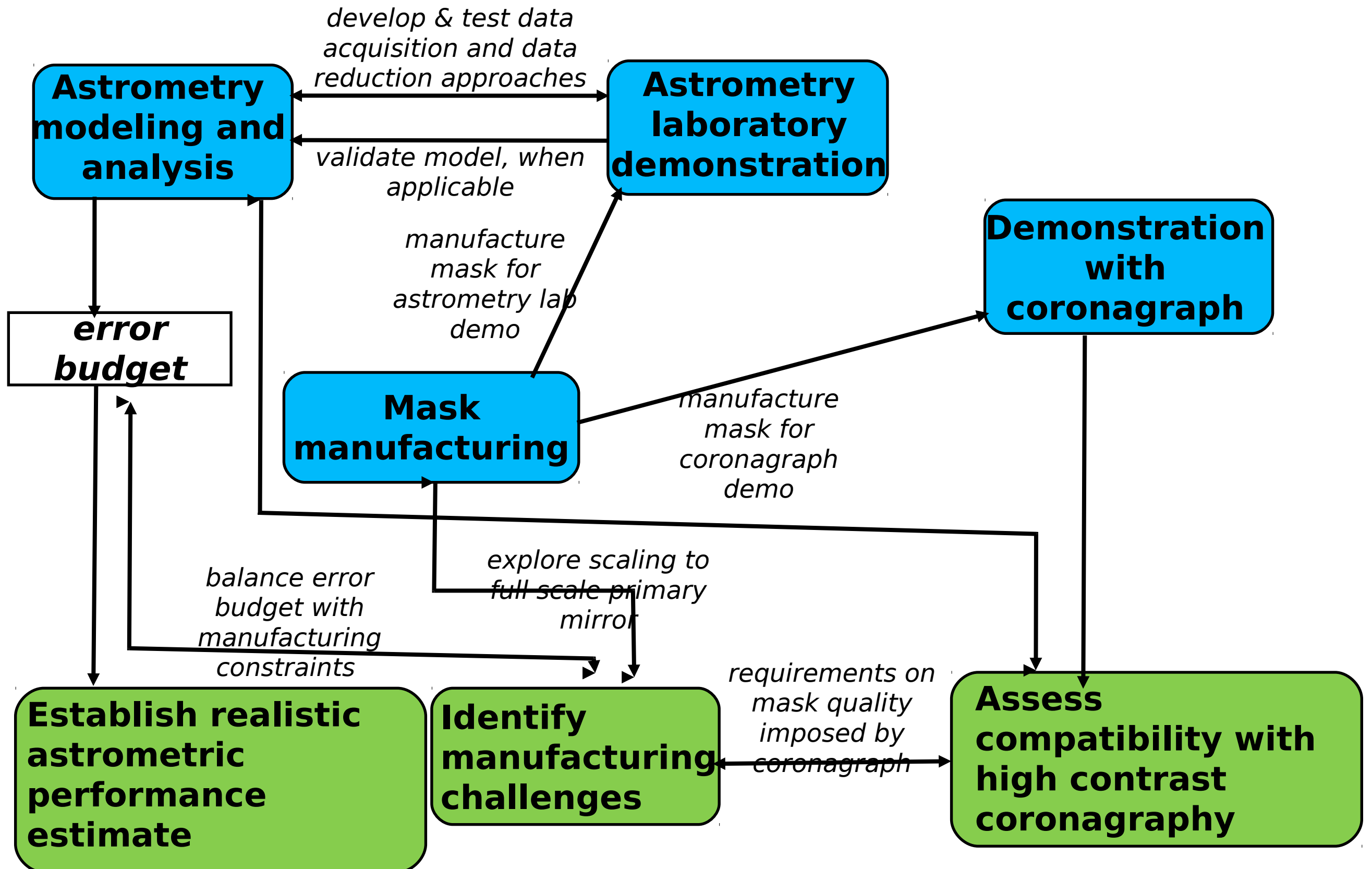
High precision CMM: $\sim 1 \text{ } \mu\text{m}$ over PECO PM seems possible

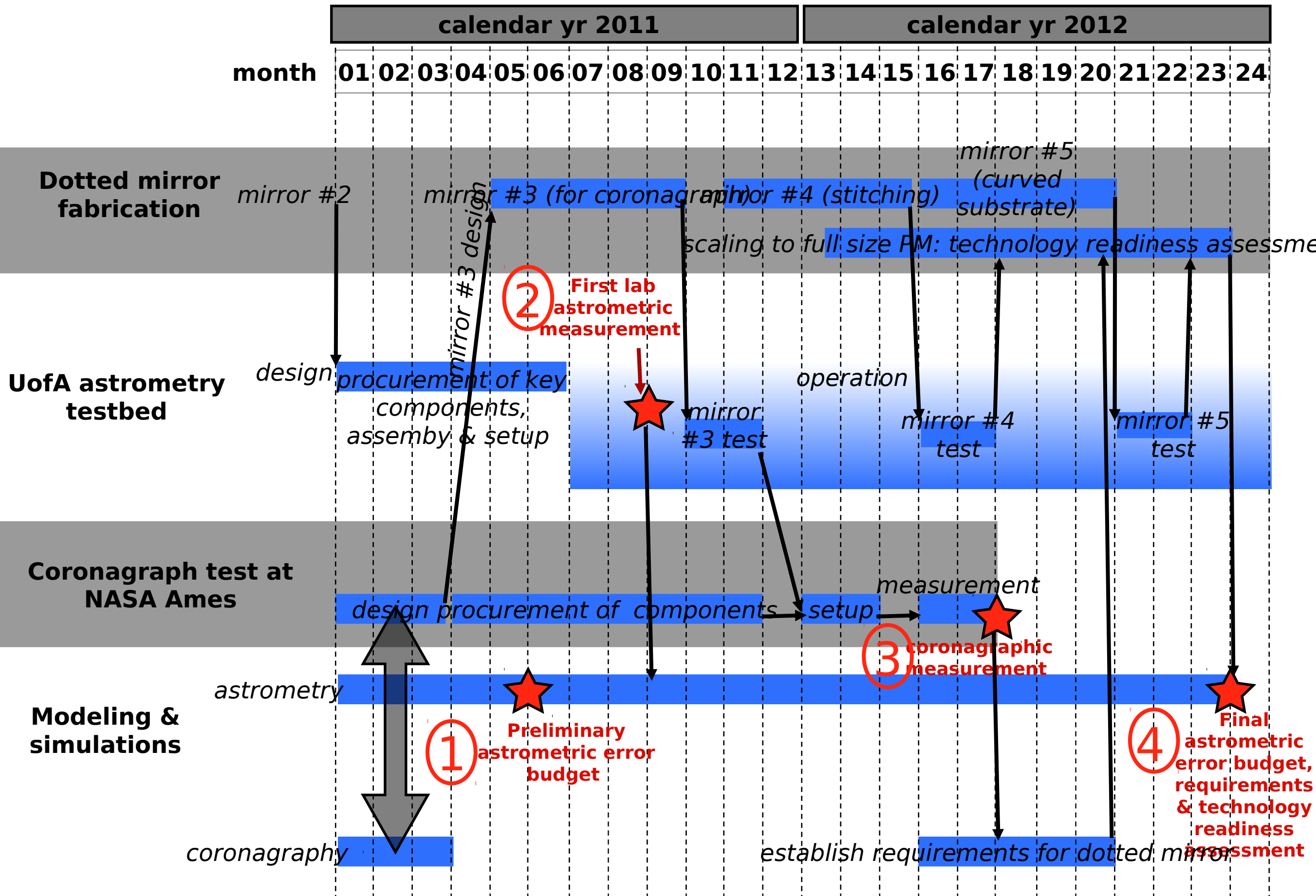
Example:

- NIST Moore 48 CMM: typical error is $130\text{nm absolute} + 200 \text{ nm per m} = 0.4 \text{ } \mu\text{m}$ on PECO PM

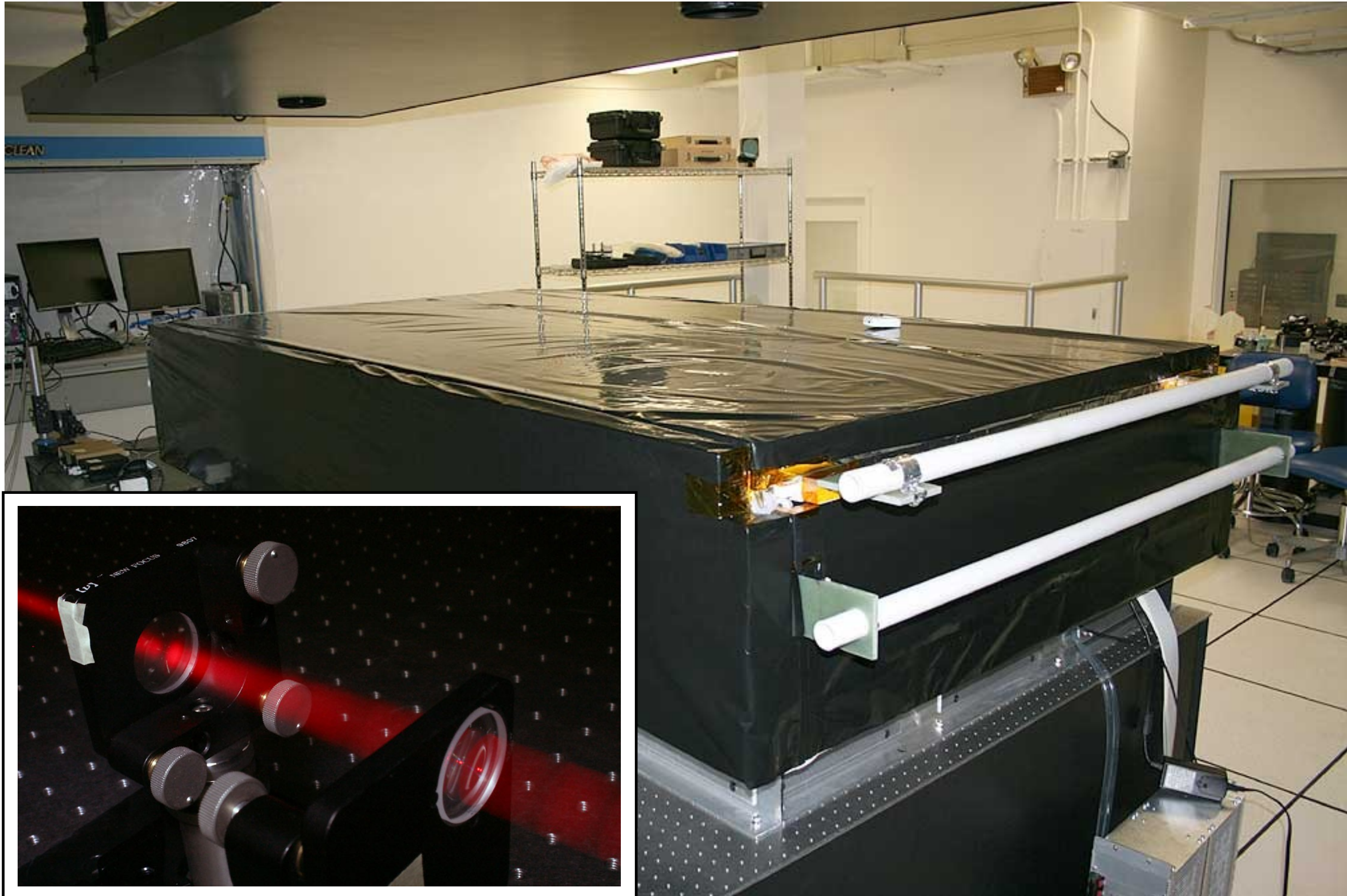
http://www.cenam.mx/cmu-mmc/Evento_2007/Presentaciones/John_Stoup-High_accuracy_CMM_measurements_at_NIST.pdf

Work plan

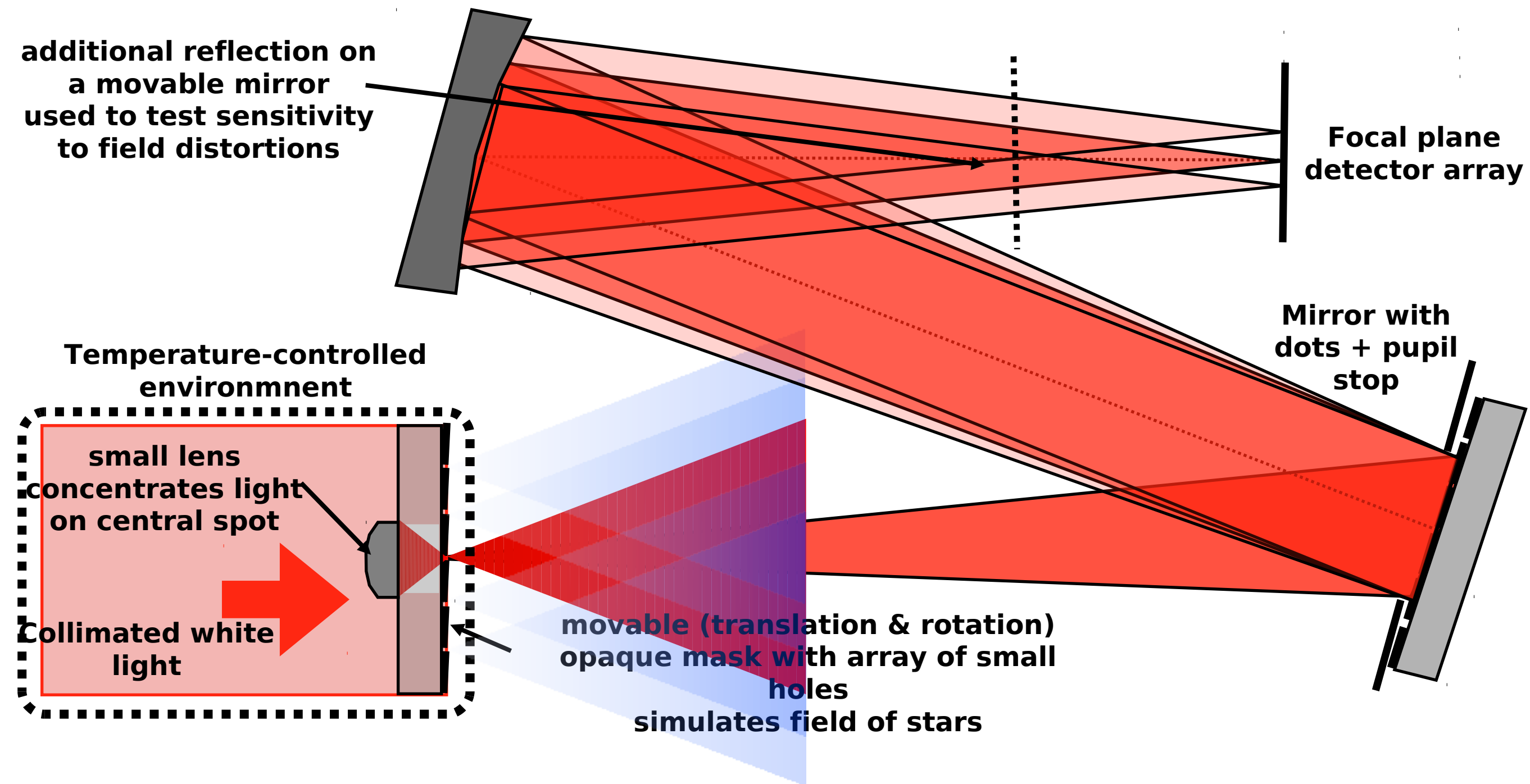




An existing coronagraph testbed at NASA Ames will be used to test compatibility of the dotted mirror with high contrast coronagraphy

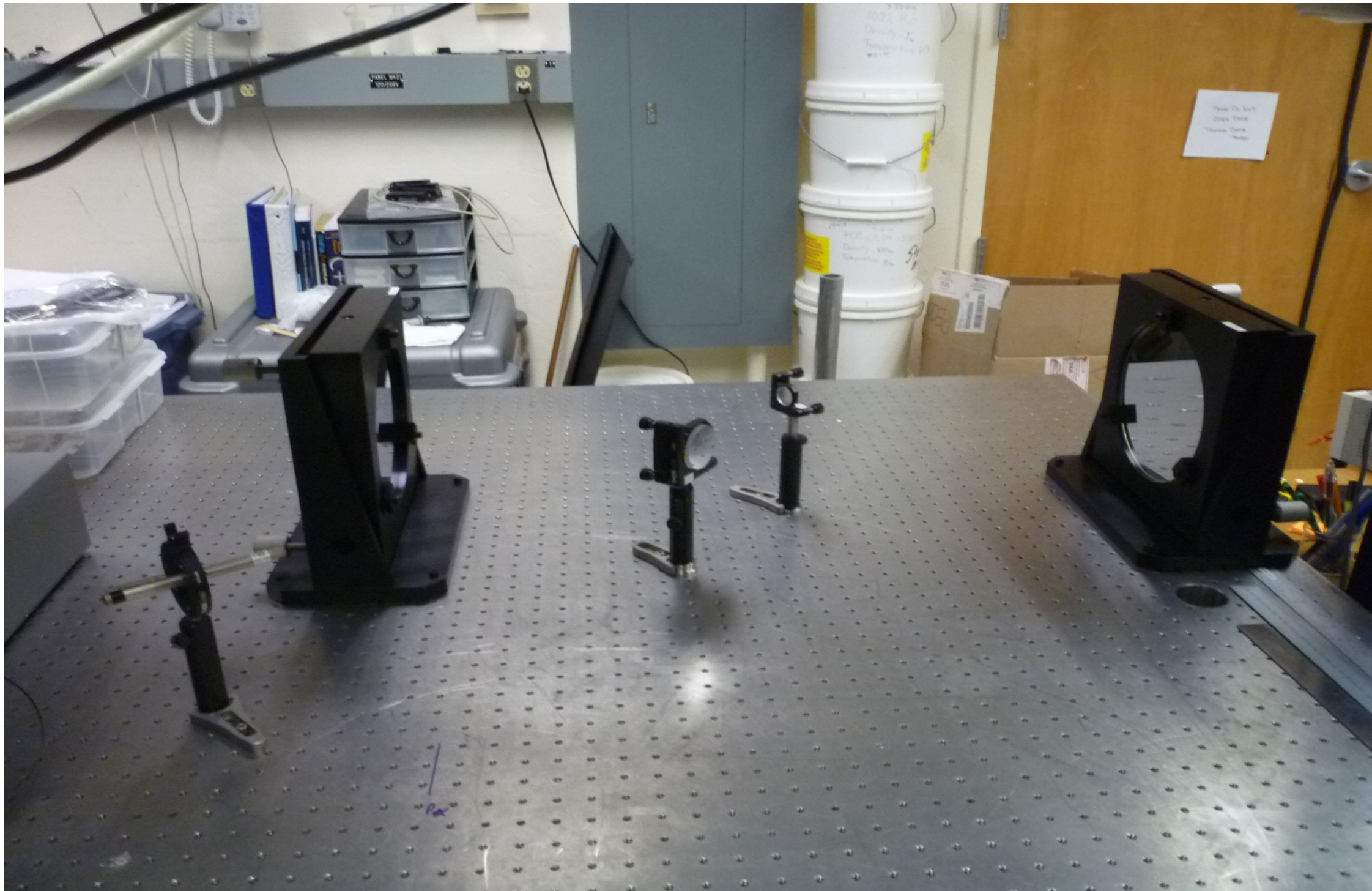


Lab demo: principle



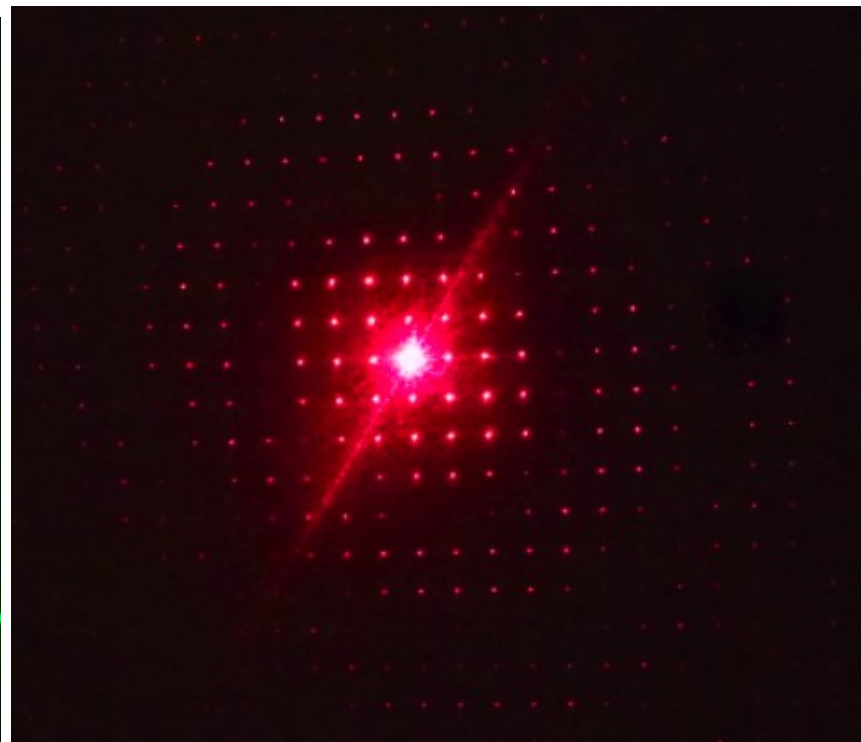
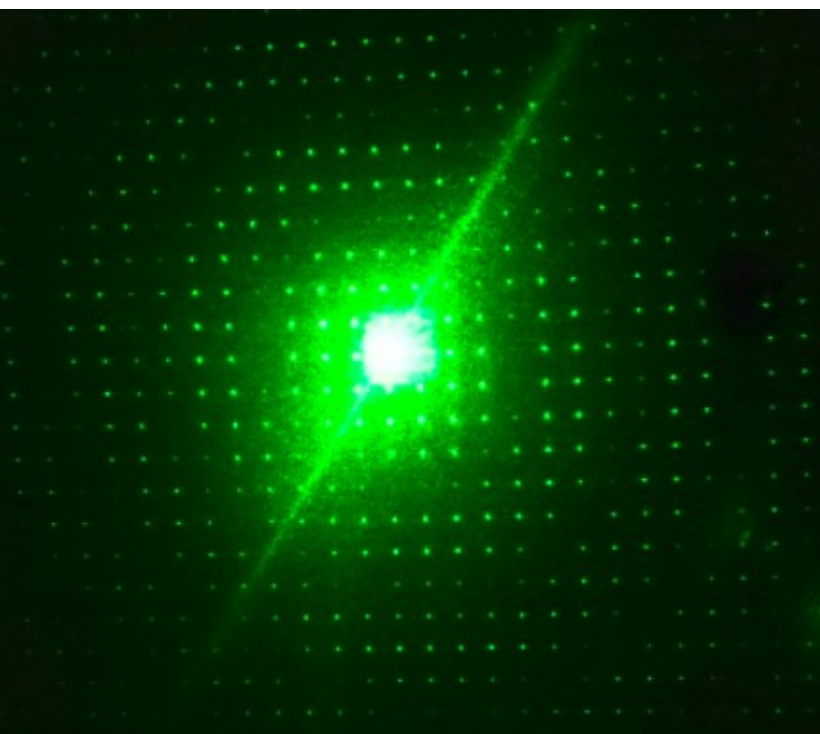
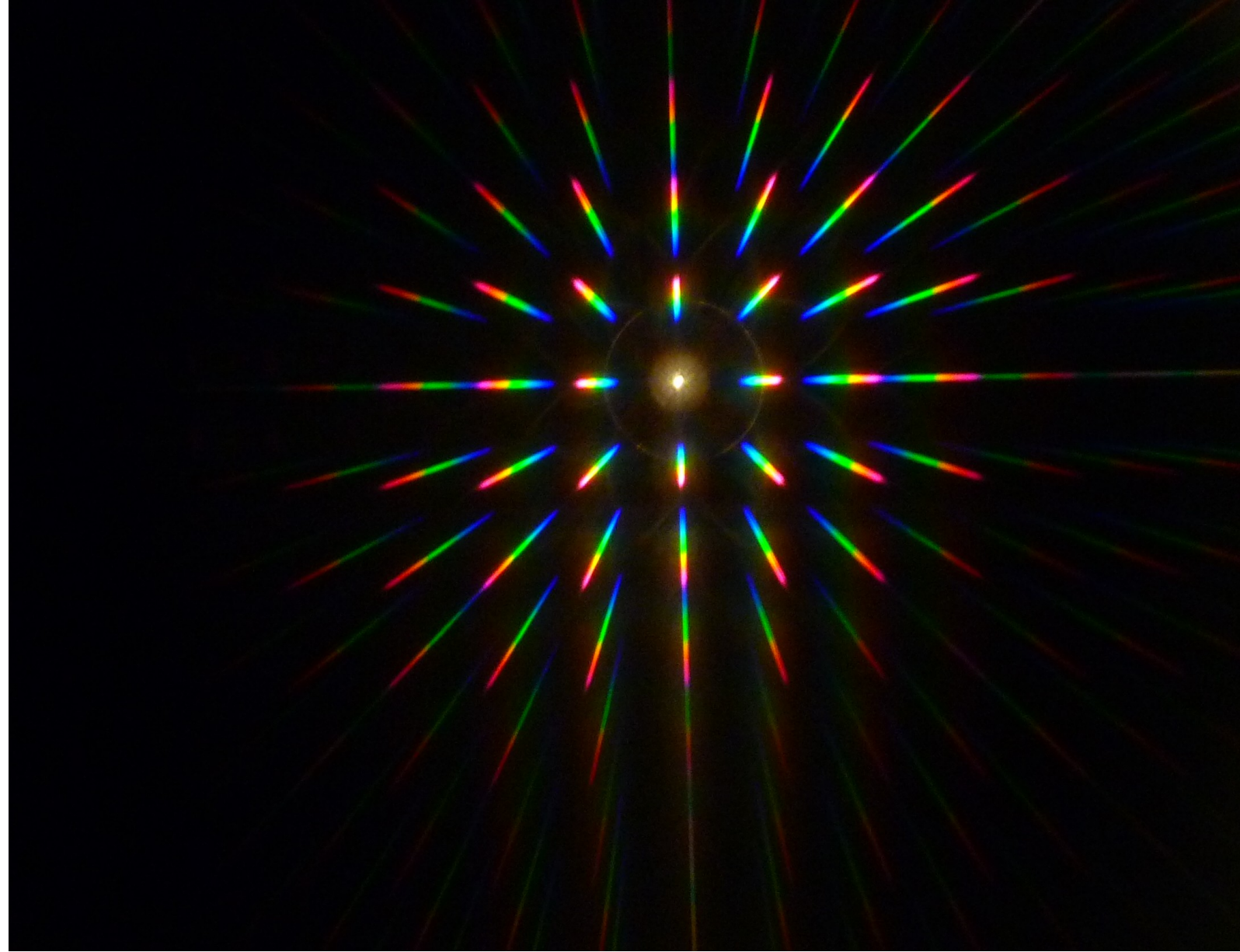
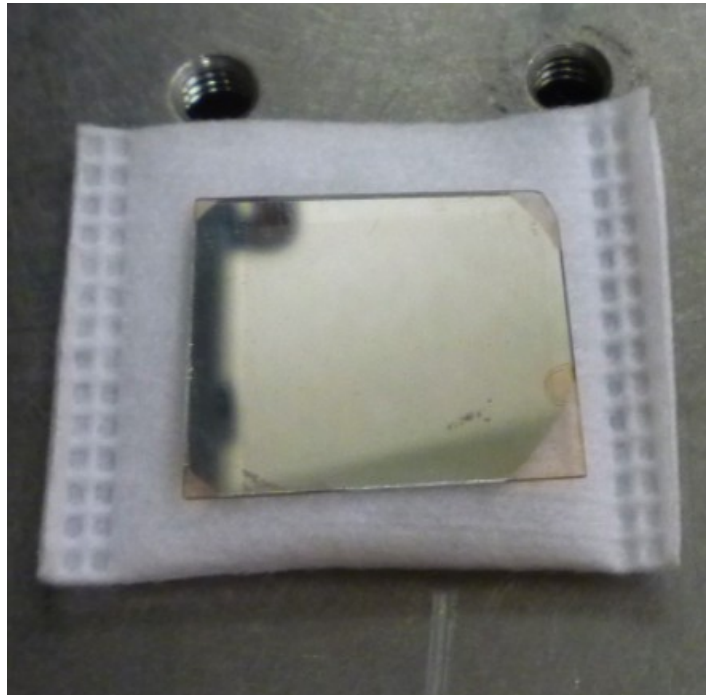
Lab demo: hardware

(lab at UofA, designed and operated by
E. Bendek and M. Ammons)

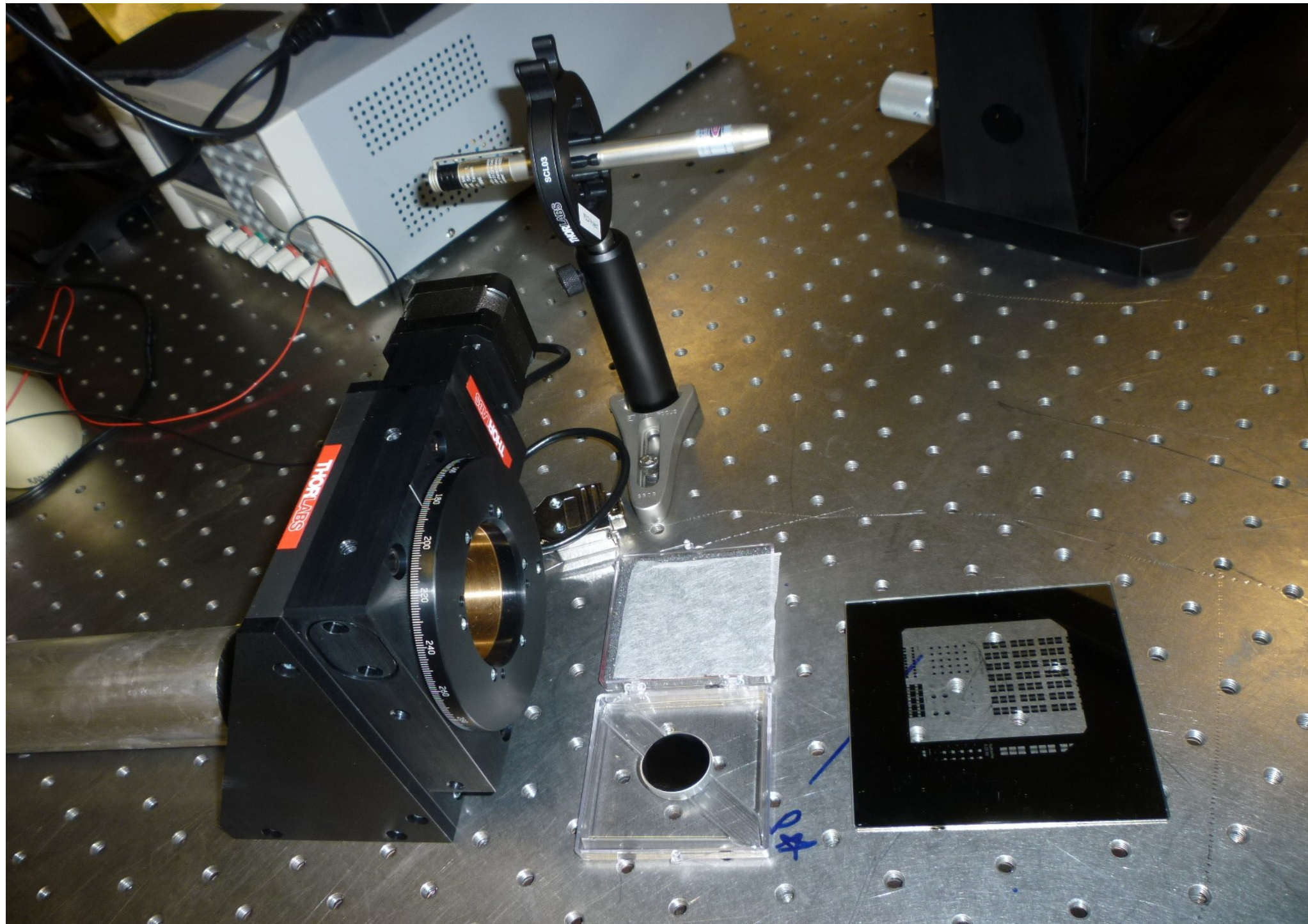


Off-axis parabolas used to collimate and focus the beam

Preliminary work on mask manufacturing and lab demo at UofA (Bendek, Ammons, Milster)



**Laser beam reflected on
first mask prototype
shows main beam
(center) + fainter
diffraction spots. Spot
spacing increases with
wavelength.**



Motorized rotation stage is used to rotate star field (= telescope roll)